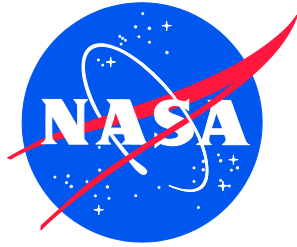


NASA/TM–2020-5008777  
NESC-NPP-18-01305



# Cryogenic Technologies for the Stratospheric Observatory for Infrared Astronomy (SOFIA) Science Instruments

*W. Lance Richards/NESC  
Armstrong Flight Research Center, Edwards Air Force Base, California*

*Michael L. Meyer  
Glenn Research Center, Cleveland, Ohio*

*Jeffrey R. Feller, and Alan C. Rhodes  
Ames Research Center, Moffett Field, California*

*Stefan Rosner  
SETI Institute, Mountain View, California*

*Dejan Stevanovic  
Universities Space Research Association, Columbia, Maryland*

*Ali Kashani  
Millennium Engineering & Integration Co., Arlington, Virginia*

## NASA STI Program . . . in Profile

Since its founding, NASA has been dedicated to the advancement of aeronautics and space science. The NASA scientific and technical information (STI) program plays a key part in helping NASA maintain this important role.

The NASA STI program operates under the auspices of the Agency Chief Information Officer. It collects, organizes, provides for archiving, and disseminates NASA's STI. The NASA STI program provides access to the NTRS Registered and its public interface, the NASA Technical Reports Server, thus providing one of the largest collections of aeronautical and space science STI in the world. Results are published in both non-NASA channels and by NASA in the NASA STI Report Series, which includes the following report types:

- **TECHNICAL PUBLICATION.** Reports of completed research or a major significant phase of research that present the results of NASA Programs and include extensive data or theoretical analysis. Includes compilations of significant scientific and technical data and information deemed to be of continuing reference value. NASA counter-part of peer-reviewed formal professional papers but has less stringent limitations on manuscript length and extent of graphic presentations.
- **TECHNICAL MEMORANDUM.** Scientific and technical findings that are preliminary or of specialized interest, e.g., quick release reports, working papers, and bibliographies that contain minimal annotation. Does not contain extensive analysis.
- **CONTRACTOR REPORT.** Scientific and technical findings by NASA-sponsored contractors and grantees.

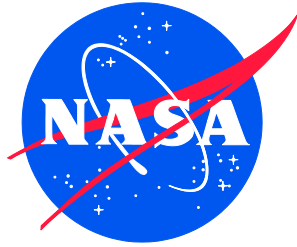
- **CONFERENCE PUBLICATION.** Collected papers from scientific and technical conferences, symposia, seminars, or other meetings sponsored or co-sponsored by NASA.
- **SPECIAL PUBLICATION.** Scientific, technical, or historical information from NASA programs, projects, and missions, often concerned with subjects having substantial public interest.
- **TECHNICAL TRANSLATION.** English-language translations of foreign scientific and technical material pertinent to NASA's mission.

Specialized services also include organizing and publishing research results, distributing specialized research announcements and feeds, providing information desk and personal search support, and enabling data exchange services.

For more information about the NASA STI program, see the following:

- Access the NASA STI program home page at <http://www.sti.nasa.gov>
- E-mail your question to [help@sti.nasa.gov](mailto:help@sti.nasa.gov)
- Phone the NASA STI Information Desk at 757-864-9658
- Write to:  
NASA STI Information Desk  
Mail Stop 148  
NASA Langley Research Center  
Hampton, VA 23681-2199

NASA/TM-2020-5008777  
NESC-NPP-18-01305



# Cryogenic Technologies for the Stratospheric Observatory for Infrared Astronomy (SOFIA) Science Instruments

*W. Lance Richards/NESC  
Armstrong Flight Research Center, Edwards Air Force Base, California*

*Michael L. Meyer  
Glenn Research Center, Cleveland, Ohio*

*Jeffrey R. Feller, and Alan C. Rhodes  
Ames Research Center, Moffett Field, California*

*Stefan Rosner  
SETI Institute, Mountain View, California*

*Dejan Stevanovic  
Universities Space Research Association, Columbia, Maryland*

*Ali Kashani  
Millennium Engineering & Integration Co., Arlington, Virginia*

National Aeronautics and  
Space Administration

Langley Research Center  
Hampton, Virginia 23681-2199

October 2020

## **Acknowledgments**

The authors would like to thank the diligent reviewers of this paper: Tim Brady, Mike DiPirro, Dan Dorney, Steve Gentz, Jon Holladay, Dean Johnson, Joe Minow, Steve Rickman, and Dave Schuster. Your inputs are greatly appreciated.

The use of trademarks or names of manufacturers in the report is for accurate reporting and does not constitute an official endorsement, either expressed or implied, of such products or manufacturers by the National Aeronautics and Space Administration.

Available from:

NASA STI Program / Mail Stop 148  
NASA Langley Research Center  
Hampton, VA 23681-2199  
Fax: 757-864-6500



# **NASA Cryogenics Technical Discipline Team Guidance Position Paper**

## **Cryogenic Technologies for the Stratospheric Observatory for Infrared Astronomy (SOFIA) Science Instruments**

**September 10, 2020**

## Report Approval and Revision History

NOTE: This document was approved at the September 10, 2020, NRB. This document was submitted to the NESC Director on September 22, 2020, for configuration control.

Approved:	<i>Original Signature on File</i>	9/23/20
	NESC Director	Date

Version	Description of Revision	Office of Primary Responsibility	Effective Date
1.0	Initial Release	Dr. W. Lance Richards	9/10/2020
1.1	Added reviewer's changes, added Figure 5.7-2	Dr. W. Lance Richards	9/30/2020

## Table of Contents

<b>1.0</b>	<b>Notification and Authorization</b> .....	<b>8</b>
<b>2.0</b>	<b>Signature Page</b> .....	<b>9</b>
<b>3.0</b>	<b>Team List</b> .....	<b>10</b>
3.1	Acknowledgements .....	10
<b>4.0</b>	<b>Executive Summary</b> .....	<b>11</b>
<b>5.0</b>	<b>Survey of SOFIA SIs</b> .....	<b>13</b>
5.1	The SOFIA Observatory.....	13
5.2	Resolving Power versus Wavelength of SOFIA SIs .....	14
5.3	Echelon-Cross-Echelle Spectrograph (EXES) .....	15
5.4	Field-Imaging Far-Infrared Line Spectrometer (FIFI-LS) .....	16
5.5	Faint Object infraRed CAmera for the SOFIA Telescope (FORCAST).....	18
5.6	German REceiver for Astronomy at Terahertz frequencies (GREAT) .....	19
5.7	High-resolution Airborne Wideband Camera Plus (HAWC+).....	21
5.8	High Resolution Mid-infrarEd Spectrometer (HIRMES) .....	23
<b>6.0</b>	<b>SI Environment and Constraints</b> .....	<b>25</b>
6.1	SOFIA Operations .....	25
6.2	Mission/Sortie Phases and Durations .....	26
6.3	Flight Preparation Timeline.....	26
6.4	Typical Flight Timelines .....	27
6.5	SI Environments During Deployment .....	28
6.6	Thermal Environments .....	28
6.7	Main Cabin Temperatures .....	29
6.8	Cargo Hold Temperatures .....	29
6.9	SI Accessibility.....	30
6.10	In-Flight SI Access .....	31
6.11	Availability of Electrical Power .....	31
6.12	Electrical Power Interruptions .....	32
6.13	Electrical Power Distribution and Allocation.....	32
6.14	Power Gear, Quality, and Overcurrent Protection.....	33
6.15	SI Mass and Volume Constraints .....	34
6.16	SOFIA Cryocooler System.....	35
6.17	SOFIA Cryocooler System Power Constraints.....	37
6.18	SOFIA Cryocooler System Dynamic Environments.....	37
6.19	Airworthiness Constraints .....	38
<b>7.0</b>	<b>Vibrational Environment with Design Guidelines</b> .....	<b>39</b>
7.1	Objectives .....	39
7.2	Telescope Assembly .....	39
7.3	Sources of Vibration.....	40
7.4	Observation Segments .....	40
7.5	Acceleration Measurements .....	40
7.6	Comparison with Test Standards .....	44
7.7	Design Guidelines .....	45
7.8	Proposed Vibration Test Curve .....	46
7.9	Approaches to Vibration Isolation.....	46
7.10	HAWC+ Lessons Learned.....	48
7.11	HIRMES Design Example.....	49
<b>8.0</b>	<b>Cryogenic Technologies Available to SI Developers</b> .....	<b>50</b>
8.1	Overview .....	50
8.2	Pulse Tube (PT) and Gifford-McMahon (GM) Refrigerators .....	51

8.3	Example: Cryomech PT407-RM PT Refrigerator.....	53
8.4	Example: TransMIT PTD-406C PT Refrigerator.....	54
8.5	Temperature Oscillation Damping Pot .....	55
8.6	$^4\text{He}$ and $^3\text{He}$ Sorption Refrigerators (SRs): Overview .....	56
8.7	Pumped Helium Pot.....	56
8.8	Helium SR .....	57
8.9	Typical SR Capacities .....	59
8.10	Example: Infrared Telescope for Space (IRTS) $^3\text{He}$ SR.....	60
8.11	Example: Chase Research Cryogenics $^4\text{He}$ SR .....	62
8.12	$^4\text{He} - ^3\text{He}$ SR .....	62
8.13	Example: Chase Research Cryogenics $^4\text{He} - ^3\text{He}$ SR.....	63
8.14	Adiabatic Demagnetization Refrigerator (ADR): Overview .....	64
8.15	ADR Principles of Operation .....	64
8.16	ADR Paramagnetic Salt Pill Manufacture.....	67
8.17	ADR Practical Design Limits .....	68
8.18	Example: XRS ADR.....	68
8.19	Example: HAWC+ ADR .....	69
8.20	Example: HIRMES ADR .....	71
8.21	Dilution Refrigerator (DR): Overview .....	71
8.22	DR Principles of Operation .....	72
8.23	Traditional Wet DR .....	73
8.24	Dry DR .....	74
8.25	Single-Cycle DR.....	75
8.26	Tiltable Single-Cycle DR .....	76
8.27	Continuously Operating Cold Cycle DR .....	77
8.28	Example: MUSCAT Cold Cycle DR.....	79
8.29	Example: Planck Open Cycle DR .....	79
8.30	Heat Switches: Overview .....	79
8.31	Mechanical Heat Switches.....	80
8.32	Gas Gap Heat Switches .....	81
8.33	Example: Astro-H Gas Gap Heat Switch .....	81
8.34	Passive Gas Gap Heat Switch.....	82
8.35	Thermal Straps.....	83
<b>9.0</b>	<b>Thermal Conductance at Low Temperatures .....</b>	<b>84</b>
9.1	Thermal Conductivity of Aluminum and Copper: Overview .....	84
9.2	Thermal Conductivity of Copper as a Function of RRR .....	85
9.3	Effects of Annealing on Thermal Conductivity.....	86
9.4	Thermal Conductivity of Aluminum and Copper: Summary .....	87
9.5	Thermal Contact Resistance: Constriction .....	88
9.6	Thermal Contact Resistance: Thermal Boundary.....	88
9.7	Thermal Boundary Resistance Models.....	89
9.8	Thermal Contact Resistance at Room Temperature .....	90
9.9	Thermal Contact Resistance at Low Temperatures .....	90
9.10	Copper Contact Conductance with Several Interface Materials.....	91
9.11	Copper Contact Conductance of Bolted Joints .....	92
<b>10.0</b>	<b>Summary of Cryogenic Technologies and General Guidance .....</b>	<b>94</b>
10.1	PT and GM Refrigerators .....	94
10.2	$^4\text{He}$ and $^3\text{He}$ SRs .....	95
10.3	ADRs .....	96
10.4	DR: Overview.....	96
10.5	DRs: Discussion of Variants.....	97



10.6	Heat Switches .....	98
10.7	General Guidance Concerning SI Cryostat Design .....	98
<b>11.0</b>	<b>Acronyms List .....</b>	<b>99</b>
<b>12.0</b>	<b>References.....</b>	<b>101</b>

### List of Figures

Figure 5.1-1.	SOFIA. The Telescope is Visible through the Opened Door .....	13
Figure 5.1-2.	SOFIA. Cutaway showing the Telescope, SI, and Work Stations .....	14
Figure 5.2-1.	Resolving Power versus Wavelength of Several SOFIA SIs.....	15
Figure 5.4-1.	Left: FIFI-LS SI Mounted to the Telescope Assembly (TA). Right: Cutaway View.....	17
Figure 5.5-1.	Left: FORCAST SI Mounted to the Telescope Assembly (TA). Right: Cutaway View..	18
Figure 5.6-1.	Left: GREAT SI Mounted to the Telescope Assembly (TA). Right: Cutaway View showing One Cryostat.....	19
Figure 5.6-2.	Left: GREAT SI Prior to Mating with the Telescope Assembly (TA). Right: Two PT-Cooled Cryostats Installed .....	20
Figure 5.7-1.	Cutaway View of the HAWC+ SI .....	22
Figure 5.7-2.	HAWC+ Mounted to the Telescope Assembly (TA).....	22
Figure 5.8-1.	Cutaway View of the HIRMES SI.....	24
Figure 6.2-1.	Notional SOFIA observing Flight Profile.....	26
Figure 6.3-1.	Notional SOFIA Flight Preparation Timeline.....	27
Figure 6.4-1.	Example Day of Flight Operations for (left) an SI using LHe + ADR, and (right) an SI using PTs instead of LHe and LN <sub>2</sub> .....	27
Figure 6.9-1.	SOFIA Parked on the Tarmac.....	30
Figure 6.16-1.	Panorama of the Aft Upper Deck of SOFIA where the Cryocooler System Compressors (grey boxes) and Other Equipment are Housed .....	36
Figure 6.16-2.	Two Pairs of Pressurized Helium Flex Lines Connect the Two Cryocoolers with the Compressors in the Upper Deck .....	36
Figure 7.2-1.	The Telescope Assembly (TA) .....	39
Figure 7.5-1.	Accelerometer Locations .....	41
Figure 7.5-2.	Vibrational data (a <sup>2</sup> /Hz vs. Hz) from Flight 356 (HAWC+). Left: 0 – 150 Hz. Right: Same Data, but from 0 – 50 Hz.....	41
Figure 7.5-3.	A Closer Look at Flight Segment 3 from Flight 356 (HAWC+) .....	42
Figure 7.5-4.	Flight Segments 1 and 3 from Flight 362 (EXES).....	43
Figure 7.5-5.	Flight Segment 3 from Flight 356 (EXES) and Flight 362 (EXES) .....	43
Figure 7.5-6.	Data from a 3-axis Accelerometer Mounted at the TA Flange for Flight 380 (FORCAST), Flight Segment 3, with High Turbulence (left) and No Turbulence (right).....	44
Figure 7.6-1.	Environmental Test Standards Compared with SOFIA Data .....	45
Figure 7.8-1.	Proposed Vibration Test Curve.....	46
Figure 7.9-1.	Schematic Equation of Motion of a Cryogenic Component showing the Three Approaches to Vibration Isolation .....	46
Figure 7.9-2.	HAWC+ Suspension System .....	47
Figure 7.9-3.	HIRMES ADR (set up for modal testing) with Magnetic Eddy Current Damper .....	48
Figure 7.11-1.	HIRMES Ti-Truss System.....	49
Figure 8.1-1.	Summary of Refrigeration Technologies Available to SI Developers.....	50
Figure 8.2-1.	Left: GM Cold Heat; Right: PT Cold Head.....	51
Figure 8.2-2.	Comparison of Vibration Levels in Comparable GM and PT Cold Heads.....	52
Figure 8.3-1.	Drawings of the Cryomech PT407-RM Cold Head, Flex Lines, and Compressor Options.....	53
Figure 8.3-2.	Performance Map for the Two-stage Cryomech PT407-RM PT Refrigerator .....	54
Figure 8.4-1.	Tilt Dependence of the TransMIT PTD-406C PT Cold Head .....	55

Figure 8.5-1.	Cryomech PT Cold Head Equipped With A Temperature Oscillation Damping Pot.....	56
Figure 8.7-1.	Left: Diagram of a Pumped Helium Pot; Right: Saturated Vapor Pressure versus Temperature Curves for $^4\text{He}$ and $^3\text{He}$ .....	57
Figure 8.8-1.	Closed Cycle Helium SR .....	58
Figure 8.8-2.	Relevant Helium Properties .....	58
Figure 8.8-3.	Gas Adsorption on a Surface .....	59
Figure 8.10-1.	The IRTS $^3\text{He}$ SR.....	60
Figure 8.10-2.	The IRTS $^3\text{He}$ SR.....	61
Figure 8.10-3.	Left: On-orbit Temperature Profile of the IRTS Refrigerator; Right: Temperature Profiles of $^4\text{He}$ and $^3\text{He}$ SRs during a Sounding Rocket Flight .....	61
Figure 8.11-1.	Left: Chase Research Cryogenics Type GL4 $^4\text{He}$ SR. Right: Measured GL4 Capacity Curve.....	62
Figure 8.12-1.	Tandem $^4\text{He} - ^3\text{He}$ SR.....	63
Figure 8.13-1.	Left: Chase Research Cryogenics Type GL7 $^4\text{He} - ^3\text{He}$ SR. Right: Measured GL7 $^3\text{He}$ Cold Head Capacity Curve .....	63
Figure 8.15-1.	Simple Schematic of a Single Stage ADR.....	64
Figure 8.15-2.	Example of a $J = 5/2$ Refrigerant .....	65
Figure 8.15-3.	Entropy Curves for Various Paramagnetic Salts (at applied magnetic fields of 0 and 2 T).....	66
Figure 8.15-4.	Molar Entropy $S$ versus Temperature $T$ for CMN Salt, with Lines of Constant applied Magnetic Field $B$ .....	67
Figure 8.16-1.	ADR Salt Pill Manufacture.....	67
Figure 8.18-1.	XRS ADR. Left: Salt Pill Removed from the Bore of the Magnet; Right: Superconducting Magnet made by Cryomagnetics, Inc .....	69
Figure 8.19-1.	HAWC+ ADR System.....	70
Figure 8.22-1.	$^3\text{He} - ^4\text{He}$ Phase Diagram and Comparison of the DR with the Pumped $^3\text{He}$ Pot .....	72
Figure 8.23-1.	Left: Schematic of a $^3\text{He}$ -Circulating DR; Right: Janis Research Company DR Insert for a LHe Dewar. Expression for the Refrigeration capacity (bottom) .....	73
Figure 8.24-1.	A Dry DR.....	74
Figure 8.25-1.	Left: A Single Cycle DR; Right: Measured Cooling Power at the Mixing Chamber showing a $T^2$ Dependence, in Agreement with Theory .....	75
Figure 8.26-1.	A Tiltable DR Developed for Astrophysical Applications .....	76
Figure 8.27-1.	A Continuously Operating Cold Cycle DR .....	77
Figure 8.27-2.	A Continuously Operating Cold Cycle DR .....	78
Figure 8.28-1.	The MUSCAT DR developed by Chase Research Cryogenics. ....	78
Figure 8.29-1.	Planck Open Cycle DR Developed by Institut Neel and Air Liquide.....	79
Figure 8.30-1.	Various Cryogenic Heat Switches with Ranges of Applicability .....	80
Figure 8.31-1.	Mechanical Heat Switch as used in HIRMES .....	80
Figure 8.32-1.	Gas Gap Heat Switch.....	81
Figure 8.33-1.	The Astro-H Gas Gap Heat Switch.....	82
Figure 8.34-1.	Passive Gas gap heat Switch. Left: ON; Right: OF. ....	83
Figure 8.34-2.	Passive Gas Gap Heat Switch. Fully Disassembled on the left; Fully Assembled on the right.....	83
Figure 8.36-1.	Commercially Available carbon, Copper, and Aluminum Thermal Straps.....	84
Figure 9.2-1.	Thermal Conductivity of Copper: Dependence on Residual Resistance Ratio RRR.....	86
Figure 9.3-1.	Thermal Conductivity Values for 5N purity Vacuum-Annealed and Oxygen-Annealed Copper at a Temperature of 1 K .....	87
Figure 9.5-1.	Two Solids with Thermal Conductivities $k_1$ and $k_2$ Making Contact Over a Circular Region of Radius $a$ .....	88
Figure 9.6-1.	Contact of Two Surfaces at a Microscopic Level .....	89

Figure 9.8-1.	Contact Conductance of Copper (left) and Aluminum (right) Alloys Near Room Temperature .....	90
Figure 9.10-1.	Copper-copper Pressed Contact Conductance between 2 and 20 K Using Various Interface Materials .....	91
Figure 9.10-2.	Copper-copper Pressed Contact Conductance between 40 and 90 K using Various Interface Materials .....	91
Figure 9.11-1.	Exaggerated Depiction of Elastic Deformation in Bolted Plates .....	92
Figure 9.11-2.	Experimental Set-Up For Measuring The Contact Resistance of Bolted Joints at Cryogenic Temperatures .....	93
Figure 9.11-3.	Measured contact Resistance Values of Bolted Joints at Cryogenic Temperatures .....	94

**List of Tables**

Table 5.3-1.	EXES Key Information .....	16
Table 5.4-1.	FIFI-LS Key Information .....	17
Table 5.5-1.	FORCAST Key Information .....	18
Table 5.6-1.	GREAT Key Information, including upGREAT LFA and HFA, and 4GREAT .....	21
Table 5.7-1.	HAWC+ Key Information .....	23
Table 5.8-1.	HIRMES Key Information .....	25
Table 6.13-1.	Sub-allocation of the Total Allocation of 6.5 kVA Available for SI Use .....	33
Table 6.14-1.	Additional Information on the SOFIA Power Source Equipment .....	33
Table 6.15-1.	Mass Allocation and Constraints of SI Elements .....	34
Table 8.4-1.	Key Specifications of the TransMIT PTD-406C PT .....	54
Table 8.15-1.	Common ADR Paramagnetic Salt Refrigerants .....	65
Table 9.10-1.	Contact Resistance Values of Bolted Joints at Room Temperature .....	92

## **1.0 Notification and Authorization**

This work was performed at the request of Jeanette Le, the Program Chief Engineer for Stratospheric Observatory for Infrared Astronomy (SOFIA). While this report emphasizes sub-Kelvin technologies, the background and environmental information and the design guidance are relevant to the entire cryogenic system.

The High Resolution Mid-infrared Spectrometer (HIRMES) Science Instrument (SI) was under development during this study but has since been canceled. It nonetheless remains as a valuable example of a fully “dry” sub-Kelvin cryostat.

Commercially available technologies are discussed by way of example. However, the NESC Cryogenics Technical Discipline Team does not endorse any vendor or product.

The key stakeholder for this report is the SOFIA Program and Jeanette Le, the Program Chief Engineer for SOFIA, and the prospective SOFIA SI developer, who may not have extensive experience with cryogenics or cryostat design.

Official SOFIA documentation is held in the SOFIA requirements library. Check the SOFIA documentation library prior to use for the purposes of meeting SOFIA requirements. For more information on SOFIA documentation and requirements, please contact the SOFIA Program office at NASA Ames Research Center.

## 2.0 Signature Page

Submitted by:

*Team Signature Page on File – 10/09/20*

---

Dr. W. Lance Richards                      Date

Significant Contributors:

---

Mr. Michael L. Meyer                      Date

---

Dr. Jeffrey R. Feller                      Date

---

Mr. Alan C. Rhodes                      Date

---

Mr. Stefan Rosner                      Date

---

Dr. Dejan Stevanovic                      Date

---

Dr. Ali Kashani                      Date

Signatories declare the findings, observations, and NESC recommendations compiled in the report are factually based from data extracted from program/project documents, contractor reports, and open literature, and/or generated from independently conducted tests, analyses, and inspections.

### 3.0 Team List

Name	Discipline	Organization
<b>Core Team</b>		
Lance Richards	NESC Lead	NESC Chief Engineer; AFRC
Michael Meyer	NESC Co-Lead	NESC NASA Technical Fellow for Cryogenics; GRC
Jeffrey Feller	Technical Lead	NESC NASA Deputy Technical Fellow for Cryogenics; ARC
Alan Rhodes	SOFIA SI Development Manager	ARC
Stefan Rosner	SOFIA SI Development and Cryocooler Systems Engineer	SETI Institute; ARC
Dejan Stevanovic	SOFIA SI Development Engineer / Analyst	Universities Space Research Association; ARC
Ali Kashani	Cryogenics SME: Cryocoolers and Materials at Low Temperatures	MEI Technologies, Inc.; ARC
Peter Shirron	Cryogenics SME: Sub-Kelvin Cryostat Design	GSFC
<b>Consultants</b>		
Sonny Yi	Cryogenics SME: Cryogenic System Design	The Aerospace Corporation
Natalie Spivey	SOFIA Structural Dynamics SME	AFRC
<b>Business Management</b>		
Rebekah Hendricks	Program Analyst	LaRC/MTSO
<b>Assessment Support</b>		
Melissa Strickland	Project Coordinator	LaRC/AMA
Erin Moran	Technical Editor	LaRC/AMA

### 3.1 Acknowledgements

The authors would like to thank the diligent reviewers of this paper: Tim Brady, Mike DiPirro, Dan Dorney, Steve Gentz, Jon Holladay, Dean Johnson, Joe Minow, Steve Rickman, and Dave Schuster. Your inputs are greatly appreciated.

## 4.0 Executive Summary

The intended audience for this position paper is the prospective SOFIA Science Instrument (SI) developer, who may not have extensive experience with cryogenics or cryostat design. The objective is to provide an introductory handbook that (1) concisely summarizes SOFIA requirements, (2) describes components and techniques that enable cryostats to reach temperatures ranging from 4 K to 50 mK, and (3) warns of common pitfalls that an SI developer might encounter.

The following topics are discussed:

- Constraints on the SI, especially where they might impact the design and operation of the SI cryostat. These include
  - Procedural constraints dictated by the strict pre-flight and flight timelines;
  - Volume, mass, and center of gravity (CG) constraints; and
  - Environmental constraints, primarily the thermal (i.e., possible temperature excursions) and vibrational environments.
- An overview of SIs that have been developed, emphasizing the various cryogenic components with SOFIA flight heritage.
- A lengthy discussion of cryogenic refrigerators and other thermal control components, including their principles of operation, operating constraints, potential capabilities, flight heritage (SOFIA or otherwise), and their overall applicability to SOFIA SIs.

Key considerations for SI developers:

- Most of the SI cryostats that have flown thus far are “wet”, meaning that they employ a reservoir of expendable liquid helium (LHe) to reach 4 K. With the development in recent years of SOFIA’s on-board cryocooler system (consisting of two helium compressors, along with supporting equipment, capable of driving two commercial pulse tube (PT) or Gifford-McMahon (GM) cold heads), fully dry cryostats are realizable. The GREAT SIs employ 4 K PTs and no liquid cryogens. The cancelled HIRMES SI would have employed two PTs.
- Most of the technologies discussed are used to bridge the gap between 4 K and operating temperatures as low as 50 mK. They include  $^4\text{He}$  and  $^3\text{He}$  sorption refrigerators (SRs), adiabatic demagnetization refrigerators (ADRs), and dilution refrigerators (DRs). These technologies are applicable to both wet cryostats (cryogen-based) and dry cryostats (PT- or GM-based).
- Vibrational heating can easily overwhelm the cooling capacity of low temperature refrigerators (e.g., ADRs and DRs). The colder the stage the more attention must be given to vibration isolation and damping.
- An ADR has flown successfully (HAWC+ SI). The HIRMES SI also employed an ADR. DRs have no SOFIA heritage, but are possible alternatives to ADRs. Several DR variants are discussed. DRs can potentially reach lower temperatures and/or higher cooling capacities than current ADR designs.

- Thermal straps are important components at all stages of the cryostat. However, the thermal conductivity of aluminum and copper can vary dramatically at low temperatures, as can pressed contact conductances. These large uncertainties must be factored into any thermal margin analysis.
- Below 4 K, it is difficult to systematize thermal margins because of heavily design-dependent factors such as parasitics (which can be comparable to the gross refrigeration capacity) and large variations in materials properties.



## 5.0 Survey of SOFIA SIs

### 5.1 The SOFIA Observatory

SOFIA (Figures 5.1-1 and 5.1-2) is a Boeing 747SP aircraft modified to carry a 2.7-meter (106-inch) reflecting telescope (with an effective diameter of 2.5 meters or 100 inches). Flying into the stratosphere at 38,000-45,000 feet puts SOFIA above 99 percent of Earth's infrared-blocking atmosphere, allowing astronomers to study the solar system and beyond in ways that are not possible with ground-based telescopes. SOFIA is made possible through a partnership between NASA and the German Aerospace Center (DLR).

SOFIA's SIs — cameras, spectrometers, and polarimeters — operate in the near-, mid- and far-infrared wavelengths, each suited to studying particular phenomena. Spectrometers spread light into its component colors, in the same way that a prism spreads visible light into a rainbow, to reveal the chemical fingerprints of celestial molecules and atoms.

Polarimeters are sensitive to the effect magnetic fields have on dust in and around celestial objects, allowing astronomers to learn how magnetic fields affect the birth of stars and other objects. Unlike space-based telescopes, SOFIA lands after each flight, so its instruments can be exchanged, serviced or upgraded to harness new technologies. Because these new instruments can be tested and adjusted, SOFIA can explore new frontiers in the solar system and beyond and serve as a testbed for technologies that may one day fly in space.



*Figure 5.1-1. SOFIA. The telescope is visible through the opened door.*

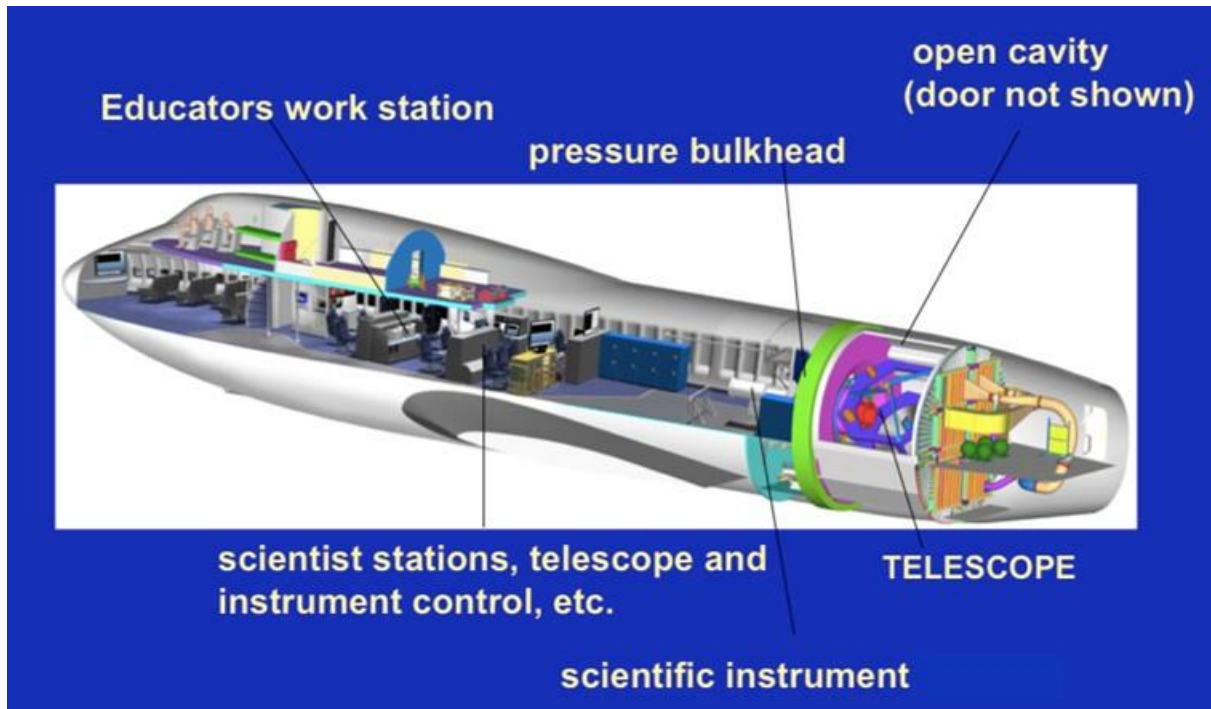


*Figure 5.1-2. SOFIA. Cutaway showing the telescope, SI, and work stations.*

## 5.2 Resolving Power versus Wavelength of SOFIA SIs

Figure 5.2-1 shows the resolving power versus wavelength, from near to far infrared and beyond, of several SOFIA SIs, including the predicted footprint of HIRMES, which has since been cancelled. The footprints of the James Webb Space Telescope (JWST) and the Atacama Large Millimeter/submillimeter Array (ALMA), the world's largest radio telescope, have been included for reference.

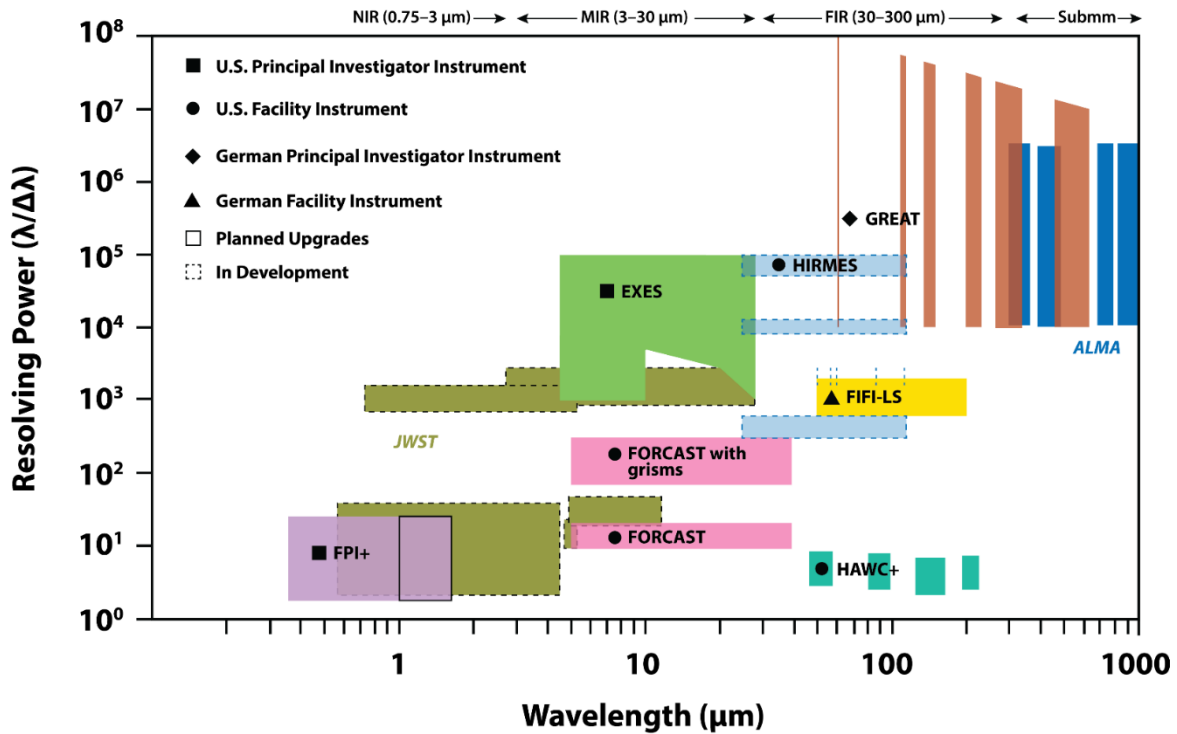


Figure 5.2-1. Resolving power versus wavelength of several SOFIA SIs. For reference, JWST and ALMA are also included.

### 5.3 Echelon-Cross-Echelle Spectrograph (EXES)

EXES is a LHe cooled instrument. The cryostat is approximately 24 inches in diameter and 72 inches long.

There are three layers of radiation shielding within EXES: a vapor cooled shield tied only to the cryogen fill tubes, one attached to the liquid nitrogen (LN<sub>2</sub>) reservoir, and the third attached to the LHe reservoir.

All optics except for the entrance window/lens are attached to the LHe-cooled stage. Baffling tubes connected to the liquid nitrogen level reduce thermal emission impinging on the internal optics. Within the LHe level, the optics are all tied to a rigid optics box constructed out of aluminum and the detector headerboard is isolated with G10 fiberglass and is actively maintained at a uniform temperature. Refer to Table 5.3-1 for more information.

**Table 5.3-1. EXES key information.**

<b>Instrument Overview</b>	
Instrument functionality	Echelle spectrograph with imaging (basic source identification) and pupil viewing capability
Operating wavelength ( $\lambda$ )	4.5-28.3 $\mu$ m
Resolving power ( $R=\lambda/\Delta\lambda$ )	high (50,000 – 100,000), medium (5000 – 20,000) low (1000 – 3000)
Cooling methodology	LN <sub>2</sub> and helium
Nominal instrument temperature	4K
Detector/spatial resolution	Si:As 256x256 (baseline); upgraded to 1024x1024
Detector temperature	7K
Operation time (cryogen hold time)	36h LN <sub>2</sub> and 24h LHe

## 5.4 Field-Imaging Far-Infrared Line Spectrometer (FIFI-LS)

The FIFI-LS detector is cooled to 1.8 K by pumping on the 3.12 liter superfluid helium tank (see Figure 5.4-1). An oil-free mechanical scroll pump (the SOFIA Vacuum Pump System (VPS)), external to the cryostat, is used.

A hold time (limited by the capacity of the superfluid helium tank) of 18 hours is achieved.

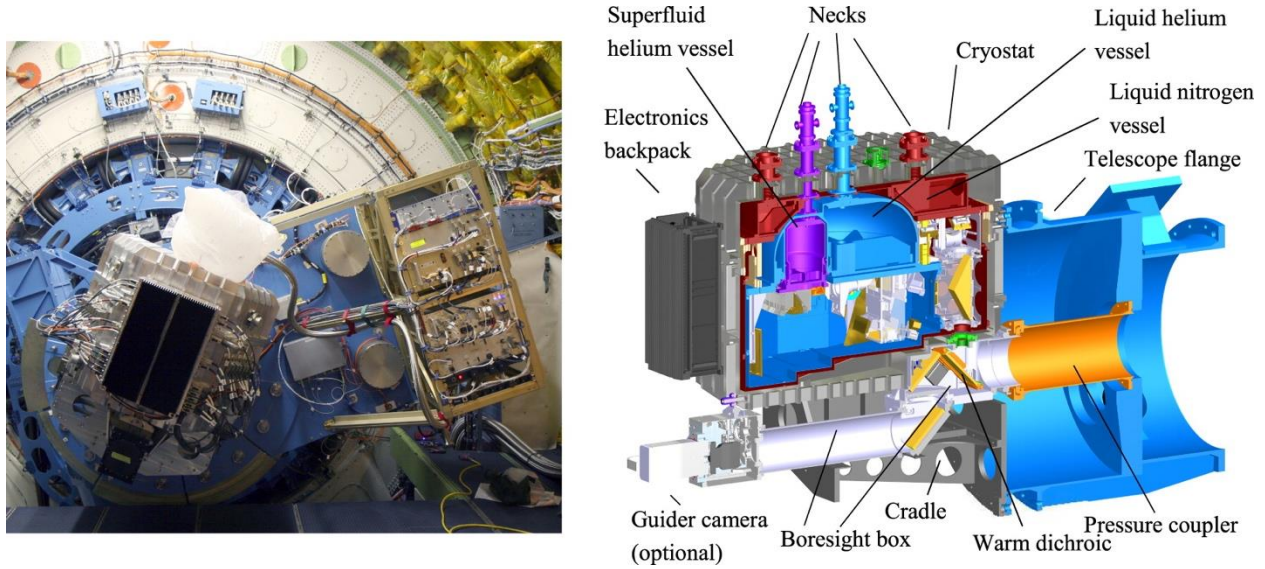


**Figure 5.4-1. Left: FIFI-LS SI mounted to the Telescope Assembly (TA). Right: Cutaway view. (Fischer, 2018).**

**Table 5.4-1. FIFI-LS key information.**

<b>Instrument Overview</b>	
Instrument functionality	Integral field, far-infrared imaging spectrometer
Operating wavelength ( $\lambda$ )	Blue channel: 51 – 120 $\mu$ m Red channel: 115 – 200 $\mu$ m
Resolving power ( $R=\lambda/\Delta\lambda$ )	500-2000
Cooling methodology	LN <sub>2</sub> (31.5 l tank); LHe (35 l tank) and superfluid helium (3.12 l tank)
Nominal instrument temperature	Entrance optics @80K (LN <sub>2</sub> ); internal optics @4K (LHe)
Detector/spatial resolution	400 pixels of Germanium Gallium-doped (Ge:Ga) photoconductors
Detector temperature	1.7-1.9K (superfluid He)
Operation time (cryogen hold time)	LN <sub>2</sub> (28h); LHe (50h) and superfluid helium (18h)

## 5.5 Faint Object infraRed CAmera for the SOFIA Telescope (FORCAST)

FORCAST is a mid-infrared camera and spectrograph cooled using LHe. Its hold time is 72 hours (Figure 5.5-1).

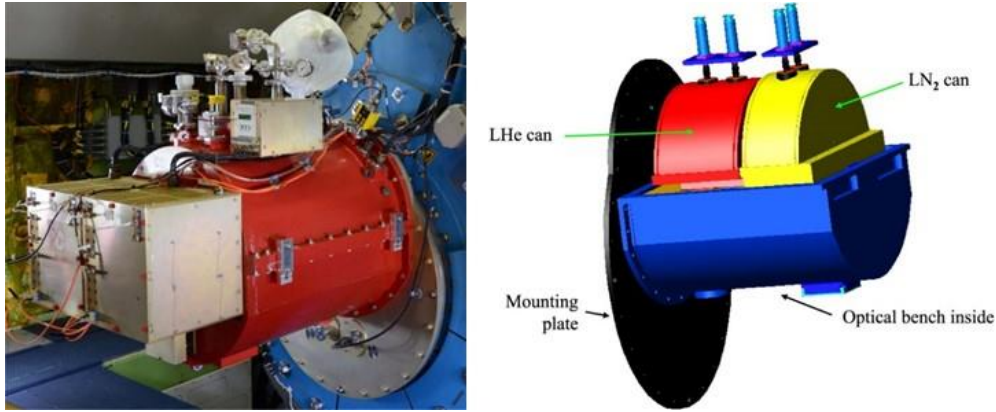


*Figure 5.5-1. Left: FORCAST SI mounted to the Telescope Assembly (TA). Right: Cutaway view. (Herter, 2018).*

**Table 5.5-1. FORCAST key information.**

Instrument Overview	
Instrument functionality	Dual-channel mid-infrared camera and spectrograph
Operating wavelength ( $\lambda$ )	5 – 40 $\mu$ m
Resolving power ( $R=\lambda/\Delta\lambda$ )	Long-slit low-resolution: $R=100\text{--}300$ (with gratings); Short-slit, cross-dispersed high resolution spectroscopic modes: $R=800\text{--}1200$ (with gratings)
Cooling methodology	LN <sub>2</sub> (20.7 l tank); LHe (30.4 l tank)
Nominal instrument temperature	Field stop and collimator @80K (LN <sub>2</sub> ); dichroic, filters and detectors @4K (LHe)
Detector/spatial resolution	The Short Wavelength Channel (SWC) ( $\lambda < 25 \mu\text{m}$ ): Si:As blocked-impurity band (BIB) 256x256 pixel array The Long Wavelength Channel (LWC) ( $\lambda > 25 \mu\text{m}$ ): Si:Sb BIB 256x256 pixel array
Detector temperature	4K
Operation time (cryogen hold time)	72h (both cryogen tanks)



## 5.6 German REceiver for Astronomy at Terahertz frequencies (GREAT)

These are the first “dry” cryostats (i.e., no expendable liquid cryogens are used) developed for use aboard SOFIA. There are three channels: upGREAT LFA, upGREAT HFA and 4GREAT.

Each cryostat uses a commercial low-frequency, 2-stage Pulse Tube Cold head (TransMIT PTD-406C).

The initial Phase 1 “pathfinder” airborne cryocooler system developed for the upGREAT LFA channel integrated a single, gimbal-mounted, air-cooled Sumitomo helium compressor (Model CSA-71A) along with a 400 Hz to 60 Hz frequency converter. For the Phase 2 cryocooler system, the Sumitomo compressor was replaced by two permanently mounted, independently controlled Cryomech CP2870 liquid-cooled compressors, each capable of driving a 2-stage 4K cold head. (Figures 5.6-1 and 5.6-2). The coolant is a mixture of de-ionized water and IceClear® HD, heavy duty, extended life, pre-diluted glycerin antifreeze.

The cryocooler infrastructure developed for GREAT is now an observatory mission system that is available for use by future instruments.

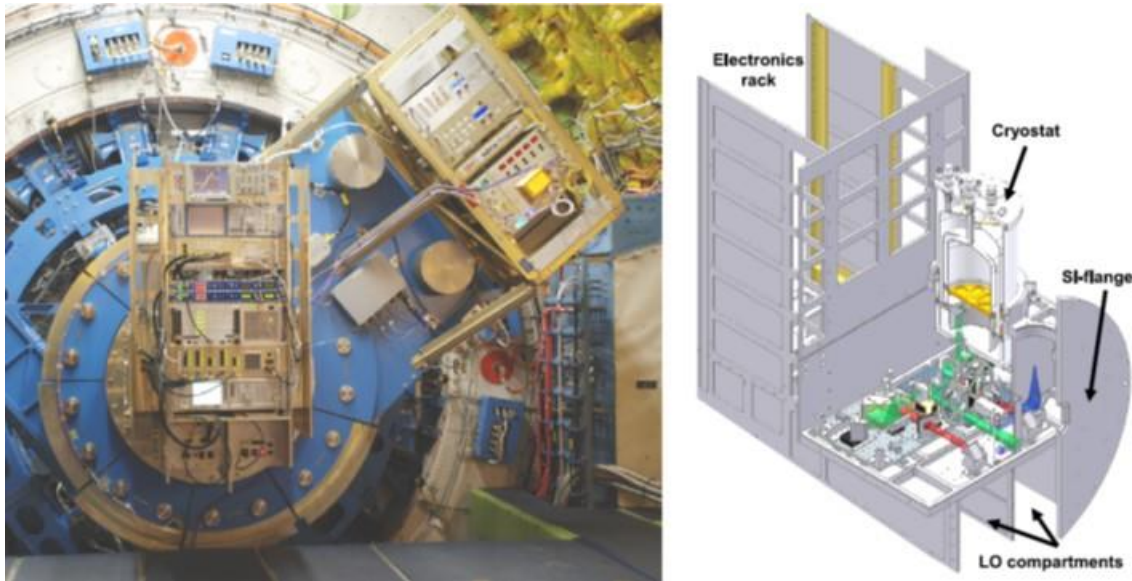


*Figure 5.6-1. Left: GREAT SI mounted to the Telescope Assembly (TA). Right: Cutaway view showing one cryostat. (Heyminck, 2018).*

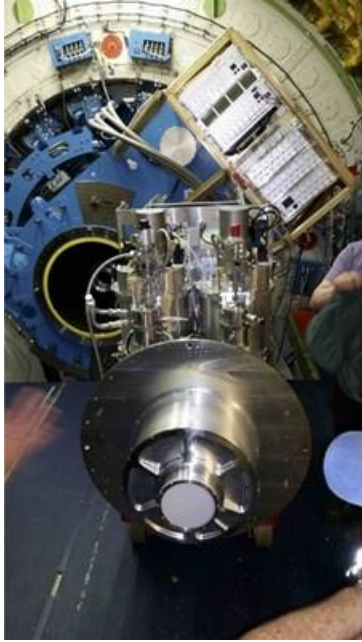


*Figure 5.6-2. Left: GREAT SI prior to mating with the Telescope Assembly (TA). Right: Two PT-cooled cryostats installed. (Heyminck, 2018).*



**Table 5.6-1. GREAT key information, including upGREAT LFA and HFA, and 4GREAT.**

<b>Instrument Overview</b>	
Instrument functionality	Dual-channel terahertz heterodyne receiver
Operating wavelength ( $\lambda$ )	63.15 – 611.8 $\mu$ m (0.490–4.747 THz)
Resolving power ( $R=\lambda/\Delta\lambda$ )	up to $R=10^8$
Cooling methodology	GREAT: LN <sub>2</sub> /LHe (Cryovac DE) – 4 channels L1, L2, M, H (decommissioned) upGREAT / 4GREAT: PT cooler (TransMIT PTD-406C) for 0.7W@4.2K
Nominal instrument temperature	4K
Detector/spatial resolution	GREAT: 4x single pixel waveguide-coupled hot-electron bolometers (HEB) upGREAT LFA: NbN HEB arrays: 2x7 pixel 1.88 – 1.93 THz Low Frequency Array upGREAT HFA: 1x7 pixels 4.7 THz High Frequency Array 4GREAT: 4x1 pixels centered at 0.43, 1.00, 1.37, 2.54 THz
Detector temperature	<4.5K
Operation time (cryogen hold time)	GREAT: 20h upGREAT: continuous (with 2x Cryomech Helium compressors on board the aircraft)

### **5.7 High-resolution Airborne Wideband Camera Plus (HAWC+)**

HAWC+ is the first sub-Kelvin instrument to fly on SOFIA. It employs an ADR built at NASA GSFC that reaches temperatures below 200 mK. The ADR is staged off of a nominally 1 K SR, which in turn is staged off of a 4 K LHe bath (Figure 5.7-1). Additionally, see Sec. 8.19 and Figure 8.19-1 for a thermal block diagram and a rendering of the layout of the <sup>4</sup>He SR and the <sup>3</sup>He heat switch on the LHe cold plate.

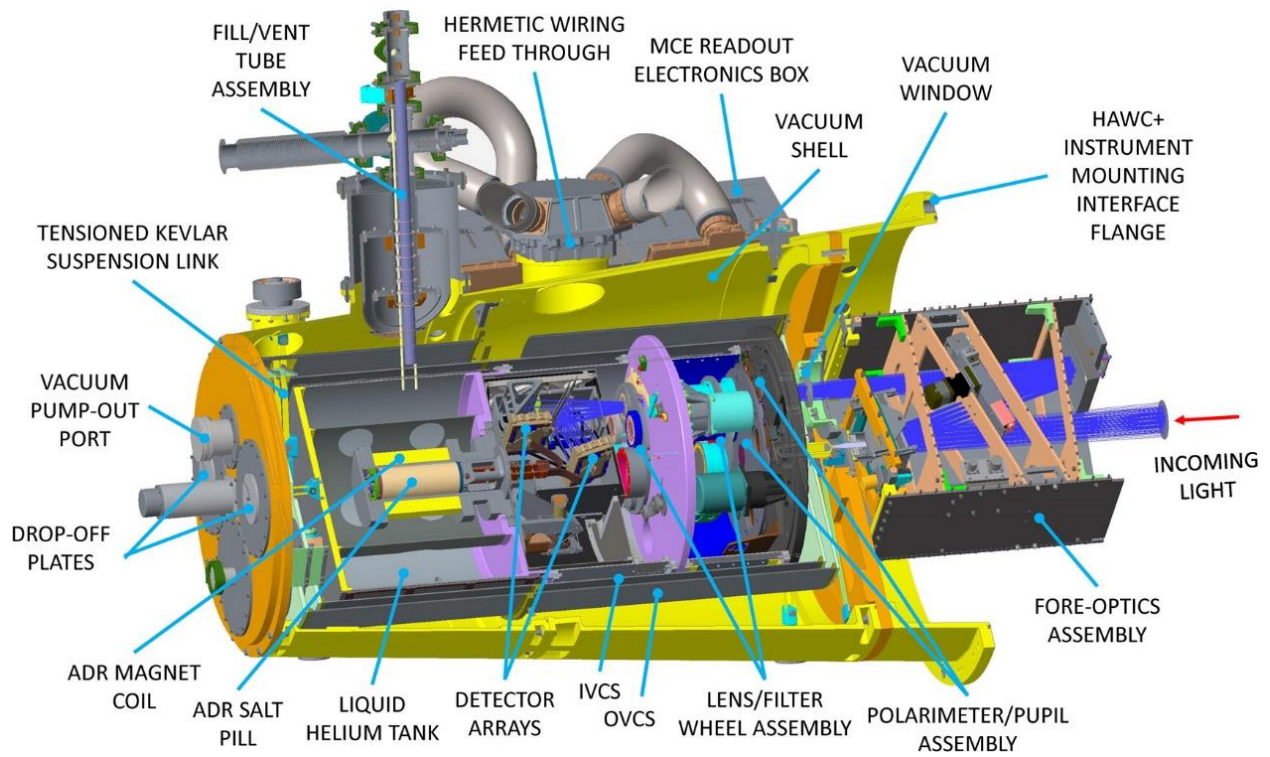


**Figure 5.7-1. Cutaway view of the HAWC+ SI. (Harper, 2018).**

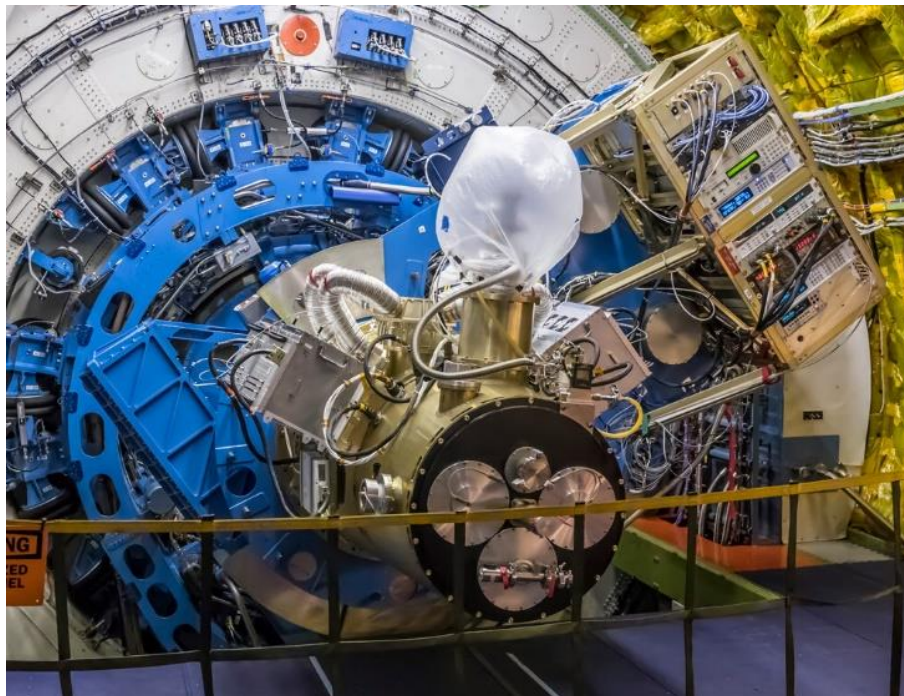


**Figure 5.7-2. HAWC+ mounted to the telescope assembly (TA) (Harper, 2018).**

**Table 5.7-1. HAWC+ key information.**

<b>Instrument Overview</b>	
Instrument functionality	Imaging camera and polarimeter
Operating wavelength ( $\lambda$ )	50 – 214 $\mu\text{m}$
Resolving power ( $R=\lambda/\Delta\lambda$ )	N/A
Cooling methodology	LHe (70 l tank), precooled by LN <sub>2</sub> Detector: closed-cycle <sup>4</sup> He sorption cooler (33 liters) and ADR with a 920g ferric ammonium alum (FAA) salt pill and 8T capable magnet (2T operational field).
Nominal instrument temperature	4.2K
Detector/spatial resolution	Transition Edge Sensor (TES) bolometers: 3x 32x40 pixel arrays: two for the reflective component and one for the transmitted component of linear polarization.
Detector temperature	<200mK
Operation time (cryogenic hold time)	~9h (ADR limited)

## 5.8 High Resolution Mid-infrared Spectrometer (HIRMES)

The HIRMES project was recently cancelled. It would have been the first fully dry sub-Kelvin SI. Its design is similar to that of HAWC+ in that it employs an ADR (this one built at High Precision Devices). However, the LN<sub>2</sub> and LHe baths were replaced by the first and second stages, respectively, of two PT refrigerators (Figure 5.8-1).

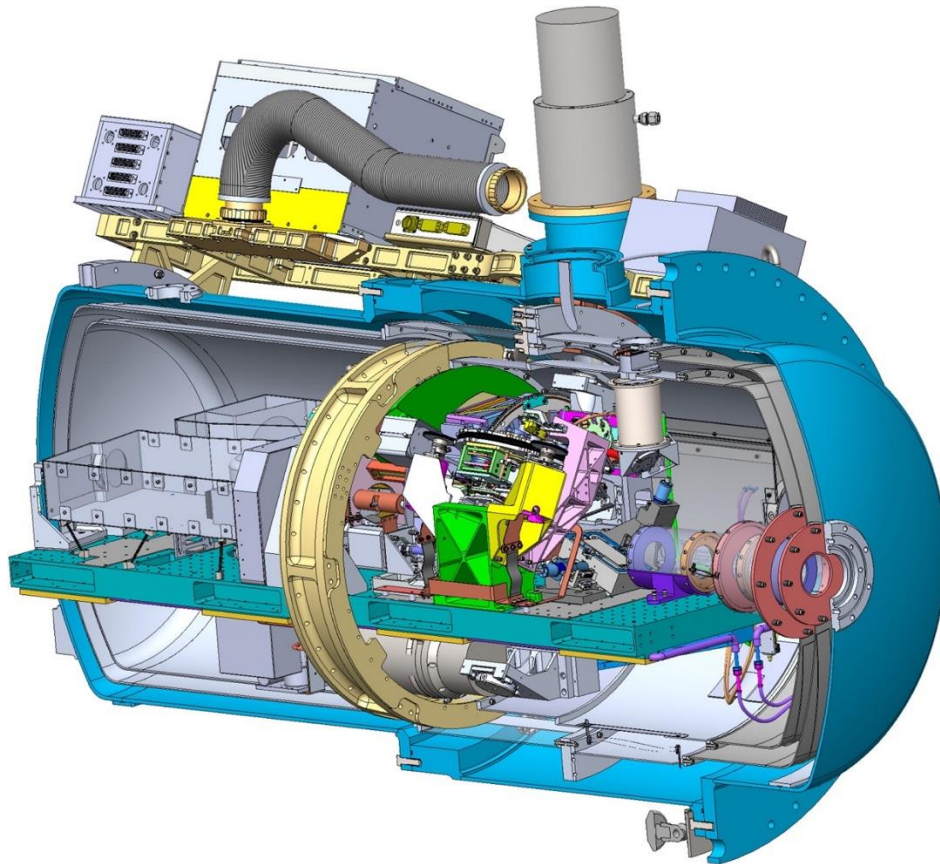


*Figure 5.8-1. Cutaway view of the HIRMES SI. (Richards, 2018).*

**Table 5.8-1. HIRMES key information.**

<b>Instrument Overview</b>	
Instrument functionality	High resolution spectrometer (dispersive grating combined with Fabry-Perot Interferometer tunable narrow-band filters (FPIs))
Operating wavelength ( $\lambda$ )	25 – 122 $\mu\text{m}$
Resolving power ( $R=\lambda/\Delta\lambda$ )	3 FPI driven spectral modes: high (100,000 – 50,000), medium (~12,000) and low (635 – 325) spectral resolution
Cooling methodology	2x PT cooler (TransMIT PTD-406C) Detector: $^4\text{He}/^3\text{He}$ and $^4\text{He}$ SRs with an ADR
Nominal instrument temperature	4K
Detector/spatial resolution	TES bolometers: low-resolution: 64x16 pixel array; high-resolution: 8 rows of 1x16 pixel array (wavelength optimized pixel size in each of the rows)
Detector temperature	<75mK
Operation time (cryogenic hold time)	>10h (ADR limited)

## 6.0 SI Environment and Constraints

### 6.1 SOFIA Operations

The SOFIA Observatory features a 2.7 m (unvignetted) Cassegrain reflector telescope integrated within an unpressurized, open cavity in the fuselage of a highly modified Boeing 747-SP aircraft. The 747-SP represents the “Special Performance” model of the 747, which is 48 feet shorter than the standard 747-100 but with the same engines, wingspan and fuel tanks, making it lighter and extending its range. In addition, the tail of the SP is taller and wider to compensate for handling changes associated with the shortened fuselage.

An added pressure bulkhead separates the unpressurized telescope cavity from the crew cabin, providing a comfortable “shirtsleeve” environment for the flight crew, mission crew and PI team/observers, as well as the SI.

SOFIA flight operations are normally based out of NASA Armstrong Flight Research Center (AFRC) Building. 703 (KPMD) in the Mojave Desert city of Palmdale, California, northeast of Los Angeles.



- Elevation: 2,543 feet (775 m) above Mean Sea Level.
- Ambient temperature extremes can range from 19 °F (-7.2 °C) or lower to 114 °F (45.6 °C) or higher.
- The average relative humidity is 65%.

Operations fly from remote sites for extended (2+ months) or much shorter “suitcase” deployments; for example, Christchurch, New Zealand (typically in the June ~ July timeframe).

## 6.2 Mission/Sortie Phases and Durations

The present nominal flight cadence is 4 flights per calendar week, each of ~10 hours duration.

A notional observing flight profile is shown in Figure 6.2-1. Note that the length of each observing leg is dependent on the observation, and that SOFIA is able to climb to higher flight levels as fuel is consumed.

There are currently discussions surrounding a proposed increase in cadence to 6 flights per calendar week, each of ~8 hours duration (programmatically impacts are now being assessed).

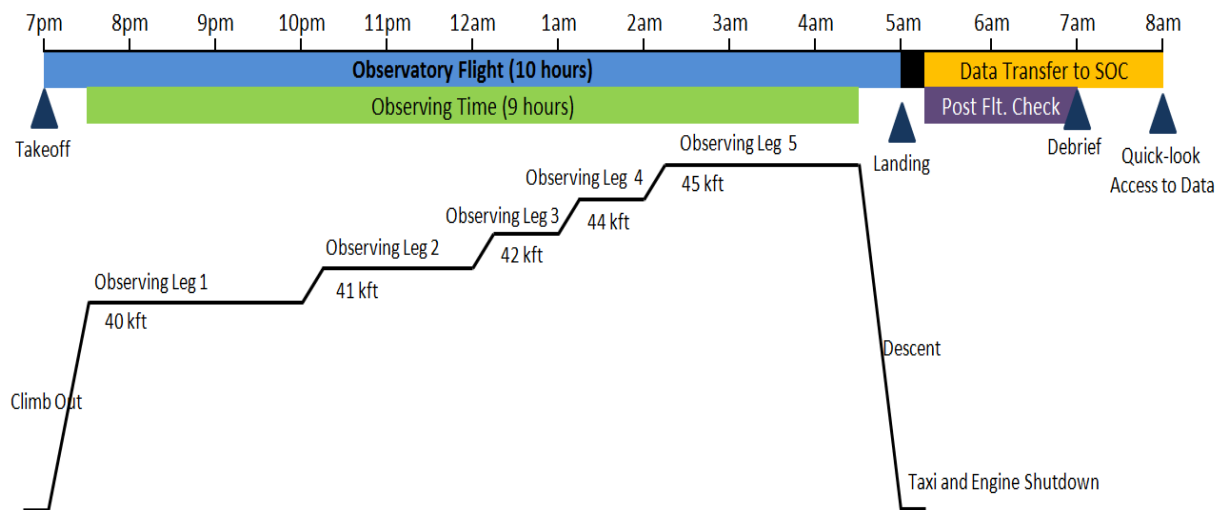


*Figure 6.2-1. Notional SOFIA observing flight profile.*

## 6.3 Flight Preparation Timeline

Figure 6.3-1 shows a notional timeline of the week leading up to a typical observing flight.

An SI is subjected to a number of environments in preparation for a flight series and for each observing flight:

- Shipping / transportation from SI developer’s institution to AFRC B703, Palmdale, CA.
- SI lab / Preflight Integration Facility (PIF) @ AFRC B703.
- Installation / deinstallation aboard SOFIA.
- Hangar Ops.
- Line Ops.
- Preflight tow-out.
- Taxi and take-off.

- Flight.
- Landing and taxi.
- Parked on tarmac.

## Flight Preparation Timeline

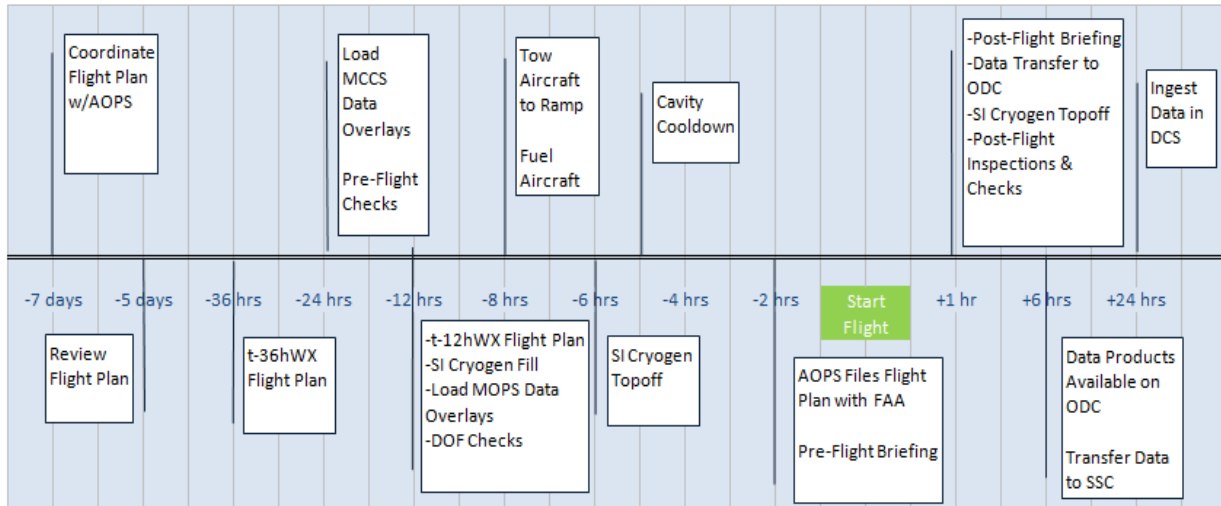


**Figure 6.3-1. Notional SOFIA flight preparation timeline.**

### 6.4 Typical Flight Timelines

Typical timelines for Day of Flight operations for observing flights, highlighting steps relevant to closed-cycle cooling technologies, are detailed in Figure 6.4-1.

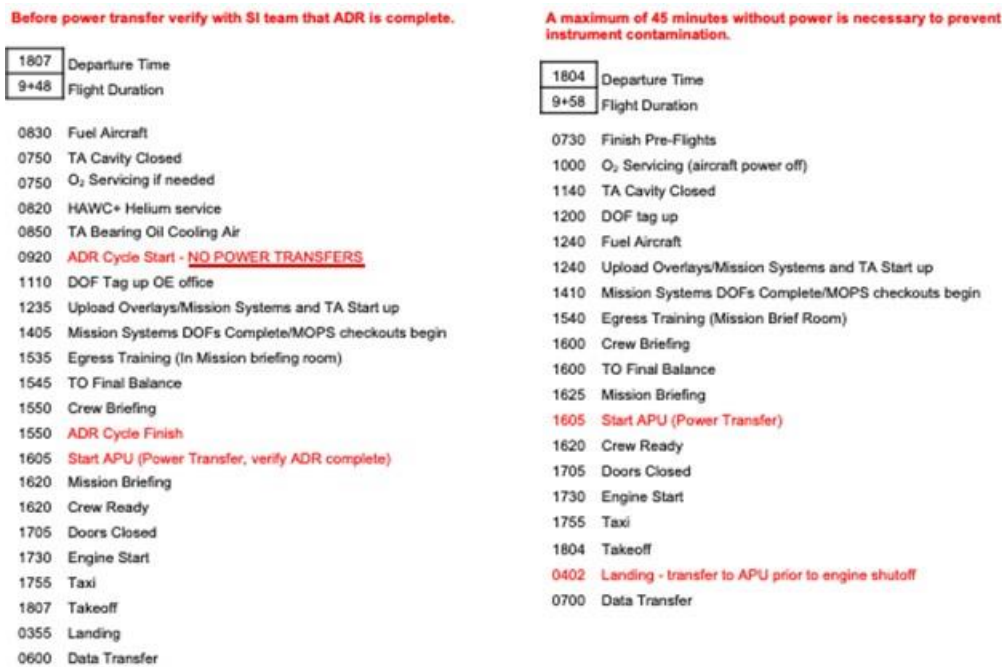


**Figure 6.4-1. Example Day of Flight operations for (left) an SI using LHe + ADR, and (right) an SI using PTs instead of LHe and LN<sub>2</sub>.**

## 6.5 SI Environments During Deployment

A SI must be built to survive the following four deployment environments:

1. “Dead-headed” (non-operational) transportation on shock-mounted SI Shipping Assembly in SOFIA Cargo Hold (or the cargo hold of a commercial aircraft). The cryostat is hermetically sealed when not mounted on the telescope assembly to protect against water vapor and other contamination. Ferry flights to remote deployment sites (e.g., Christchurch, New Zealand) may involve one or more stops and layovers for refueling and crew rest / change-out (e.g., Hickam AFB in Honolulu, HI).
2. Dead-headed transportation in the cargo holds of commercial aircraft. There have been times when the SOFIA Program has shipped a warm SI to or from a deployment site.
3. SI lab at deployment operations site (often more rudimentary than home facilities at AFRC B703).
4. Diversion to alternate landing sites (due to poor weather conditions at nominal deployment site). Alternate landing sites may not have necessary facilities/amenities to ensure 24/7 power and/or air conditioning support (i.e., power, AC carts). This could potentially jeopardize continuous SI cooling operations and therefore the near-term flight schedules.
5. Parked on tarmac. SOFIA typically does not have access to protected accommodations (e.g., a hangar) during deployments, and will generally be parked out on the tarmac exposed to the elements during the day between flights. Typically, SOFIA deploys to Christchurch, NZ in the ~June to August timeframe (i.e., during the southern hemisphere winter). As such, elevated cabin temperatures during extended ground operations on tarmac are generally not an issue during typical deployments, however shorter “suitcase deployments” to alternate sites (e.g., Daytona, FL) could potentially expose SIs to elevated temperatures for extended periods on tarmac.

## 6.6 Thermal Environments

The pressurized cabin of SOFIA, though usually described as a comfortable “shirtsleeve” environment for the crew (and installed SI), can subject the SI cryostat (and other equipment) to temperature excursions that can potentially impact SI performance.

The SOFIA Environmental Control System (ECS) is fundamentally the stock Boeing 747-SP ECS with some important modifications that affect cabin zone temperature controllability.

A custom Telescope Cavity Environmental Control System (CECS) has been developed and integrated to control the environment within the unpressurized telescope cavity and mitigate effects that could be detrimental to the telescope optics and observations – especially those associated with condensation on cold-soaked mirror surfaces during the observatory descent from the cold, dry stratosphere into the much more humid troposphere.

Some ECS air ducts have been blocked and others rerouted/redirected to address the fact that the “payload” of this 747 is quite different from that of a standard airliner accommodating hundreds of passengers with a highly dispersed heat load (typically SOFIA carries only ~15 to 25 people, but instead includes ~90 kVA of non-standard electrical loads associated with the observatory.



Efforts to improve the ECS cabin zone temperature control have had some success. However there remain certain operating conditions and constraints that challenge the ability to maintain “comfortable” temperatures in all locations. In particular, extended ground operations (in the hangar or especially on the tarmac during hot high desert daytime conditions while operating the onboard Cryocooler System) can test the limits of the ECS and available ground air conditioning cart(s).

## 6.7 Main Cabin Temperatures

An effort to survey and characterize the range of operational SOFIA cabin temperature conditions was undertaken in 2016. SOF-NASA-REP-SV03-2115, *2016 Cabin Temperature Characterization Results*, documents the temperature range in the portion of the SOFIA aft main cabin where the SI is integrated over a full year of flight and ground operations.

- The maximum recorded temperature in this area during 2016 was 83.7 °F (28.7 °C).
- The minimum recorded temperature in this area during 2016 was 57.0 °F (13.9 °C).

Typically, SOFIA main cabin temperatures are maintained within a tighter range but do tend to be cooler than some find comfortable during observing flights and can get quite warm during the day between flights.

The SOFIA Program has imposed the following SI environmental requirement, based on this cabin temperature survey, with some margin [ref. SOF-AR-SPE-SE01-2028D ParID 3.4.1]:

- SOFIA SIs shall be operable within the SOFIA main cabin with ambient temperatures ranging from 55 °F (12.8 °C) to 85 °F (29.4 °C).
- In the context of this requirement, “operable” means that the SI meets all functional, performance and safety / airworthiness requirements through the entire defined range of ambient temperatures.
- It should be noted that temperature excursions outside of this required temperature range are possible (e.g., when an SI is being transported to a remote deployment site in the cargo hold of SOFIA), but while permanent SI degradation or damage to components should be considered for such cases, SI operability (while meeting functional and performance requirements) need not be assured outside of this range.

## 6.8 Cargo Hold Temperatures

The temperature environment within the SOFIA Cargo Hold has not yet been well characterized (i.e., for SIs that are transported to / from remote deployment sites using an SI Shipping Assembly).

SOF-NASA-REP-SV03-2115, *2016 Cabin Temperature Characterization Results*, includes a section titled *Analysis of air temperature in the FLL* that references temperature measurements recorded in the Forward Lower Lobe (FLL) in 2014 as documented in SOF-DSI-REP-3131.0-0001\_R00, however it is not clear how representative this temperature range is for SIs within an SI Shipping Assembly loaded in the Cargo Hold.

- The maximum recorded temperature in the FLL was 98.6 °F (37.0 °C).
- The minimum recorded temperature in the FLL was 51.8 °F (11.0 °C).

It should be noted that there are no accommodations for providing power or compressed helium cryocooler interfaces to SIs or support equipment in the SOFIA Cargo Hold.

SI components that are susceptible to damage due to non-operational exposure to elevated temperatures (e.g., ADR salt pill, entrance window, etc.) may require measures to protect them from such exposure.

SIs that use expendable liquid cryogens (i.e., LN<sub>2</sub> and/or LHe) for “passive” cooling should also be aware that the hazard related to displacement of air by the cryogen evaporate in the confined volume of the Cargo Hold would need to be assessed and potentially mitigated before the SI can be transported in the Cargo Hold with liquid cryogens.

An O<sub>2</sub> monitor has been temporarily installed to support the transportation of the HAWC+ SI with some LN<sub>2</sub>.

## 6.9 SI Accessibility

SIs remain accessible to instrument operators and scientists aboard SOFIA within certain constraints, both while on the ground and while airborne.

SI Access on the ground: When SOFIA is parked (in the AFRC B703 Hangar or out on the flight line tarmac), access for SI operations and routine maintenance (e.g., cryogen fills) is generally available during nominal 1<sup>st</sup> and 2<sup>nd</sup> shift (Figure 6.9-1).

Certain aircraft operations require that non-essential personnel remain clear of SOFIA (e.g., refueling, O<sub>2</sub> refills, engine test runs, EMI / EMC testing, etc.).



*Figure 6.9-1. SOFIA parked on the tarmac.*

## 6.10 In-Flight SI Access

In-flight, SI equipment in the forward-facing bays of the PI Rack(s) are always accessible, though personnel must remain seated with seatbelts / harnesses during taxiing, take-off and initial ascent, approach and landing.

Access to the portions of the SI mounted to the Telescope Assembly (TA) (i.e., the SI assembly/cryostat and SI equipment in the Counterweight Rack (CWR)) is possible, within the constraints of APP-DF-PRO-OP02-2043, *Procedure for Crossing the TA Barrier during Flight*.

Per SOF-AR-SPE-SE01-2028, *SOFIA Science Instrument System Specification*, ParID 3.9.1: The design, operations and in-flight access of SOFIA SIs shall be consistent with the following operational constraints and limitations:

- Access to the SI Forward Side while the telescope is inertially stabilized and tracking (only those portions accessible with the TA Barrier raised).
- Access to the SI Top, Port and Starboard Sides to the flange while the TA is braked.
- Access to the Forward Side of the counterweight rack while the TA is braked at a nominal elevation of 20 degrees.
- Access to the SI Bottom Side while the TA is braked and caged.

While in flight, before proceeding aft of the PI Rack(s) and approaching the TA and SI, it is necessary to request access from the Mission Director (MD), who will notify and coordinate the request with the flight crew and safety technician aboard the flight.

SI equipment needed to support in-flight Control & Monitoring functions should be manifested within the PI Rack(s), where possible, to avoid the need for routine inflight access to the SI Assembly cryostat / CWR.

## 6.11 Availability of Electrical Power

The SI, the Cryocooler System, and Vacuum Pump System (VPS) are all powered by SOFIA Observatory Bus #4. This is by design, as it allows the SI and the observatory mission systems necessary to support the SI to be powered on a quasi-continuous 24/7 basis (i.e., between flights), while limiting the number of flight systems that need to be brought online. However, the 24/7 power provided for an SI is not ideal from the standpoint of SOFIA operations, even though it has been done. The preference is to power down the SI between flights.

Power to these systems is subject to transients and/or interruptions, planned and occasionally unplanned, such as:

- Relatively short transients, typically less than 1 second in duration (and often more likely to be on the order of milliseconds), such as those associated with the routine transfer of power from ground to aircraft power (and vice-versa) which must not damage the SI.
- Routine operational periods without Observatory power (e.g., during tow-out of aircraft from hangar to flight line in which the SI is typically without power for 30 to 60 minutes, or during servicing of flight crew oxygen which, when needed, results in a 10 to 20 minutes power interruption between flights).

- Relatively long power outages (i.e., “blackouts”) of up to several hours in duration, which may require an orderly shutdown to “safe” the SI.
- Unannounced application or restoration of power, which may indicate the use of a manually resettable contactor to protect sensitive electronics.

## 6.12 Electrical Power Interruptions

Per SOF-AR-SPE-SE01-2028, *SOFIA Science Instrument System Specification*, ParID 3.1.1, SIs shall be tolerant of such power transients, interruptions and reapplication without permanent functional or performance degradation.

For SIs that utilize the VPS or Cryocooler System, developers should also consider the likelihood that a power interruption may impact the nominal operation of these supporting observatory systems.

Further details regarding planned / routine power transients / interruptions and impacts to SIs that use the Cryocooler System may be found in APP-DA-PLA-PM17-2076, *Cryocooler System Concept of Operations (ConOps)*, Sections 2.4 and 2.5.

Typically, such SIs are transported cold from the Instrument Readiness Room (IRR) lab or Preflight Integration Facility (PIF) in AFRC B703 to the hangar floor and SOFIA for installation on the TA. In some cases, it is important that SI warm-up during transportation and installation be minimized (e.g., to prevent the high vacuum within the cryostat from degrading due to revolatilization of gases that have been condensed and cryotrapped on cold internal surfaces). SI transportation and installation procedures should be designed, and staffing pre-coordinated, to minimize the elapsed time between disconnections of the SI from the GSE cryocooler infrastructure in the IRR / PIF to installation and the interface of the SI to the SOFIA flight Cryocooler System so that active cooling can be resumed.

“Single-shot” SI refrigeration technologies that are sensitive to power interruptions (e.g., ADRs during pre-flight “cycling”) will require that Day of Flight timelines be carefully coordinated with SOFIA Aircraft Operations and USRA Mission Operations (MOPS) to ensure that there are no untimely power transfers or transients.

## 6.13 Electrical Power Distribution and Allocation

SOFIA SIs, as well as several observatory mission systems that directly support SIs, are provided power sourced from 400 Hz power from Observatory Bus #4. The power available to SOFIA SIs is converted from the 400 Hz native aircraft power via a combination of Uninterruptible Power Supplies (UPS), Frequency Converters (FC) and DC Power Supplies.

All of the power available to SIs is provided at the PI Patch Panel “doghouse” on the main deck, just aft of the PI Rack(s), from U401 receptacles J0, J1, J2 and J3, as defined within ICD SE03-2029 (MCCS\_SI\_05).

SIs distribute power within their PI Rack, and route it aft to the SI Assembly (cryostat) on the Telescope Instrument Mounting Flange (IMF) and to the Counterweight Rack (CWR) via the PI Patch Panel U400 and the TA Patch Panel U402, as defined within ICD SE03-036 (TA\_SI\_01).

A total allocation of 6.5 kVA is available for use by SIs in accordance with ICD SE03-2038 (GLOBAL\_POWER\_BUDGET). This 6.5 kVA is sub-allocated to the various individual power interfaces, as defined in ICD SE03-2029 (MCCS\_SI\_05) and summarized in Table 6.13-1 below.

It should be noted that the power needed to operate observatory mission systems, such as the VPS and the Closed Cycle Cryocooler (CCC) System, though sourced from the same Observatory Bus #4, is independent of the 6.5 kVA allocated to the SI.

The Cryocooler System is allocated 20 kVA for the operation of two helium compressors as well as the supporting liquid coolant loop pumps, heat exchanger fans, instrumentation and controller.

Power needed to operate the SI Cold Head(s) (e.g., PT rotary valves, etc.) must be provided by the SI from its 6.5 kVA allocation, per ICD SE03-2066 (CRYO\_SI\_02).

**Table 6.13-1. Sub-allocation of the total allocation of 6.5 kVA available for SI use.**

Type of Power	Maximum SI Power
230 VAC, 50 Hz, Uninterruptible Power Supply (UPS)	1 kVA
115 VAC, 60 Hz, Frequency Converter (FC)	3.5 kVA
115 VAC, 60 Hz, Uninterruptible Power Supply (UPS)	2 kVA
28 VDC, Uninterruptible Power Supply (UPS)	84 W

## 6.14 Power Gear, Quality, and Overcurrent Protection

Additional information on the SOFIA Observatory power source equipment upstream of the SI power interfaces, including identification of the specific UPS or FC, power quality specifications, and overcurrent protection devices is presented in Table 6.14-1. Note that the UPS Backup Times reported are based on power loads higher than the power allocated to an SI via ICD SE03-2029 (MCCS\_SI\_05) and are considered conservative.

**Table 6.14-1. Additional information on the SOFIA power source equipment.**

U401	Voltage	Freq.	Power	Source Device	Device MFR + P/N	Voltage Stability	Freq. Stability	Total Harmonic Distortion (THD)	UPS Backup Time (min) @ load	CB Rating	CB P/N
J0	230 VAC	50 Hz	1 kVA	UPS C	Nova GRS11-5K50-115/200-230-10012	±3% of 230 VAC	±1.5% of 50 Hz	5% max	8 minutes (min) @ 5 kVA	25 A	MS25244-25 or #3TC7-25
J1	115 VAC	60 Hz	3.5 kVA	FC 5	Unitron PS-94-444-29B	±1% of 115 VAC	±0.1% of 60 Hz	1.5% typ. / 2% max.	N/A	35 A	MS25244-35
J2	120 VAC	60 Hz	2 kVA	UPS D	Falcon ED4-5000RM-3/1-6-CIS	±3% of 120 VAC	±1 Hz	3% max. linear load 5% max. non-linear load	10 minutes (min) @ 3 kVA load	25 A	MS25244-25
J3	28 VDC	DC	84 W	28VDC Bus 4 (UPS)	Acumentrics ACG2500-282K	±5% of 28 VDC	N/A	N/A	8.5 minutes @ 2 kW load	5 A	MS25244-5

## 6.15 SI Mass and Volume Constraints

The mass of SOFIA SI elements are allocated and constrained as stated in Table 6.15-1.

The center of gravity (CG) of the SI Assembly and CWR, and the overturning moment of the PI Rack equipment payload, are also constrained within the referenced Table 6-15-1 ICDs.

SI Assembly CG operational variations (i.e., change in CG over time due to depletion of expendable liquid cryogen, where applicable) is additionally constrained within SE03-037 (TA\_SI\_02).

Additional mass constraints on integrated SI + GSE Handling Carts due to aircraft floor loading apply.

**Table 6.15-1. Mass allocation and constraints of SI elements.**

SI Element	Mass Limit	Comments	ICD Reference
SI Assembly (Cryostat)	600.0 kg	All SI items mounted to TA flange	SE03-037 (TA_SI_02)
Counterweight Rack (CWR)	55.8 kg to 105.7 kg	Total SI equipment payload for CWR, including equipment mounting H/W, fasteners, cables, Electronic Interface Channels or ballast weights (not including 37.7 kg mass of CWR structure or 6.4 kg mass of CWR mounting hardware)	SE03-2027 (SI_CWR_01)  SE03-051 (TA_SI_05)
PI Rack(s)	272.7 kg	Total SI equipment payload for each PI Rack (not including ~29.1 kg mass of PI Rack structure itself)  136.4 kg payload / rack bay	SE03-2015 (SI_AS_01)

SOFIA SI physical envelopes are constrained as defined within ICD SE03-002 (GLOBAL\_09)—see Table 6.15-2.

**Table 6.15-2. SI volume constraints.**

SI Envelope	Comments	ICD SE03-002 Reference
SI Dynamic Envelope	Ensures that no portion of the TA, or any TA-mounted SI elements, will come within 101.6 mm (4.0 in.) of any static aircraft structures, over full range of TA motion. Also provides clearance for CWR support struts.	ParID 3.1 a., Figure 3.1-1A ~ D
SI Static / Servicing Envelope	Establishes a stay-out area for aircraft structures and TA components, to ensure adequate clearance for SI operations when mounted to the TA, including SI installation and removal and cryogen servicing of SIs.	ParID 3.1 b., Figure 3.1-2A ~ D
SI Installation Envelope	Ensures that the SI and associated GSE Handling / Installation Cart can be moved through the SOFIA B747SP Door 1L and aft along the reinforced aircraft main deck floor to the TA.	ParID 3.1 c., Figure 3.1-3A ~ C

## 6.16 SOFIA Cryocooler System

SOFIA 1<sup>st</sup> generation SIs were cooled by means of expendable liquid cryogens (LN<sub>2</sub> and LHe) to ~4.2 K. One 1<sup>st</sup> generation SI (FIFI-LS) uses the SOFIA VPS to lower the pressure in a LHe reservoir to effect a phase change through the lambda point to superfluid LHe-II, achieving detector temperatures of ~1.7 K.

Several of the newer channels for the GREAT SI (upGREAT LFA, upGREAT HFA, and 4GREAT) have adopted closed-cycle cryocooler (PT) technology. This allows the volume and mass previously required for liquid cryogens to be instead reallocated to detectors, mixers and read-out electronics. It also supports rejection of more heat than could be handled by LHe for the full duration of an observing flight (with necessary operational margins), allowing implementation of additional detector pixels.

The 3<sup>rd</sup> generation SOFIA SI (HIRMES) would have also used the SOFIA Cryocooler System infrastructure for its primary cryogenic cooling (to ~4 K), and additional refrigeration technologies (ADR, helium SRs) to achieve Focal Plane Array temperatures in the 70 ~ 80 mK range.

To support the cooling needs of newer SIs, the SOFIA Program has implemented a facility Cryocooler System comprising two modified COTS Cryomech CP2870 liquid-cooled helium compressors, capable of driving two SI-selected / SI-provided cold heads.

Cryocooler System-to-SI interfaces are defined within SOF-NASA-ICD-SE03-2066 (CRYO\_SI\_02).

Figure 6.16-1 is a panoramic photograph showing the SOFIA closed-cycle Cryocooler System installation located in the aft upper deck of the SOFIA observatory. The two grey boxes near the center of the image are the two modified COTS compressors. The blue inclined box is the Cryocooler System Upper Deck Control Panel with the Programmable Logic Controller (PLC)



and touchscreen Human Machine Interface (HMI). The black boxes and cable harnesses to the right are frequency converters and interface boxes used to convert ~20 kVA of 400 Hz, three phase aircraft power to 60 Hz, 3Ø power needed to operate the system.

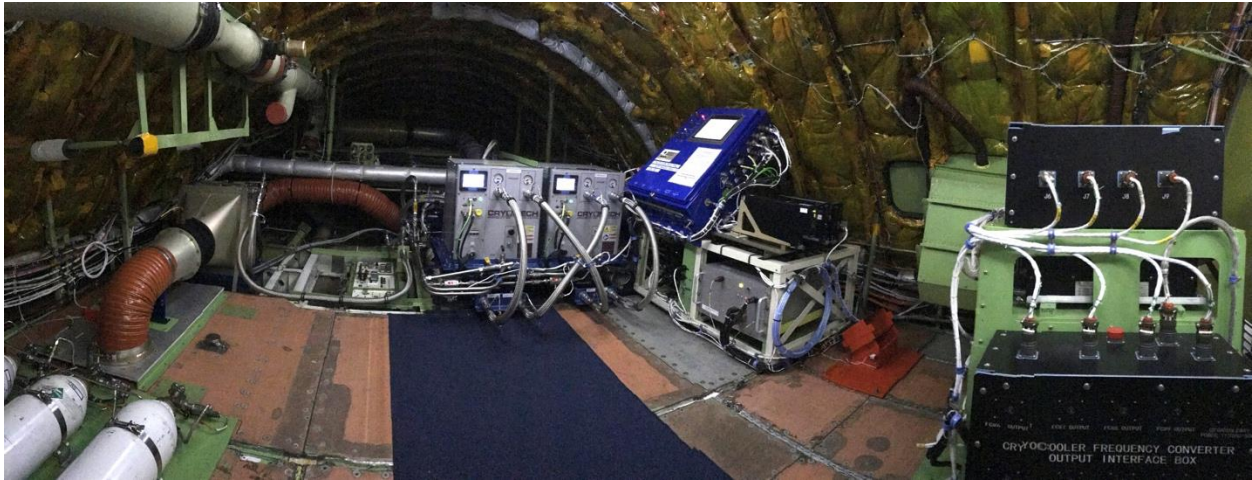


**Figure 6.16-1. Panorama of the aft upper deck of SOFIA where the Cryocooler System compressors (grey boxes) and other equipment are housed.**

The image on the left in Figure 6.16-2 shows two Supply/Return pairs of flexible pressurized helium lines routed through the Cable Load Alleviator (CLA) wrap to the Quick Disconnect (QD) SI interface patch panel. The image on the right shows the GREAT SI installed on the SOFIA telescope, with its two PT cooled cryostats / channels connected to the SOFIA Cryocooler System.

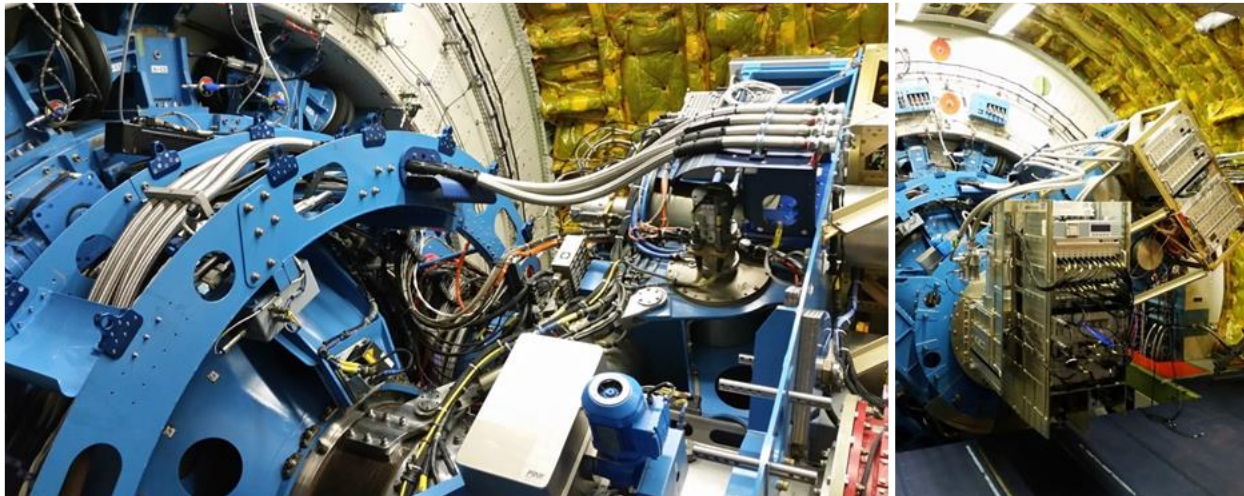


**Figure 6.16-2. Two pairs of pressurized helium flex lines connect the two cryocoolers with the compressors in the upper deck.**



## 6.17 SOFIA Cryocooler System Power Constraints

The SOFIA Closed-Cycle Cryocooler System has an allocated power budget of 20 kVA (220 VAC, 400 Hz, 3Ø aircraft power) for operation of the two Cryomech CP2870 liquid-cooled helium compressors and associated PLC controller, two control panels with touchscreen displays, liquid coolant pumps, liquid-air heat exchanger fans, instrumentation, and other miscellaneous equipment.

This system power budget excludes the power needed to operate the cold heads (e.g., PTC rotary valve motors), which must be accommodated within the SI power budget of ~6.5 kVA.

As described within APP-DA-PLA-PM17-2076, *SOFIA Cryocooler System Concept of Operations*, and SOF-NASA-ICD-SE03-2066 (CRYO\_SI\_02) Sec. 6, there are nominal lapses in power of varying durations during Day of Flight and pre-flight operations that should be anticipated and planned for:

A lapse of approximately 30 to 45 minutes is typical whenever SOFIA is towed between the hangar and the flight line. Generally, SOFIA remains unpowered from the time it is disconnected from the hangar “shore power” interface until it is connected to GSE ground power carts out on the flight line.

Flight crew breathing O<sub>2</sub> servicing between flights requires a power interruption, typically for 10 to 20 minutes.

SIIs that are particularly sensitive to such lapses (e.g., due to warm-ups that can cause the cryostat vacuum to “go soft”) may request an APU start-up and power transfer soon after SOFIA has cleared the hangar, which typically limits the aircraft tow-out power lapse to ~15 to 20 minutes. Such requests should be addressed to SOFIA Operations Engineering.

Power transfers between ground power, the SOFIA aircraft APU, and engine generator power are on the order of milliseconds and the SOFIA Cryocooler System is designed to handle these “bumplessly”. However, the aircraft engine start-up procedure requires bleed air from the already started engines that requires a Cryocooler System compressor shut-down for up to several minutes after taxiing to the runway and before take-off.

## 6.18 SOFIA Cryocooler System Dynamic Environments

### Compressors:

Due to the nominal “coordinated turn” dynamics of aircraft, the floor-mounted compressors do not experience significant effective tilt in the roll axis or quasi-steady accelerations in the lateral direction during flight. However, the accelerations experienced during taxiing, take-off and landing, and climb-out, and low frequency turbulence need to be considered.

During the development of the SOFIA Cryocooler System, the Cryomech CP2870 helium compressors underwent developmental tilt, vibration and simulated turbulence testing to demonstrate that they are able to withstand these dynamic flight environments without damage, oil-fouling of the helium, or performance degradation. In addition, the compressors, oil-mist adsorbers and molecular sieve filters are subject to regular inspections for any sign of damage or fouling, with conservative maintenance intervals.

## **Cold Heads:**

Though PT cold heads have advantages for astronomical instrumentation applications, they are more sensitive to tilting with respect to the nominal vertical orientation than GM cold heads due to the effects of gravity on natural convection.

Typically, the thermal performance of a PTC and helium compressor combination is specified / certified for operation in a nominal “vertical” orientation. Since the SI and cold heads are mounted to the SOFIA TA which has an elevation range from 20° to 60° (around the FWD – AFT “U” axis), it may be important to ensure that any degradation in thermal performance associated with tilt can be accommodated within the thermal performance margins of the SI.

## **6.19 Airworthiness Constraints**

Because closed-cycle Cryocooler Systems use pressurized helium gas as the refrigerant, they are considered to be Pressurized Vessels & Systems (PVS) and are subject to applicable codes and safety / airworthiness standards.

Per SOF-AR-SPE-SE01-2028, *SOFIA Science Instrument (SI) System Specification*, ParID 3.5.3.3.2 and Table 3.5-3:

Pressure vessels and pressurized lines and components of SOFIA SIs shall be qualified via Analysis, Inspection of Certificates of Compliance (CoCs), and undergo hydrostatic or pneumatic pressure testing to acceptance pressure levels based on the maximum normal operating pressure (MNOP) of each component and the applicable factor as defined in Table 3.5-3, *Qualification and Acceptance pressure test levels for cryogen reservoirs, other pressure vessels, lines and components*.

The MNOP for the SOFIA Cryocooler System is 400 psi, as established by Pressure Relief Valves (PRVs) protecting that system. Because the SI PTC(s) will warm up when disconnected and isolated from the Cryocooler System, the PTC must also be protected by a PRV certified to crack open @ 400 psi to relieve expanding He.

Pressurized lines and components shall be qualified to MNOP x 3.0 (MNOP x 4.0 for pressurized flexible lines), and each flight article shall be proof tested to MNOP x 2.0.

PRVs and pressurized flexible lines are subject to periodic inspections and recertification intervals (typically this involves periodically swapping out the PRVs for pre-certified flight spares, and then sending these out for refurbishment and recertification, while the flex lines need to be proof tested at MNOP x 1.0 (400 psi).

PTs shall be qualified to a test pressure of MNOP x 1.5 (600 psi) and each flight article shall be proof tested to MNOP x 1.0 (400 psi), with an additional required analysis showing positive Margin of Safety (MS) including a Factor of Safety (FS) of 4.0 (for tube diameters < 38 mm) or 2.5 (for tube diameters ≥ 38 mm).

Qualification-level (or “Burst”) testing is not generally required for COTS items with appropriate CoCs, but may be requested by the SOFIA SI Airworthiness Team (SIAT) if the design and/or fabrication details cannot be adequately substantiated.

## 7.0 Vibrational Environment with Design Guidelines

### 7.1 Objectives

The objectives of the following sections are:

- To present typical vibrational data acquired over several flights with various SIs.
- To establish a baseline vibrational model that SI designers can use to perform modeling or testing during the instrument development.
- To assist in assessing the ADR parasitic vibrational heating that can deteriorate SI detector sensitivity.
- To derive a set of basic guidelines for the SI mechanical design so the SOFIA vibrational environment is taken under consideration early in the design process.
- To discuss approaches to vibration isolation.

### 7.2 Telescope Assembly

The TA, as depicted in Figure 7.2-1, consists of (among many other elements) the mirror assemblies on the right (towards the rear of the aircraft); the mounting flange at the bulkhead on the left (to which the SI is bolted); and an empty Nasmyth tube between them.

The TA is equipped with an active vibration control system that isolates the TA from the aircraft bulkhead structure.

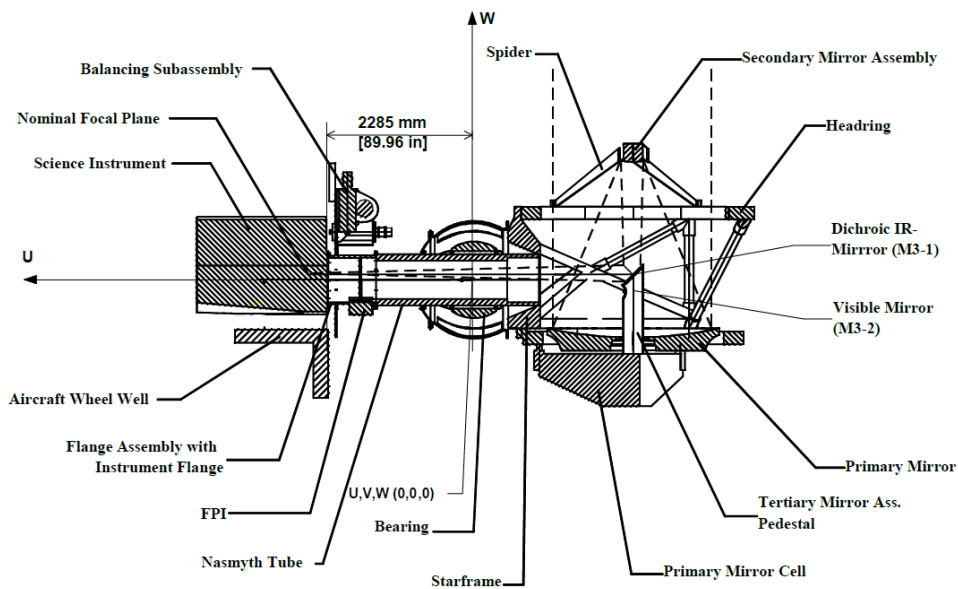


**Figure 7.2-1. The telescope assembly (TA).**

### 7.3 Sources of Vibration

The primary sources of vibration are:

- Flight induced vibration – engines, turbulent air flow and altitude (pressure/temperature) changes.
- When the TA cavity door and gate valve are opened:
  - Increase in turbulence due to the exposed TA cavity;
  - Acoustic resonance inside the telescope tube (“organ pipe” modes);
  - Effects of variable SI physical configurations and CG positions.
- Variable telescope elevation position.
- The TA’s dynamic stabilization and vibration control system is effective in attenuating frequencies above 100Hz.

### 7.4 Observation Segments

Various observation segments are referred to with respect to representative vibrational data to be presented in the following sections:

- A. Ground Segment - taxiing, takeoff, and landing; the TA is caged and braked. The TA door is closed and the gate valve is closed.
- B. Flight Segments:
  1. Aircraft climbing or descending, prior to or after the observation. The TA is caged and braked; the TA door gate valve are closed.
  2. Aircraft at the observation altitude. The TA door is opening; the TA is unbraked and the valve gate is open.
  3. Aircraft cruising at the observation altitude. The TA door is open; telescope is tracking; the dynamic stabilization system is active; the gate valve is open.

### 7.5 Acceleration Measurements

Data collected from various instruments is collated in Power Spectral Density (PSD) versus frequency plots. The focus is on vertical (Z) vibration measured at the SI tip (point 1) when the TA is in a normal observing mode (flight segment 3). The results represent vibrational responses of a complete TA+SI dynamic system which changes with every instrument.

Acceleration data were collected from accelerometers mounted at various positions on the TA and SI (see Figure 7.5-1).

*Note: New SI developers should use the data presented below with care when deriving tests or modeling random vibrational scenarios.*

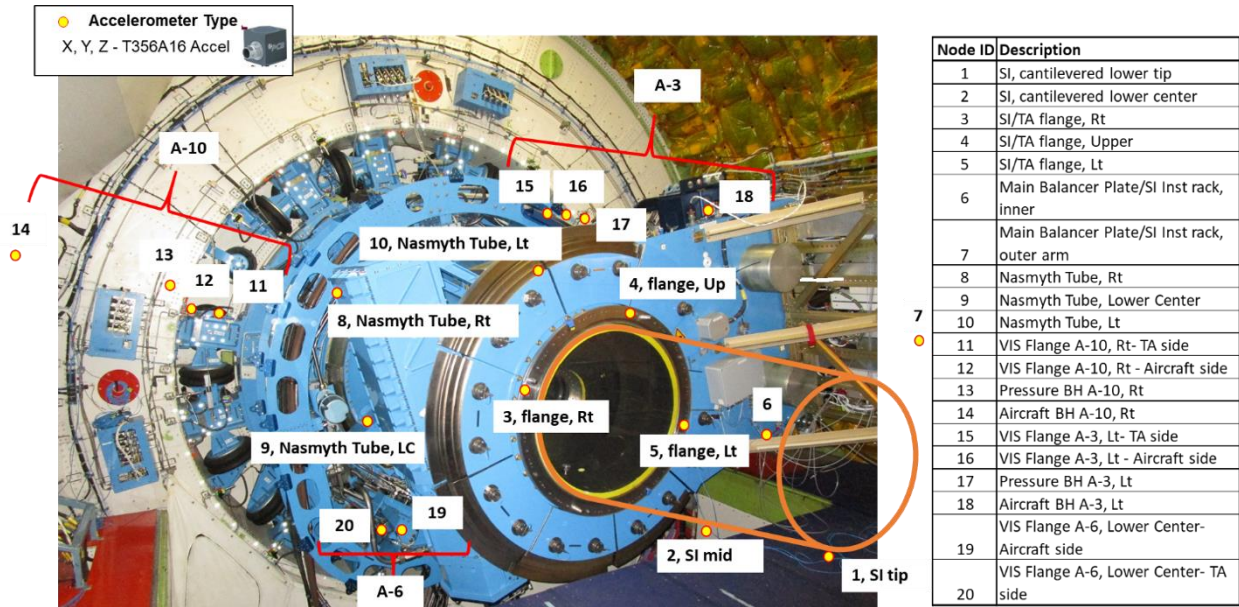


Figure 7.5-1. Accelerometer locations.

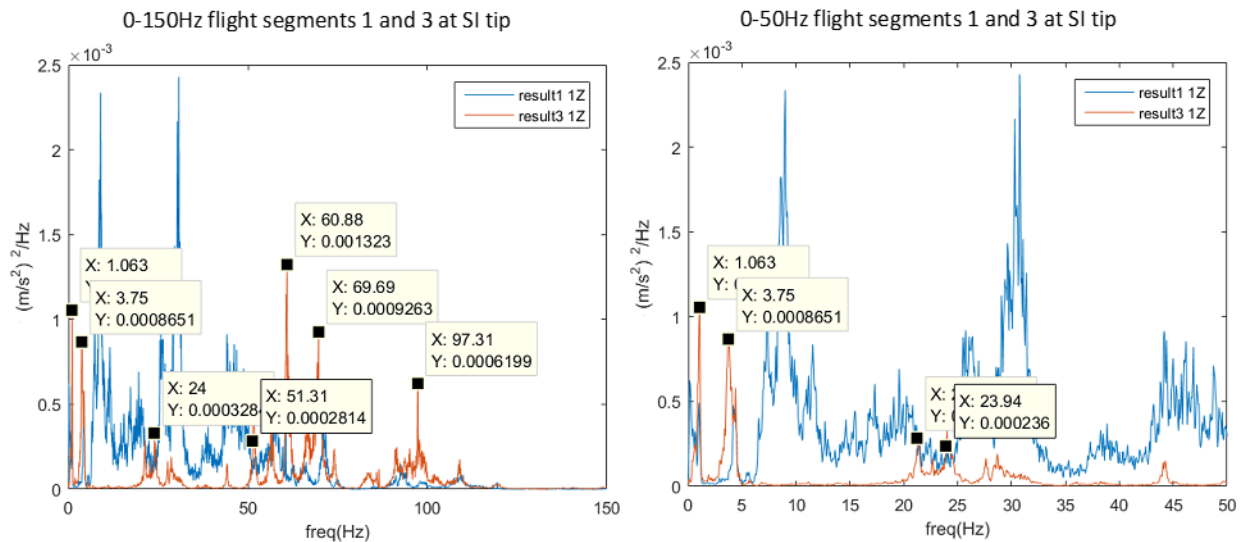
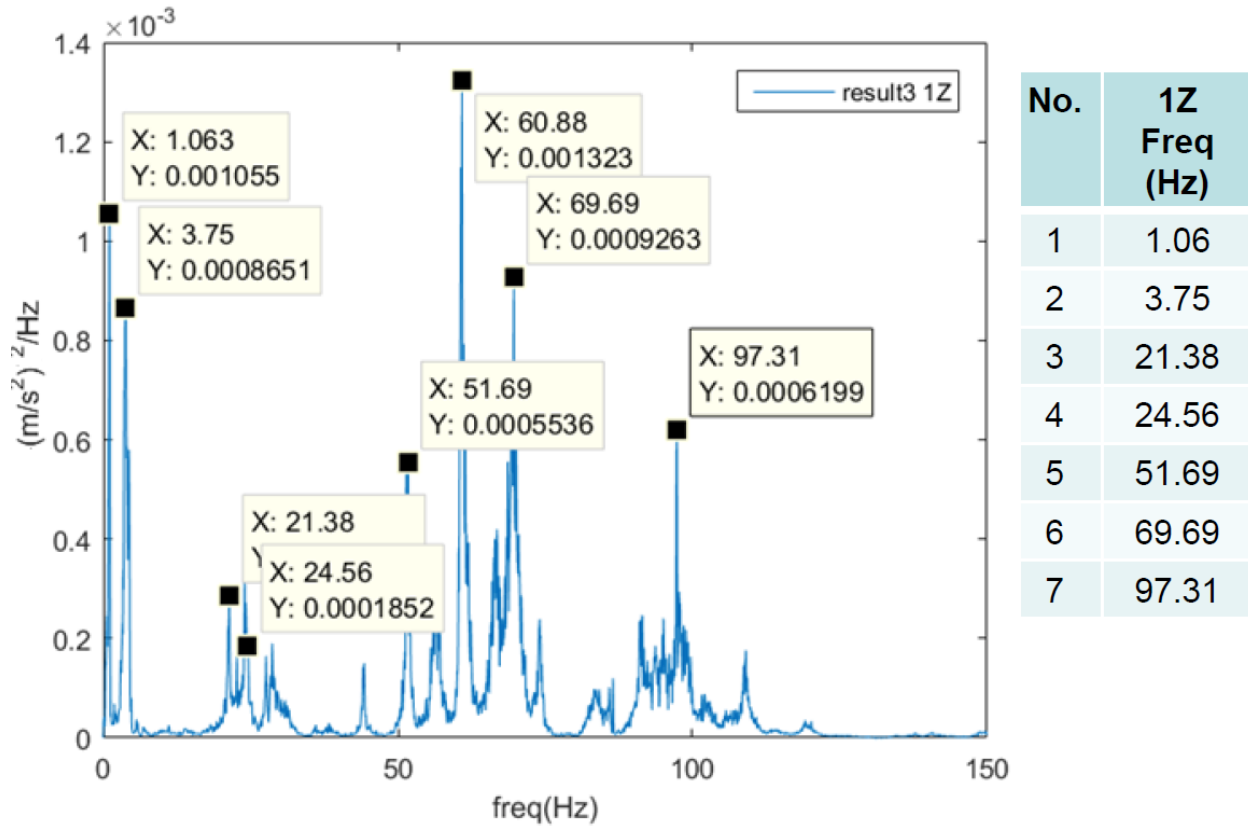


Figure 7.5-2. Vibrational data ( $a^2/\text{Hz}$  vs. Hz) from Flight 356 (HAWC+). Left: 0 – 150 Hz. Right: Same data, but from 0 – 50 Hz.

PSD plots for Flight Segments 1 and 3 from Flight 356 (HAWC+) are shown in Figure 7.5-2. Data were collected from the accelerometer mounted on the forward tip of the SI (Node 1 in Figure 7.5-1). For clarity, only data from Segment 3 is plotted in Figure 7.5-3. It is apparent that the active vibration control system attenuates most of the energy beyond 100 Hz. Below 100 Hz the SI developer must be careful to avoid resonant modes in the system, especially between 50 and 70 Hz. The peaks close to 1 Hz could be attributable to accelerometer accuracy drop (the sensitivity limit is at 0.5 Hz).

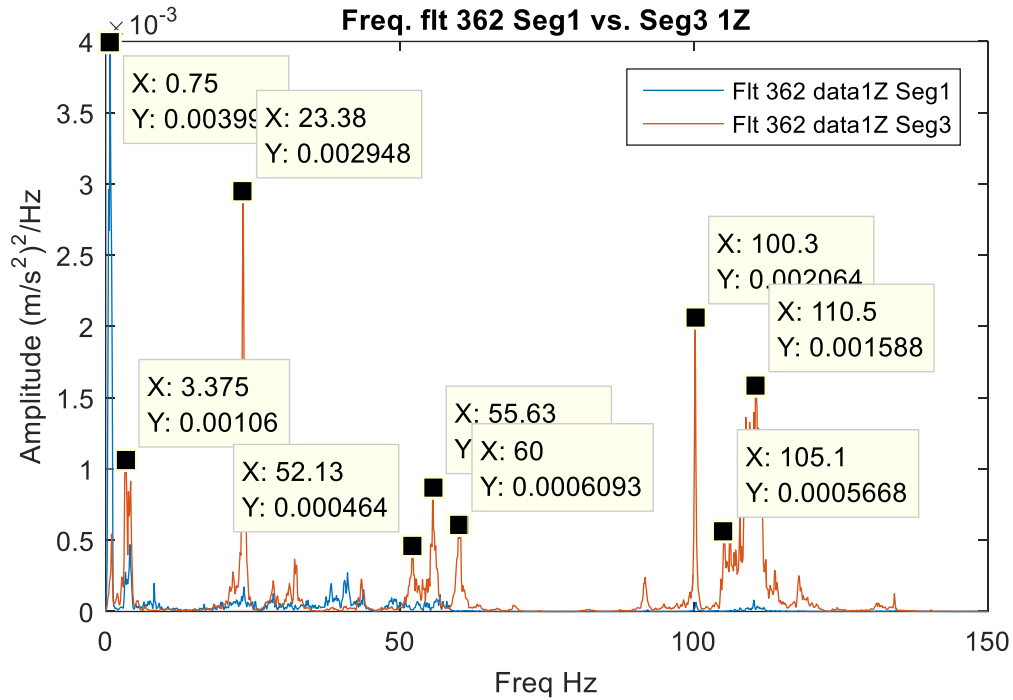


**Figure 7.5-3. A closer look at Flight Segment 3 from Flight 356 (HAWC+).**

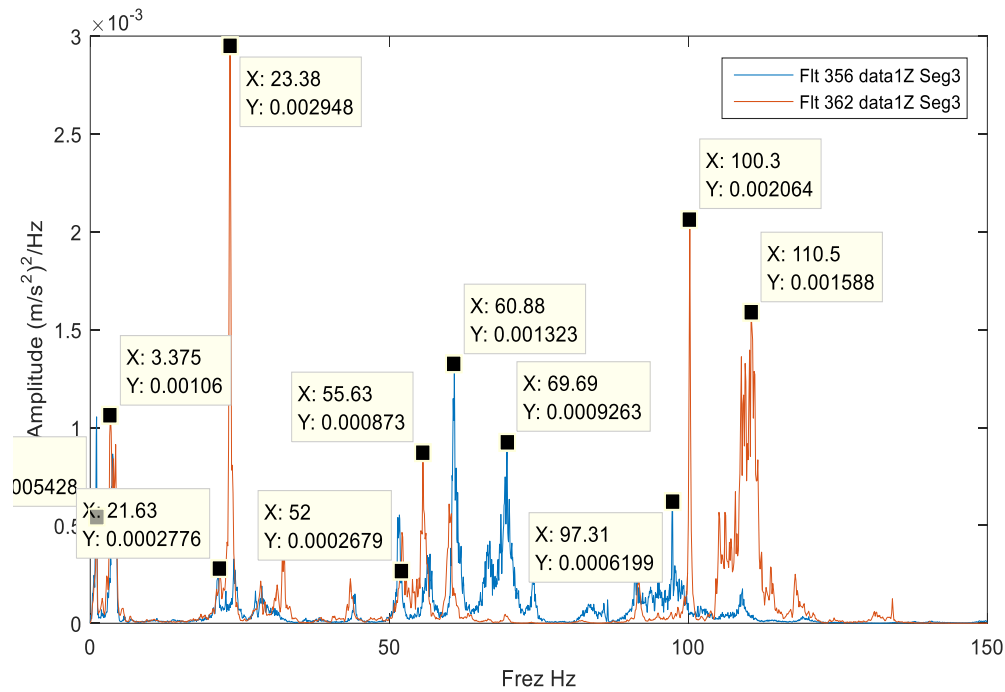
PSD data vary from flight to flight. Figure 7.5-4 shows data from Flight 362 (EXES), looking at the accelerometer at the SI tip, for Segments 1 and 3 (before and after the TA door is opened). There is much less Segment 1 vibration compared with Flight 356 (HAWC+). There is also a stronger 23 Hz resonance compared with HAWC+, possibly due to the differences in the physical configuration of the SI (EXES is longer and lighter while HAWC+ is more compact and heavier).

Figure 7.5-5 directly compares HAWC+ to EXES during Flight Segment 3, looking at the SI tip accelerometer.

Finally, measurements from Flight 380 (FORCAST), Flight Segment 3, are plotted in Figure 3.5-6, with and without turbulence.



**Figure 7.5-4. Flight Segments 1 and 3 from Flight 362 (EXES).**



**Figure 7.5-5. Flight Segment 3 from Flight 356 (EXES) and Flight 362 (EXES).**



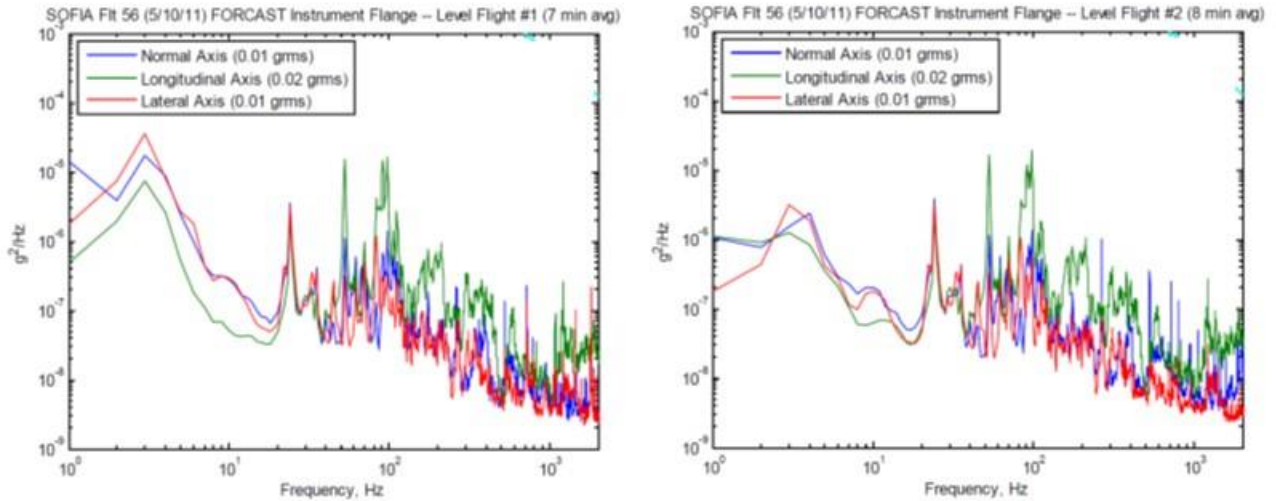


**Figure 7.5-6. Data from a 3-axis accelerometer mounted at the TA Flange for Flight 380 (FORCAST), Flight Segment 3, with high turbulence (left) and no turbulence (right). Acceleration measured in g's.**

## 7.6 Comparison with Test Standards

SOFIA mission systems are required to satisfy NASA and industry recognized environmental test standards: AFOP-7900.3-004 (DCP-O-018B) and DO-160.

DCP-O-018B has a mass loading reduction factor (-6dB) for items heavier than 160 lb. The standard is prescribed for electrical and electro-mechanical airborne equipment.

SOFIA SIs do not fall into the mission systems equipment category. Enforcing stringent vibration environmental test requirements on SOFIA instruments, particularly at the SI cryostat level, would likely be a significant technical risk to cryogenic opto-mechanical subsystems, as well as a significant cost and schedule driver. SOFIA SIs are exempted from vibration testing for airworthiness or flight certification but may opt to perform subsystem and/or component level testing and/or analysis, based on the characterized vibrational environment, for mission assurance reasons. SIs are required to demonstrate by analysis or better (e.g., environmental testing) that it will be structurally sound in flight and can survive crash loads.

In Figure 7.6-1 the environmental test standards are compared with SOFIA data. It is seen that even the 6 dB attenuated (0.78 Grms) PSD test curve is significantly more stringent than the worst measured SOFIA vibration.



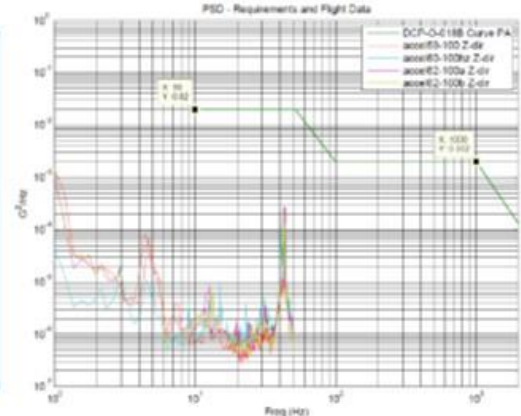
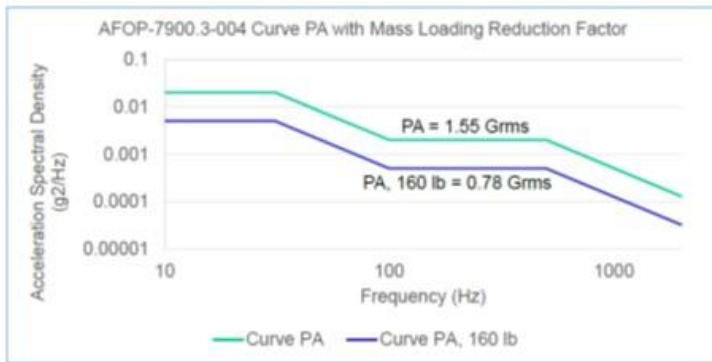


**Figure 7.6-1. Environmental test standards compared with SOFIA data. Acceleration measured in g's.**

## 7.7 Design Guidelines

The applicable standard tests could potentially limit the SI scientific performance and likely increase cost. However, the SI developers are encouraged to apply vibration testing at a sub-system or component level to increase the confidence in their computational models.

All aspects of optomechanical design must include vibrational loading and consider dynamic load effects. This is critical for the design and implementation of sub-Kelvin components (in terms of both structural integrity and vibrational heating), especially detectors and their cooling systems.

Some vital points:

- The vibrational input is at the TA flange and can be anticipated in a broad range between 1 and 100Hz.
- The cryostat design should effectively provide thermal and vibration isolation to the SI internal equipment.
- Every mechanical interface between 300K and the cold bench working temperature (usually ~4K) should be designed to act as mechanical low-pass filters.
- An ADR (or other very low temperature stage) suspension system should have its lowest natural frequency above 400Hz (at least 2 octaves above the highest input disturbance frequency).

## 7.8 Proposed Vibration Test Curve

The proposed test curve (Figure 7.8-1) envelopes most of the resonant peaks measured on SOFIA instruments. The key focus is on the spectrum between 1 and 100 Hz, which is not attenuated by the telescope active vibration control system.

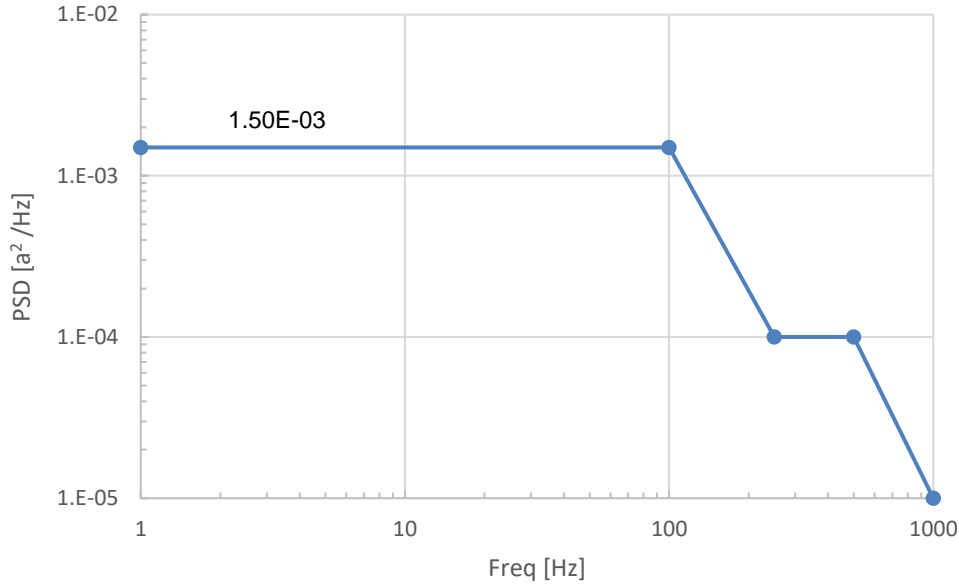


**Figure 7.8-1. Proposed vibration test curve.**

Only one peak (at ~ 25 Hz) has been recorded above the proposed test PSD level of 1.5E-3 a² / Hz (see EXES flight 362 spectrum). This can be addressed by performing a continuous or discrete narrow band sine wave sweep between 20 and 30 Hz at 3E-3 a² / Hz.

*The proposed test levels are significantly lower than the standard tests (DO-160 and DCP-O-018B).*

## 7.9 Approaches to Vibration Isolation

Vibrational heating of a component is given by (Shirron, 2019):  $P = K m g^2(f_0)$  Watts, where  $K = 24 \text{ W}/(\text{kg} \cdot \text{g}^2/\text{Hz})$  and  $g^2$  is the acceleration spectral density. If  $m \sim 0.5 \text{ kg}$  and  $f_0 \sim 100 \text{ Hz}$ , then (referring to the spectral density plots),  $P$  can be on the order of the gross cooling power of an ADR or other very low temperature stage (Figure 7.9-1).

$$m \ddot{x} + b \dot{x} + kx = F(t)$$

↑ Dissipation / Damping  
 ↓ Tuning  
 ↓ Passive Filtering & Active Vibration Control

**Figure 7.9-1. Schematic equation of motion of a cryogenic component showing the three approaches to vibration isolation.**

Vibrational heating can be mitigated by:

- *Filtering and active vibration control.* The active vibration control system dramatically attenuates vibration at the TA flange beyond 100 Hz. Moreover, the structure of the cryostat acts as a filter, and can further attenuate vibration. On HAWC+, spring washers were inserted at the Kevlar® suspension anchor point assemblies (Figure 7.9-2); this greatly reduced the vibration coupling between the TA flange and the optical bench (Harper, 2018).
- *Tuning.* Decreasing the mass and/or increasing the stiffness shifts the vibrational spectrum to higher frequencies, preferably to well beyond 100 Hz.
- *Damping.* In the end, the energy pumped into a resonant mode by the forcing function must either be dissipated in the component (through internal or joint friction), thus heating the component, or damped (dissipated at some higher temperature where the heating is more easily dealt with). HIRMES employs a magnetic eddy current damper (see Figure 7.9-3).

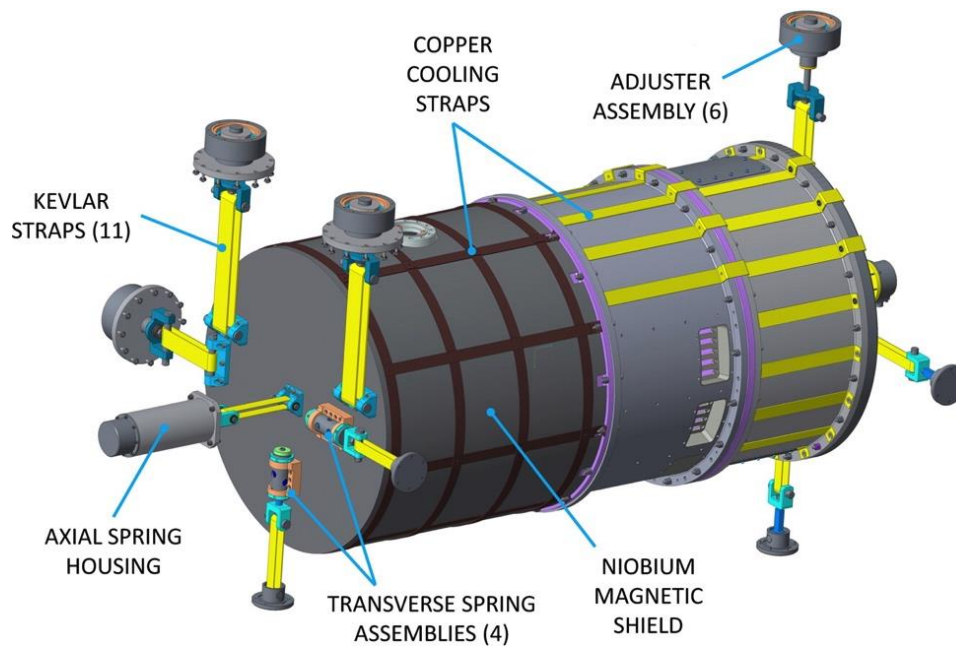


**Figure 7.9-2. HAWC+ suspension system.**

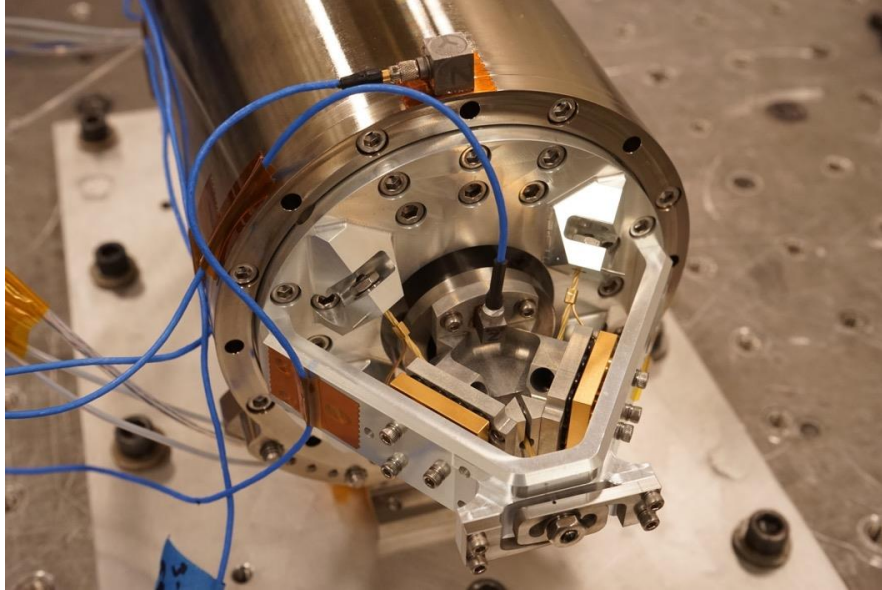


**Figure 7.9-3. HIRMES ADR (set up for modal testing) with magnetic eddy current damper. Vibrational energy would be dissipated at 4 K.**

A simple way to visualize this is to refer to Figure 7.9-1, which shows the equation of motion for a single degree of freedom:

- $x$  is the displacement of the component from its mechanical equilibrium.
- $m$  is the mass.
- The third term represents the restoring force.
- The second term represents dissipation.
- $F$  is the direct forcing function. It ultimately traces back to the TA via the cryostat structure. Everything in between acts like a mechanical filter, including the active vibration control.

Setting  $F = 0$ , and assuming that  $b$  is small, gives the normal mode frequency  $\omega_0 = \sqrt{(k/m)} = 2\pi f_0$ . Of course, an actual component, like an ADR salt pill, will give a spectrum of vibrational modes.

## 7.10 HAWC+ Lessons Learned

The HAWC+ cryostat was designed to reach a final operating temperature below 100 mK. Because of vibrational heating its operating temperature is closer to 200 mK. Following are some lessons learned (private communication with Charles D. Dowell, JPL).

1. Perform quantitative mechanical modeling (normal mode and forced vibration) of the instrument early in the project (e.g., preliminary design review).
2. Design in mechanical filtering (on HAWC+, springs in the 300 – 4 K suspension) to more effectively isolate the sub-Kelvin components from the TA flange.
3. Perform quantitative vibration testing during the instrument build.

## 7.11 HIRMES Design Example

The HIRMES cryostat design includes a double hexapod truss system (Figure 7.11-1) made of Ti-6Al-4V tubes and steel rod-ends with PTFE-lined spherical bearings.

The first natural frequency of the truss system is  $\sim 30\text{Hz}$ , causing slow rigid-body movements of the internal optical bench, while effectively rejecting most of the higher frequency disturbances.

At the second level, the optical bench has the first natural frequency (simple bending resonance) at  $\sim 150\text{Hz}$ .

At the third level the ADR and detector suspension systems are tuned so that the first natural frequency is greater than 400 Hz.

The remaining vibrational energy would be dissipated either through friction at mechanical joints, or by using eddy-current (magnetic) dampers at critical components (detectors, ADR, etc.).

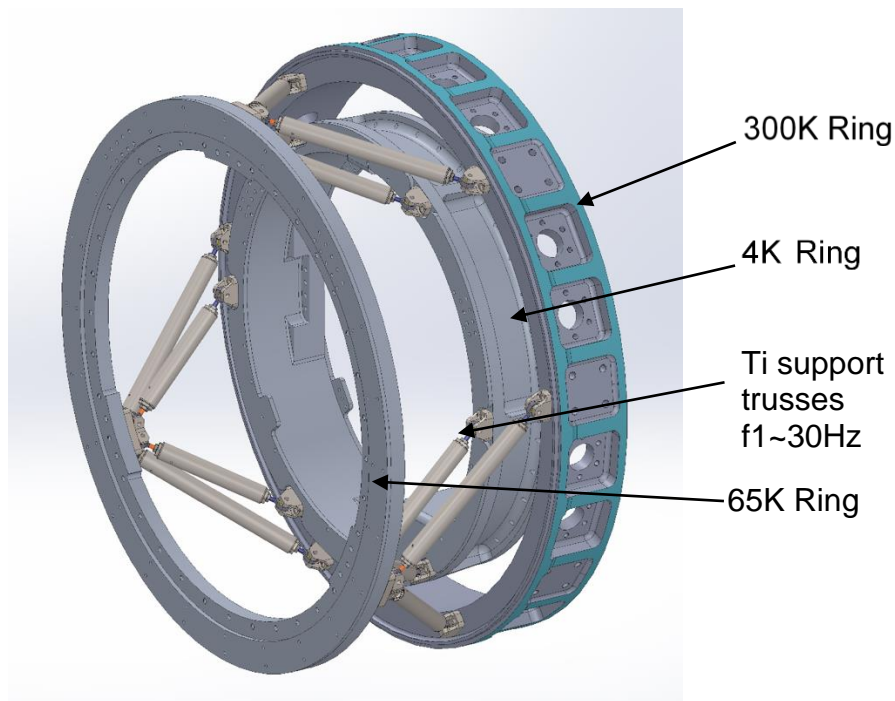


**Figure 7.11-1. HIRMES Ti-Truss System. (Richards, 2018).**

## 8.0 Cryogenic Technologies Available to SI Developers

### 8.1 Overview

The 1<sup>st</sup> generation of SOFIA SIs employed expendable liquid cryogenics, as in traditional cryostats.

GREAT introduced two-stage PT refrigerators, which eliminated the need for both the LHe bath and the LN<sub>2</sub> jacket, resulting in a “dry” cryostat.

HAWC+ introduced sub-Kelvin technologies (e.g., SR, ADR, <sup>3</sup>He gas gap heat switch).

HIRMES is the first dry sub-Kelvin SI, employing two PT refrigerators, <sup>4</sup>He and <sup>3</sup>He SRs, gas gap heat switches, and an ADR. It is expected to operate at ~ 80 mK.

*This section assumes the HIRMES approach—a dry cryostat based on commercial PT (or GM) refrigerators, and components that enable cooling to below 1 K and below 100 mK.*

The bulk of the following sections (Sections 8.2 through 8.29) discuss the operational characteristics and limitations of various refrigeration technologies available to the SI developer. These are summarized in Figure 8.1-1. Also discussed (Sections 8.30 through 8.36) are thermal switch and strap options.

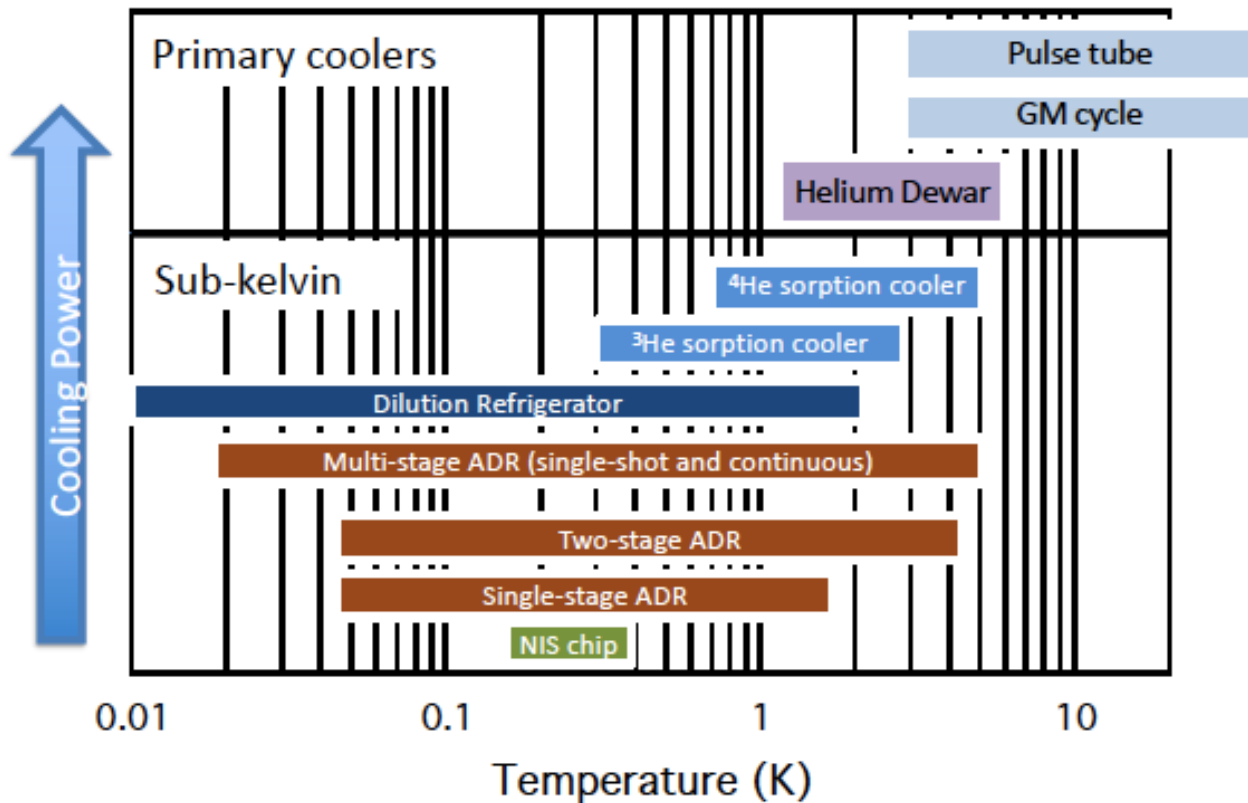


**Figure 8.1-1. Summary of refrigeration technologies available to SI developers.**



## 8.2 Pulse Tube (PT) and Gifford-McMahon (GM) Refrigerators

The SOFIA Cryocooler System can accommodate a wide range of PT and GM cold heads. Closed-cycle cryocooler cold heads are available in both single-stage and two-stage models. However, single-stage cold heads typically only achieve cryogenic temperatures in the range of ~10 to 20 K (Figure 8.2-1).

To achieve cryogenic temperatures that approximate a 4.2 K LHe bath, a two-stage cold head is required. The 1<sup>st</sup> stage of a two-stage cold head nominally approximates the temperature of a LN<sub>2</sub> bath (~77 K) or lower, depending on the heat load. It would typically be used to cool a thermal radiation shield enclosing the colder stage(s) and to intercept heat loads carried by support structures and wiring. The 2<sup>nd</sup> stage of a two-stage cold head can achieve temperatures of ~4 K or lower, depending on the heat load on both the 2<sup>nd</sup> and 1<sup>st</sup> stage heat sinks. It can be used to directly cool an instrument's sensors, as in GREAT, or to precool colder stages, as in HIRMES, which employed SRs (at ~ 1 K and ~ 0.3 K) and an ADR (at ~ 80 mK).

The thermal performance of a two-stage cold head is complex and has a large “parameter space” including compressor selection and power source (60 Hz vs. 50 Hz), helium line length and diameter (impedance and compliance), helium pressure, pulse frequency, and orifice tuning. In addition, the heat lift to the heat sinks on the 1<sup>st</sup> and 2<sup>nd</sup> stages are interdependent.

PT and GM cold heads are manufactured by companies world-wide, including TransMIT (Germany), Sumitomo (Japan, with US distributors), and Cryomech (US).

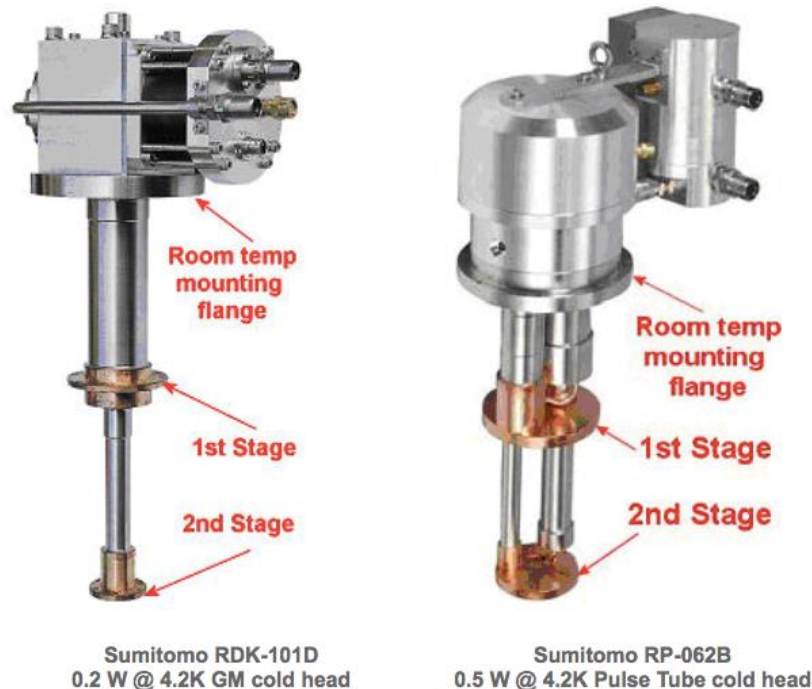


**Figure 8.2-1. Left: GM cold head; Right: PT cold head.**  
(Source: [www.janis.com](http://www.janis.com))

The PT has no moving parts, except at room temperature, while the GM has a cold displacer as in a Stirling cooler. Many PT coolers offer an optional configuration in which the motor-driven rotary valve is connected to the rest of the cold head only via a flexible He line, allowing it to be shock-mounted and mechanically isolated from sensitive optical elements. It is often suggested

that the displacer introduces reliability issues, but in practice both types are highly reliable and require little maintenance unless contaminated, as with oil from the compressor. The installed Cryomech compressors have been modified to minimize that possibility.

For the SI developer, there are three main differences:

- *Cost*: A GM cold head tends to be considerably less expensive.
- *Dependence on orientation*: The GM cold head is insensitive to orientation (i.e., tilt); the PT's performance depends strongly on orientation, especially beyond  $\pm 20^\circ$  from vertical (see Sec. 8.4).
- *Vibration*: There are three sources of vibration: the room temperature motor/valve assembly; pulsating helium in the thin-wall tubing; and the cold displacer (GM only).

A number of investigators have measured the acceleration or displacement of GM and PT cold heads. Most have looked at mechanically unloaded cold heads, whereas loading with dummy masses might yield more informative data (Figure 8.2-2).

The displacement spectral density plots at right are from a study (Tomaru, 2004) comparing two Sumitomo 4 K cold heads, one a GM and the other a PT. Note, "Cold Stage" refers to the 2<sup>nd</sup> stage cold heat sink; and "Cold Head" refers to the warm motor housing that is bolted to the outer shell of the cryostat. The peak at  $\sim 1$  Hz is the oscillation frequency of the helium.

Generally, it can be assumed that the vibration levels in a GM are 5 to 10 times higher than in a PT of comparable capacity.

Nevertheless, GM refrigerators have been successfully used for ground-based astronomy applications and therefore should not be dismissed out of hand.

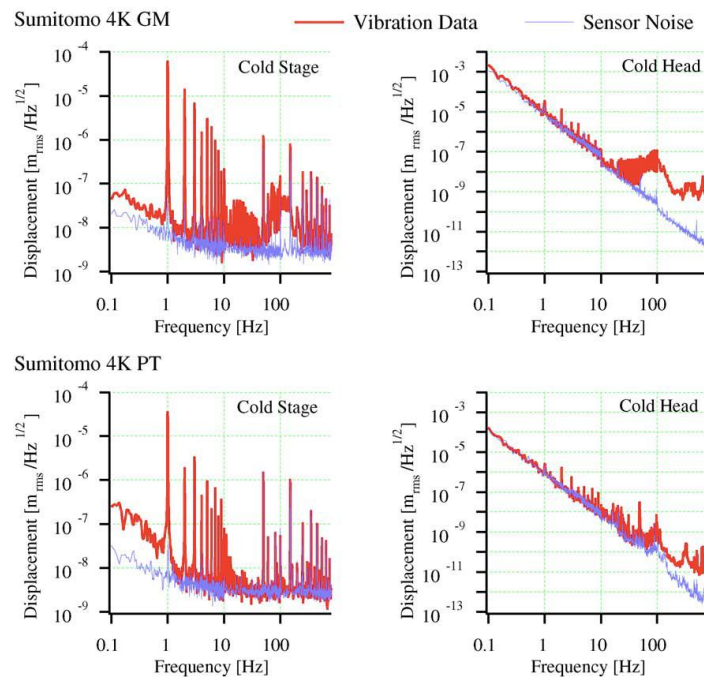


**Figure 8.2-2. Comparison of vibration levels in comparable GM and PT cold heads. (Tomaru, 2004).**



### 8.3 Example: Cryomech PT407-RM PT Refrigerator

Figure 8.3-1 shows drawings of the Cryomech PT407-RM PT cold head, along with helium flex lines and two compressor options. Two liquid cooled CPA2870 compressors and two sets of flex lines are installed on the SOFIA aircraft as part of the SOFIA Cryocooler System (see Sec. 6.16).

The cold head employs a remote motor assembly, which reduces vibrational input at the cold head mounting flange on the cryostat. Cryomech cold heads have not been used on SOFIA, but the PT407-RM is more or less equivalent to the TransMIT PTD-406C (see Sec. 8.4) which cooled the GREAT instruments.

Figure 8.3-2 is the nominal performance map, which shows the inter-relationship between the two stages.

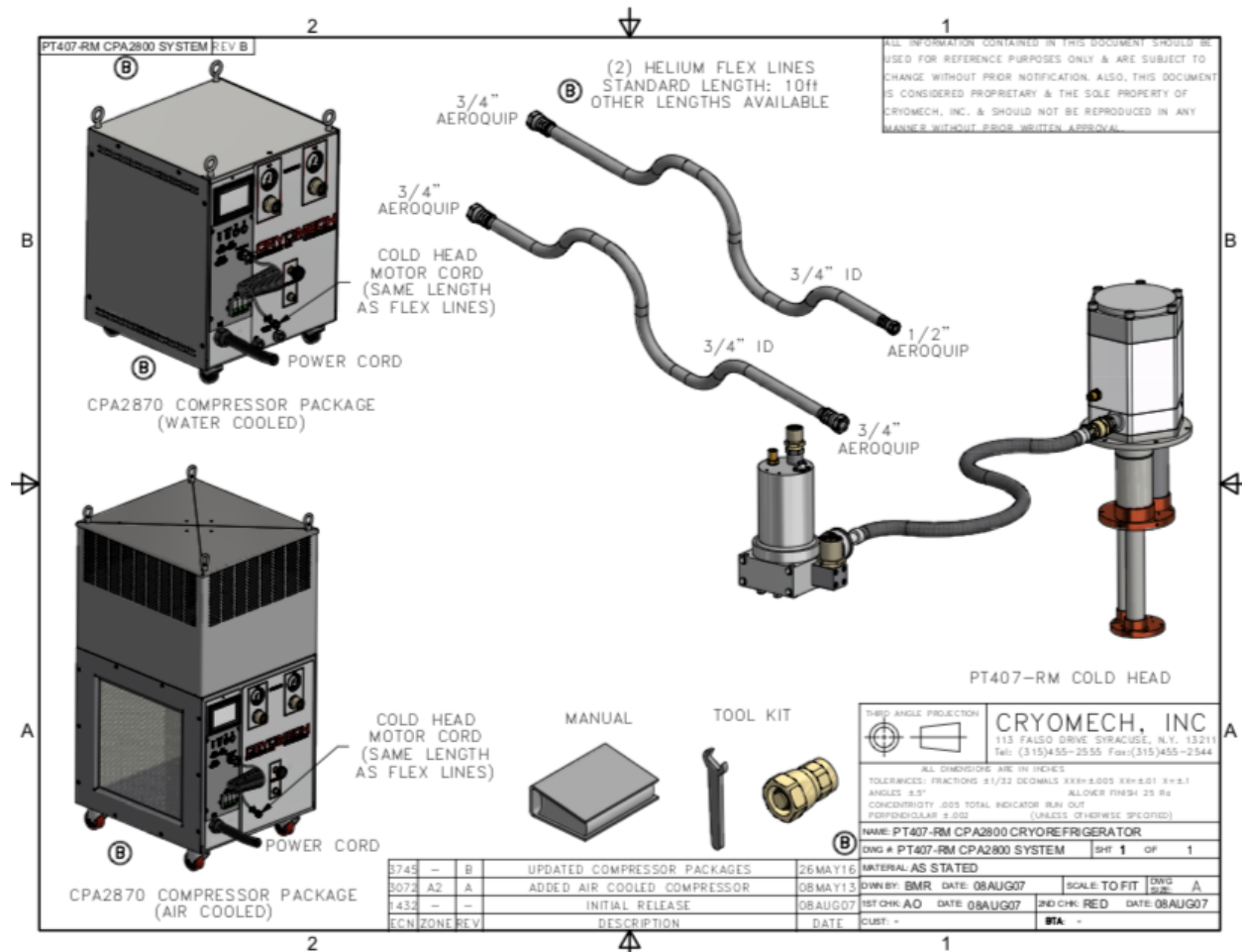
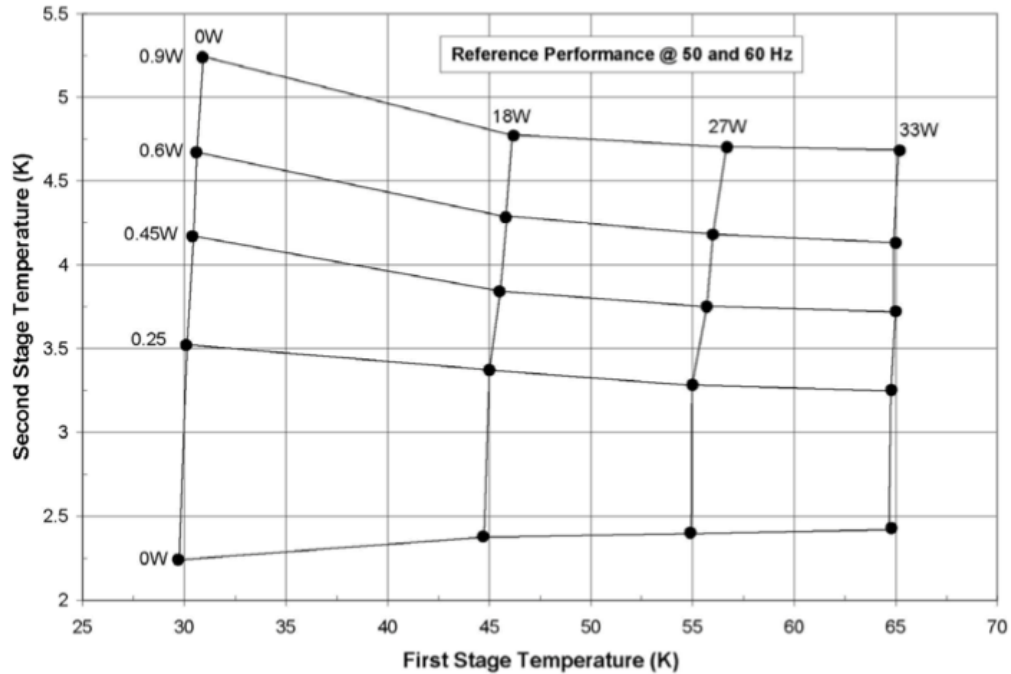


Figure 8.3-1. Drawings of the Cryomech PT407-RM cold head, flex lines, and compressor options. (cryomech.com).



**Figure 8.3-2. Performance map for the two-stage Cryomech PT407-RM PT refrigerator.**

### 8.4 Example: TransMIT PTD-406C PT Refrigerator

The TransMIT PTD-406C is used by the GREAT instruments and would have been used for the canceled HIRMES.

The GREAT team opted to work with the German company TransMIT to produce PT cold heads properly tuned to Sumitomo air-cooled compressors (selected for the Phase 1 Cryocooler System, before the dedicated liquid cooling loop was installed).

The HIRMES team elected to use the TransMIT cold heads because of their flight heritage. This somewhat simplified the airworthiness certification of the SI.

**Table 8.4-1. Key specifications of the TransMIT PTD-406C PT.**

Minimum temperature at 2 <sup>nd</sup> stage	< 2.4 K
Cooling power 2 <sup>nd</sup> stage	≥ 0.75 W @ 4.2 K
Cooling power 1 <sup>st</sup> stage	≥ 20 W @ 45 K
Cool down time to 4.2 K	< 75 minutes (no additional heat load)
Length of split line to rotary valve	75 cm
Weight of cold head with rotary valve	20 kg without vacuum vessel and radiation shield
Frequency controller for rotary valve mains supply	220 V / 50 Hz, ≤ 40 W el. power consumption

Because of gravity-driven convection in the PT, performance degrades as the cold head is tilted from its optimum vertical orientation. This effect was measured by the HIRMES team at NASA GSFC (Figure 8.4-1). In operation, the orientation will vary from -20° to +20°, as indicated by the vertical dashed lines.

During thermal testing, the PTs are run at 20° tilt.

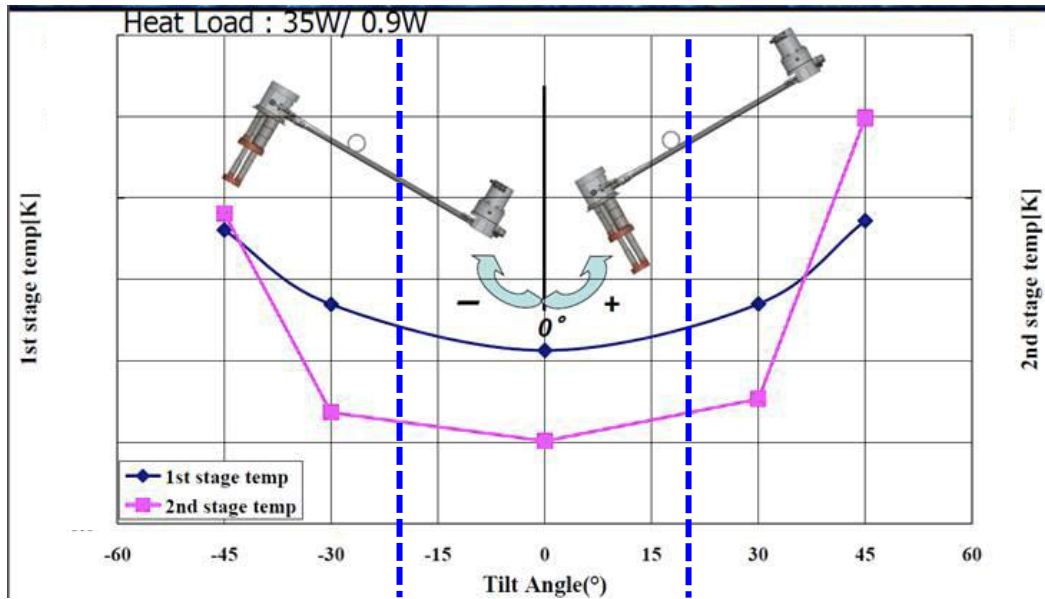


*Figure 8.4-1. Tilt dependence of the TransMIT PTD-406C PT cold head. (Source: Mark Kimball, NASA GSFC).*

## 8.5 Temperature Oscillation Damping Pot

TransMIT and Cryomech offer a damping pot option (see Figure 8.5-1) to reduce thermal oscillations at the 2<sup>nd</sup> stage heat sink. The LHe pot is in direct thermal contact with the ~4 K heat sink. Temperature oscillations are damped by condensation/evaporation of helium.

The GREAT team had intended to incorporate a 0.2 liter damping pot (Risacher, 2016). With it, temperature oscillations were reduced by a factor of 25, from 300 mK to 12 mK peak-to-peak. Ultimately, the damping pot was deemed unnecessary. Eliminating it also simplified the airworthiness certification.



*Figure 8.5-1. Cryomech PT cold head equipped with a temperature oscillation damping pot. (cryomech.com)*

## 8.6 $^4\text{He}$ and $^3\text{He}$ Sorption Refrigerators (SRs): Overview

Following are some key facts concerning SRs:

- SRs are small, low mass, and highly reliable. They can provide moderate cooling capacities: Up to  $\sim 300 \mu\text{W}$  at 1 K; up to  $\sim 30 \mu\text{W}$  at 300 mK.
- They are typically single-shot (i.e., must be recycled periodically), but with a high duty cycle of up to  $\sim 95\%$ .
- They can be configured, with multiple evaporators and sorption pumps, to provide continuous cooling. However, single-shot refrigerators are capable of providing cooling throughout the observation phase of a SOFIA flight, so continuous versions are not considered.
- They can be used to intercept heat leaks to ADRs or DRs. They can also be used as precooling stages for magnetic or DRs.
- The  $^4\text{He}$  refrigerator has SOFIA flight heritage with HAWC+.
- They are commercially available.

## 8.7 Pumped Helium Pot

The simple drawing in Figure 8.7-1 represents a  $^4\text{He}$  pot, as used in a traditional “wet” DR. The pot is pumped to lower its vapor pressure and is continuously replenished via the needle valve. Its operating temperature is around 1 K. The helium pot is similar to the superfluid helium reservoir in the FIFI-LS cryostat (Sec. 5.4), which uses an external mechanical pump. However, that is a single-shot, wet, nonrecyclable cooler.

The external pump can be replaced by a small sorption pump, contained within the cryostat. The system can then be recycled indefinitely, with high duty cycle. The result is a dry closed-cycle

SR. Note that the SR is described as “dry” even though it does contain a liquid cryogen; the point is that the cryogen is not expendable.

The operating temperature of a helium pot is simply found by following the appropriate saturated vapor pressure versus temperature curve.

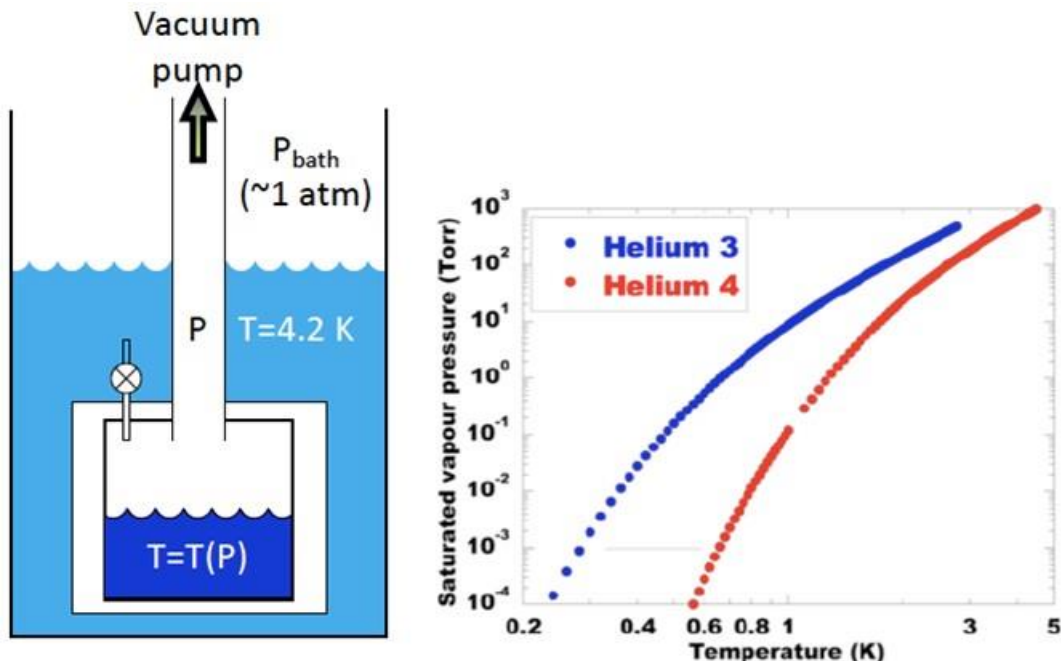


*Figure 8.7-1. Left: Diagram of a pumped helium pot; Right: Saturated vapor pressure versus temperature curves for  $^4\text{He}$  and  $^3\text{He}$ .*

## 8.8 Helium SR

The fundamental components of a SR are shown in the schematic in Figure 8.8-1. There are no moving parts.

Typically, the cold sink would be in thermal contact with a helium bath, at 4.2 K, or the second stage of a PT or GM refrigerator, at  $\sim 4 \text{ K}$  or slightly colder. For  $^3\text{He}$ , the condenser must be at  $< \sim 3 \text{ K}$ , so a  $^4\text{He}$  refrigerator might be required to cool the condenser.

The liquid in the evaporator is usually contained by a porous medium (e.g., copper sinter). This makes the unit much less sensitive to tilts (a necessary consideration for SOFIA).

Referring to Figure 8.8-1, the components of the SR are: 1. Sorption pump; 2. Pumping line; 3. Thermal link to the cold sink (condenser); 4. Evaporator (liquid  $^4\text{He}$  or  $^3\text{He}$ ); 5. Cold sink (at  $\sim 4 \text{ K}$  for  $^4\text{He}$  and  $< \sim 3 \text{ K}$  for  $^3\text{He}$ ); 6. Adsorbant heater (for recycling); 7. Thermal switch (ON for pumping; OFF for recycling).

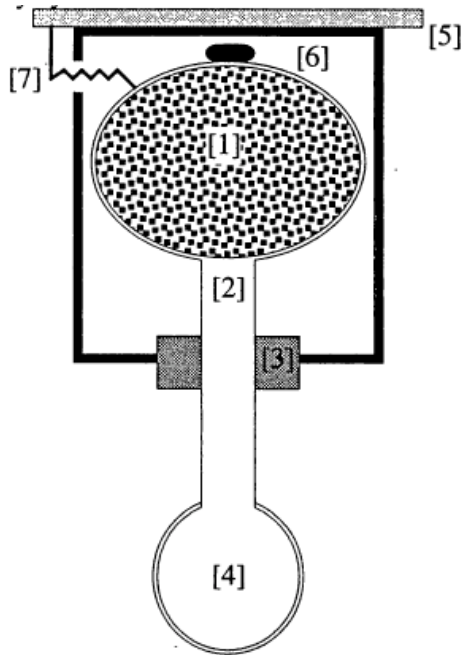


**Figure 8.8-1. Closed cycle helium SR. The various components are identified in the text. (Duband, 1996).**

	Helium-3	Helium-4
Molar mass (g/mol)	3.016	4.003
$T_{\text{NBP}}$ (K)	3.19	4.24
Critical point, temperature (K)	3.32	5.2
Critical point, pressure (Mpa)	0.116	0.223
Latent heat at $T_{\text{NBP}}$ (J/g)	7.7	21
Liquid density at $T_{\text{NBP}}$ (g/cm <sup>3</sup> )	0.059	0.125

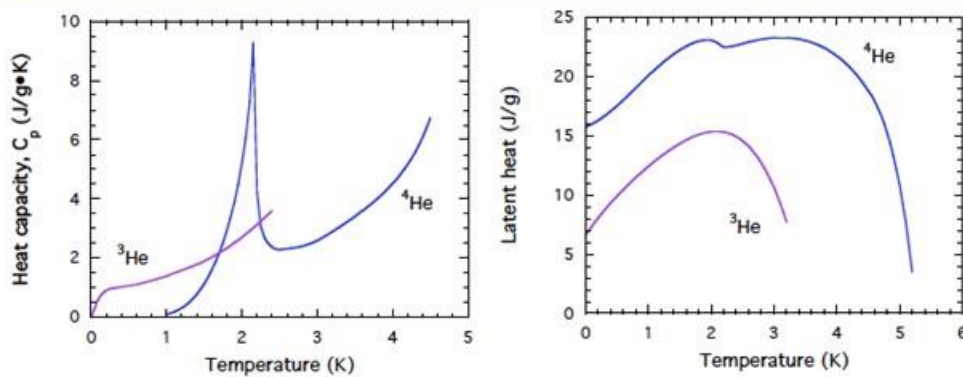


**Figure 8.8-2. Relevant helium properties.**

The sorption pump works by adsorbing helium atoms to the surface of an adsorbant. Adsorption (see Figure 8.8-3) is the adhesion of atoms or molecules to a solid surface by means of the van der Waals force. The rate of desorption is proportional to  $\exp(-\Gamma / k_B T)$ , where  $\Gamma$  is the van der Waals binding energy. The pressure is proportional to the surface coverage  $Q$  and the desorption rate.

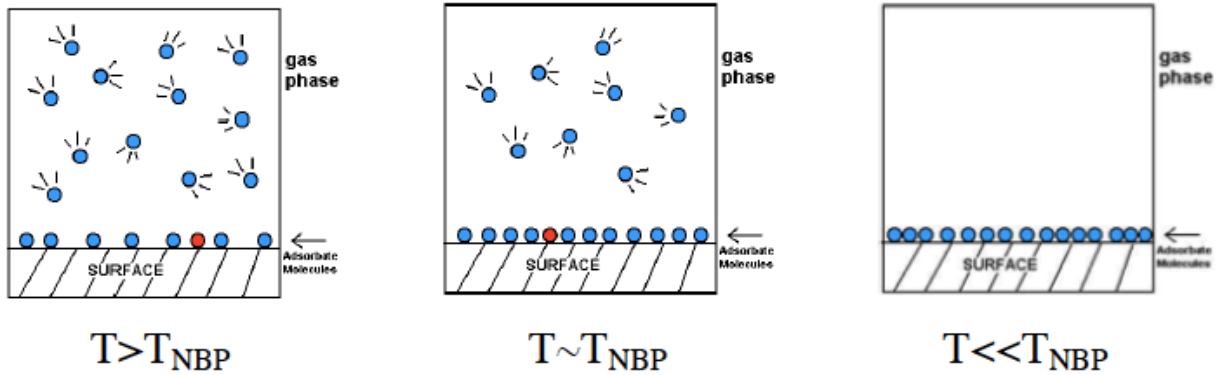


**Figure 8.8-3. Gas adsorption on a surface.**

A good adsorbant has a high binding energy  $\Gamma$  and a very large specific area (exposed surface area per unit mass).

For cryogenic applications the adsorbant of choice is charcoal. The binding energy of helium to charcoal is  $\Gamma \sim 150$  K, whereas  $\Gamma \sim 30$  K for typical surfaces like metals. The vapor pressure above monolayer films is extremely low at low temperatures. Also, charcoal has an extremely large specific area ( $1000 - 1600$  m<sup>2</sup>/g). A single helium monolayer is  $13$   $\mu\text{mol}/\text{m}^2$ .

One gram of charcoal can adsorb up to  $0.02$  mols of helium ( $\sim 500$  STP cm<sup>3</sup>).

## 8.9 Typical SR Capacities

Listed below are the energy and power capacities of typically sized SRs.

The energy capacity, per cm<sup>3</sup> of liquid, is given by (latent heat) x density:

- <sup>3</sup>He:  $0.4$  J/cm<sup>3</sup> at  $0.3$  K;      Gas charge at NTP:  $\sim 500$  cm<sup>3</sup> gas for  $1$  cm<sup>3</sup> liquid.
  - <sup>4</sup>He:  $3.2$  J/cm<sup>3</sup> at  $1.0$  K;      Gas charge at NTP:  $\sim 800$  cm<sup>3</sup> gas for  $1$  cm<sup>3</sup> liquid.
- NTP =  $294$  K,  $1$  atm.
- For a 10-hour hold time:
    - <sup>3</sup>He:  $11.1$   $\mu\text{W}/\text{cm}^3$  at  $0.3$  K.
    - <sup>4</sup>He:  $88.9$   $\mu\text{W}/\text{cm}^3$  at  $1.0$  K.
  - The device is charged at room temperature. If the total enclosed volume is  $100$  cm<sup>3</sup>, then  $5 - 8$  atm of charge is required per cm<sup>3</sup> of liquid.
  - Typical liquid volume: A few cm<sup>3</sup>.



## 8.10 Example: Infrared Telescope for Space (IRTS) $^3\text{He}$ SR

IRTS was the first Japanese telescope dedicated to infrared astronomy. The detector was cooled to 300 mK using a  $^3\text{He}$  SR mounted to a 1.9 K cold sink (Duband, 1996 and Kittel, 2004). See Figures 8.10-1 and 8.10-2 (drawing with components identified).

Following are some characteristic numbers:

- Cooling capacity: 15  $\mu\text{W}$  at 0.3 K for 8 days.
- Recycle time: 15 hours (93% duty cycle).
- Average heat load on the 1.9 K heat sink: < 2 mW.
- Total mass: 870 g.

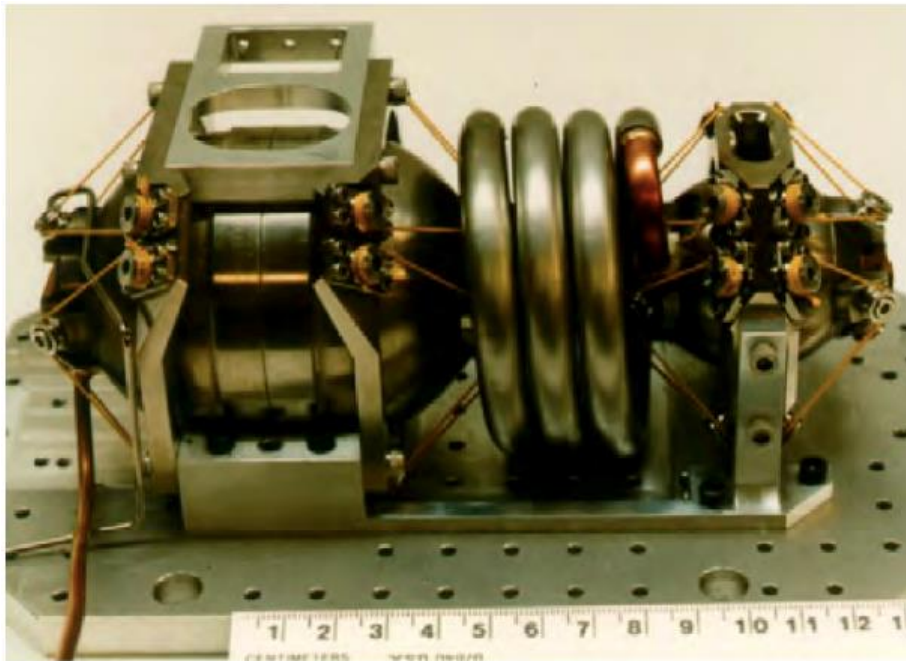
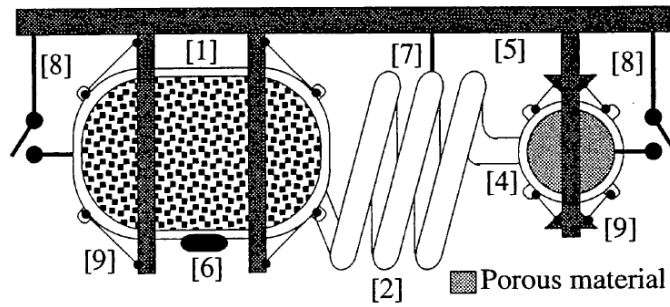


*Figure 8.10-1. The IRTS  $^3\text{He}$  SR.*

Figure 8.10-3 (*left*) shows the on-orbit temperature profile. The cause of the step at around 4 days is not known.  $^4\text{He}$  and  $^3\text{He}$  versions of the IRTS refrigerator were built for sounding rocket applications (see Figure 8.10-3 (*right*)). The arrows indicate various events in the flight, from launch to re-entry.





1. Charcoal sorption pump.
2. Pumping line.
4. Evaporator ( $^3\text{He}$  pot): Cold head.
5. 1.9 K cold sink.
6. Desorption heater.
7. Thermal link to cold sink (condenser).
8. Thermal switches.
9. Kevlar<sup>®</sup> support system.

**Figure 8.10-2. The IRTS  $^3\text{He}$  SR.**

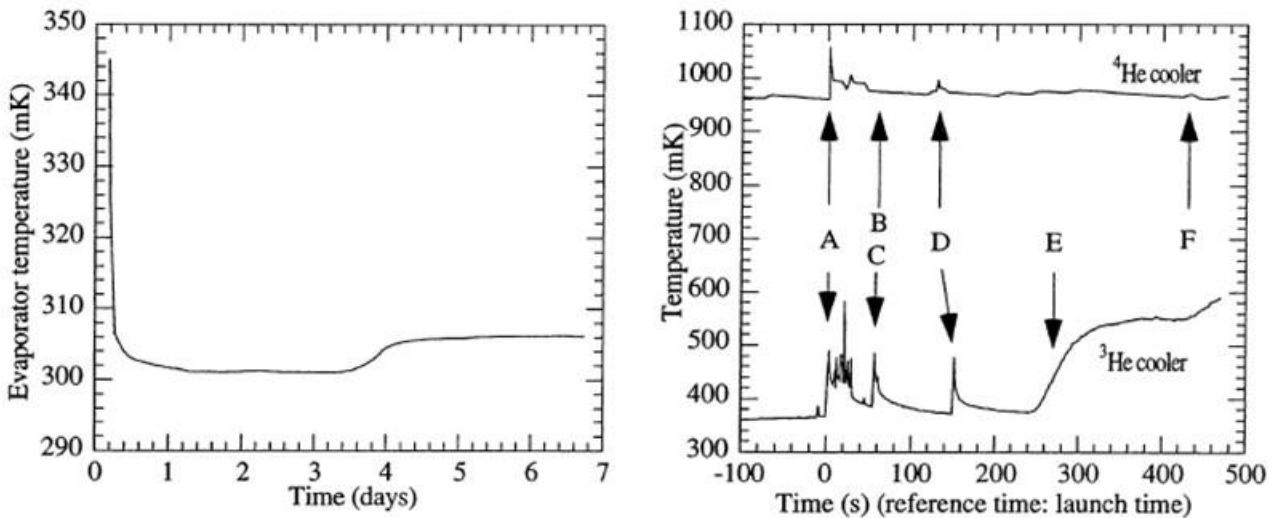


**Figure 8.10-3. Left: On-orbit temperature profile of the IRTS refrigerator; Right: Temperature profiles of  $^4\text{He}$  and  $^3\text{He}$  SRs during a sounding rocket flight.**

## 8.11 Example: Chase Research Cryogenics $^4\text{He}$ SR

An example of a commercially available  $^4\text{He}$  SR is the Chase Research Cryogenics Type GL4; see Figure 8.11-1 (*left*). Its measured cooling capacity curve (i.e., operating temperature versus applied thermal load) is plotted in Figure 8.11-1 (*right*).

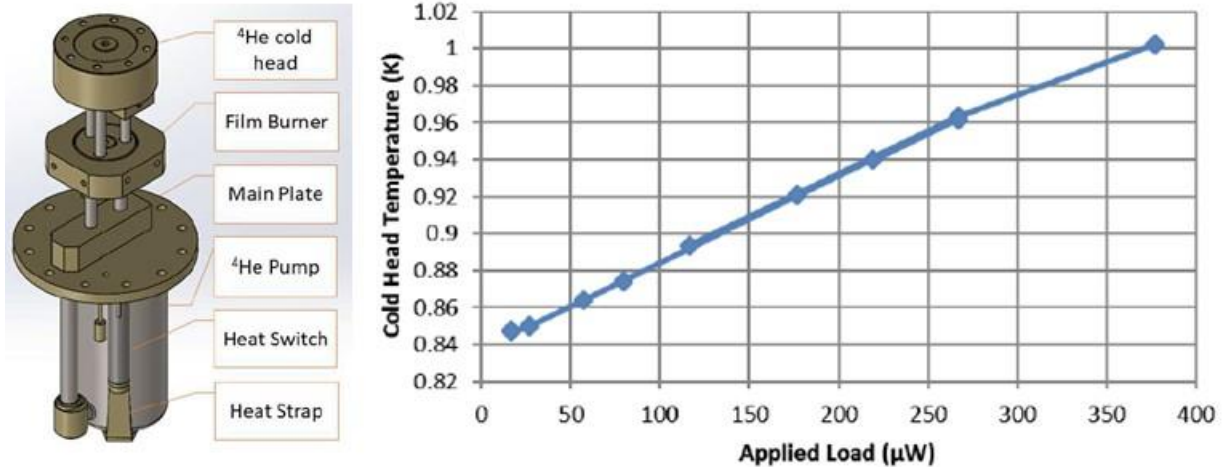


*Figure 8.11-1. Left: Chase Research Cryogenics Type GL4  $^4\text{He}$  SR. It is shown upside-down for a clear view of the cold end. Right: Measured GL4 capacity curve.*

## 8.12 $^4\text{He} - ^3\text{He}$ SR

A  $^4\text{He}$  SR can operate using the nominally 4 K second stage of a PT like the TransMIT PTD-406C.

However,  $^3\text{He}$  condenses at a lower temperature, so for many applications it makes sense to package a  $^3\text{He}$  refrigerator with a  $^4\text{He}$  refrigerator. Then, while recycling, the  $^3\text{He}$  can be condensed via the flange connected to the  $^4\text{He}$  evaporator. Both sorption pumps operate at  $\sim 4$  K. Refer to the schematic in Figure 8.12-1. Note that the IRTS  $^3\text{He}$  refrigerator did not require a tandem  $^4\text{He}$  unit, as it was mounted to a 1.9 K heat sink.

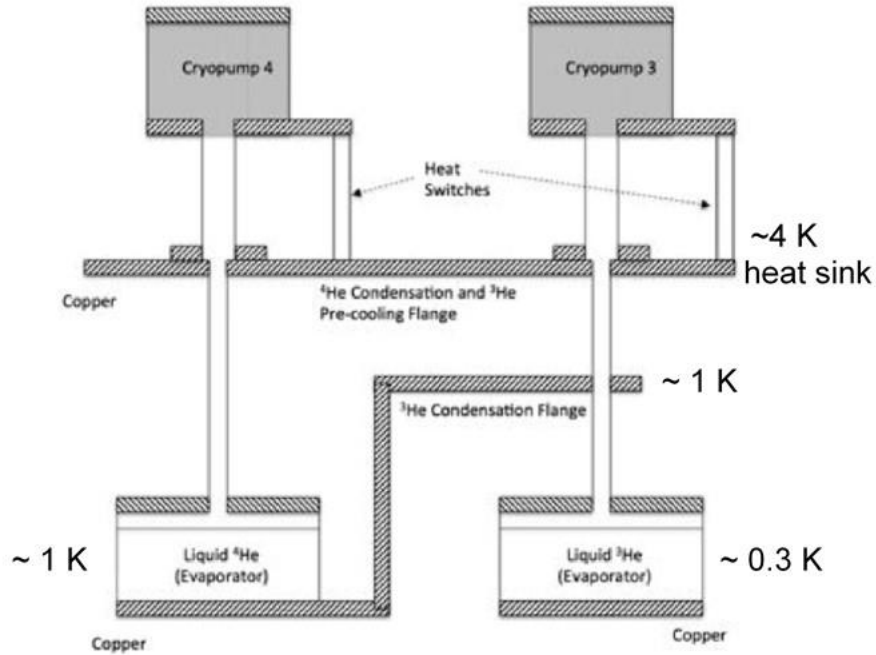


**Figure 8.12-1. Tandem  $^4\text{He} - ^3\text{He}$  SR. The purpose of the  $^4\text{He}$  unit is to cool the  $^3\text{He}$  condensation flange. (Piccirillo, 2018).**

### 8.13 Example: Chase Research Cryogenics $^4\text{He} - ^3\text{He}$ SR

Chase Research Cryogenics also makes a  $^4\text{He} - ^3\text{He}$  refrigerator, the Type GL7. See Figure 8.13-1 (left). The measured cooling capacity at the  $^3\text{He}$  cold head is plotted in Figure 8-13-1 (right).

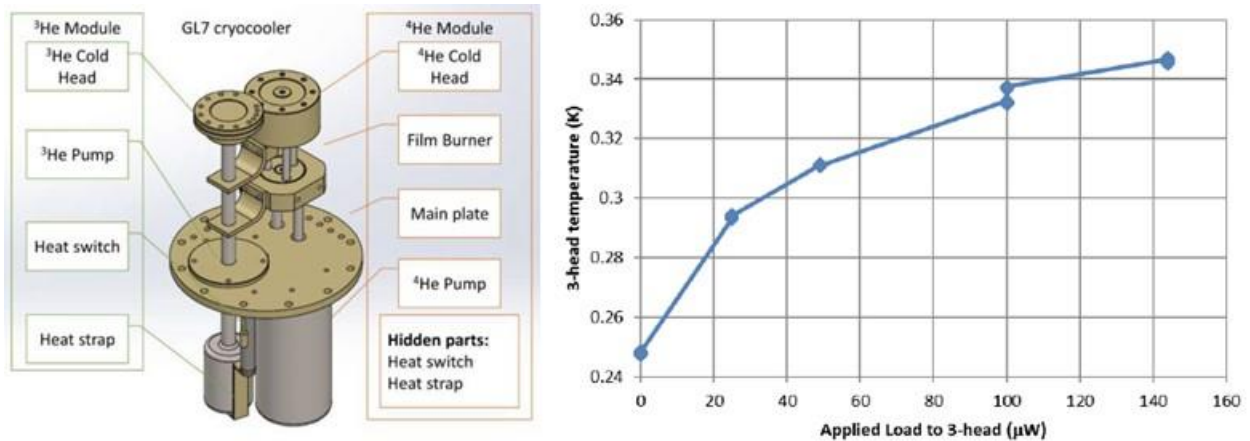


**Figure 8.13-1. Left: Chase Research Cryogenics Type GL7  $^4\text{He} - ^3\text{He}$  SR. It is shown upside-down for a clear view of the cold end. Right: Measured GL7  $^3\text{He}$  cold head capacity curve.**

## 8.14 Adiabatic Demagnetization Refrigerator (ADR): Overview

ADRs are highly efficient and reliable (solid state; no moving parts) and can operate from above 6 K to below 50 mK, depending on the salt pill material, heat sink temperature, and magnet size.

Typical ADR capacities are:

- 1 – 10 mW in the 1 – 4 K operating range.
- Drops to a few micro-Watts below 100 mK.

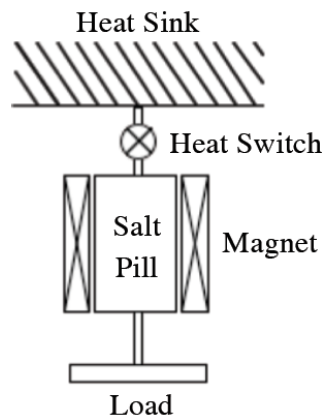
ADRs are usually single-stage, single-cycle, but multi-stage ADRs can be configured to provide continuous cooling.

For SOFIA SI applications:

- The operating temperature will typically be  $< 200$  mK, with a capacity of  $\sim 2$   $\mu$ W and a hold time of 10 – 16 hours (as with the HAWC+ ADR).
- Because of the relatively short observation time, only single-shot ADRs are considered in this report.
- The ADR is gravity-independent, and so is insensitive to the cryostat tilt.

## 8.15 ADR Principles of Operation

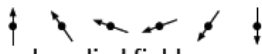
As shown in Figure 8.15-1, a single stage ADR consists of three primary components: (1) the salt pill, also called the refrigerant; (2) a superconducting magnet; and (3) a heat switch between the salt pill and the heat sink. The salt pill resides in the bore of the magnet and is thermally connected to the load.

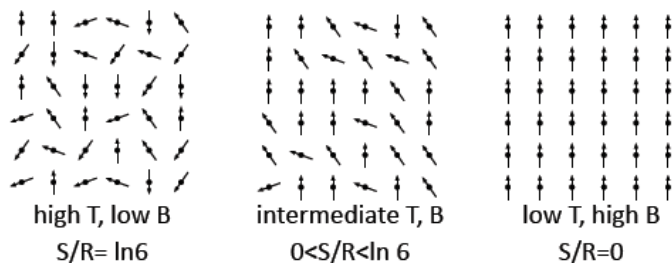


**Figure 8.15-1. Simple schematic of a single stage ADR.**

The refrigerant is an array of weakly interacting spins. Each spin can take on one of  $2J+1$  spin states  $m$ , where  $J$  is the total angular momentum quantum number.  $m$  can then be one of  $-J, -J+1, \dots, J-1, J$ . See Figure 8.15-2 for an example.

*The refrigerant is a thermal sponge:* It absorbs heat from the load by allowing the thermal energy to randomize the spins, thus increasing the entropy; it is “wrung out” by magnetizing the pill (i.e., by aligning the spins, thus decreasing the entropy) while in thermal contact with the heat sink.

- Array of magnetic spins is used to store and release heat
  - Example: Ferric Ammonium Alum (FAA):  $\text{Fe}^{3+}(\text{NH}_4)(\text{SO}_4)_2 \cdot 12\text{H}_2\text{O}$
  - $J=5/2$ ; 6 spin states  $-5/2, -3/2, -1/2, 1/2, 3/2, 5/2$  
  - Population of each state depends on temperature and applied field



- Maximum entropy change is  $R \cdot \ln 6 \sim 15 \text{ J/mol} \cdot \text{K}$ 
  - 1 mol (500 grams,  $280\text{cm}^3$ ) of FAA can store 1 J at 0.06 K

*Figure 8.15-2. Example of a  $J = 5/2$  refrigerant.*

The pill material (refrigerant) should have a high magnetic moment and high density. Ideally it should be composed of a system of non-interacting spins. In reality there will be some interaction, and below the transition temperature  $T_N$  (see Table 8.15-1), the system will spontaneously order, and the entropy will drop to zero, even in a vanishingly small magnetic field. During normal operation of the ADR the ordering is field-induced. The refrigerant is selected based on the lowest desired temperature.

*Table 8.15-1. Common ADR paramagnetic salt refrigerants.*

Material	$J$	Ion Density ( $/\text{cm}^3$ )	$T_N$ (K)
Cerium Magnesium Nitrate, CMN	1/2	$1.68 \times 10^{21}$	.0015
Chromic Potassium Alum, CPA	3/2	$2.14 \times 10^{21}$	.009
Chromic Cerium Alum, CCA	3/2	$2.1 \times 10^{21}$	.01
Ferric Ammonium Alum, FAA	5/2	$2.15 \times 10^{21}$	.026
Gadolinium Lithium Fluoride, GLF	7/2	$1.34 \times 10^{22}$	~.2
Gadolinium Gallium Garnet, GGG	7/2	$1.27 \times 10^{22}$	~.38

Entropy versus temperature for various common paramagnetic salts are plotted in Figure 8.15-3.

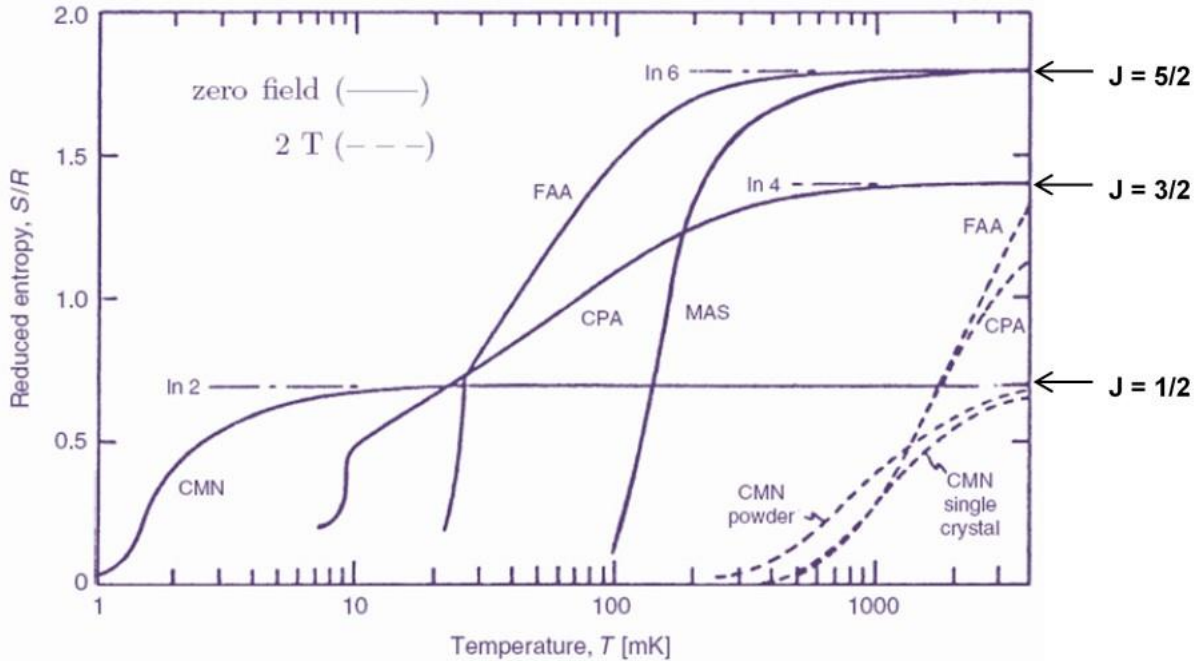


**Figure 8.15-3. Entropy curves for various paramagnetic salts (at applied magnetic fields of 0 and 2 T).**

An ADR cycle is shown in Figure 8.15-4 and described as follows:

1. Before the cycle can begin, the salt pill must be precooled—to point A ( $B = 0$ ,  $T = 100$  mK) in the diagram (Figure 8.15-4). The spin system is more or less disordered, so the molar entropy is just the maximum value  $R \log(2J+1)$ ; in this case (CMN salt),  $J = \frac{1}{2}$ .
2. This is where the thermal sponge is wrung out. The magnetic field is ramped up (isothermal magnetization), in this case to 0.1 T, while the pill is in thermal contact with the sink at  $T_{sink} = 100$  mK. The heat of magnetization is rejected to the thermal sink. The heat rejected is found by integrating  $dQ = TdS$  along the line AB; it is just  $Q_{rej} = T_{sink}\Delta S$ , which is the area of the rectangle ABDE.
3. The pill is isolated from the sink when the switch is turned off, and the field is ramped down (adiabatic demagnetization). *The entropy is a function of  $B/T$  only*: Then  $S = \text{const.}$  means that  $B/T$  is constant, which means that *if the field is decreased, then the temperature must decrease proportionally*. The system is now at point C.
4. The pill (thermal sponge) now absorbs heat from the load, and the system gradually warms up, following the  $B = 0$  curve CA. The heat absorbed from the load is the integral of  $TdS$  from C to A, which is the area of the shaded region.
  - The system is now back at point A, but steps 2 -3 can be repeated indefinitely.
  - Note that in going from C to A, the temperature is not constant. Alternatively, the system could be demagnetized to some field  $B > 0$ . The reserve field can then be used to regulate the load temperature.



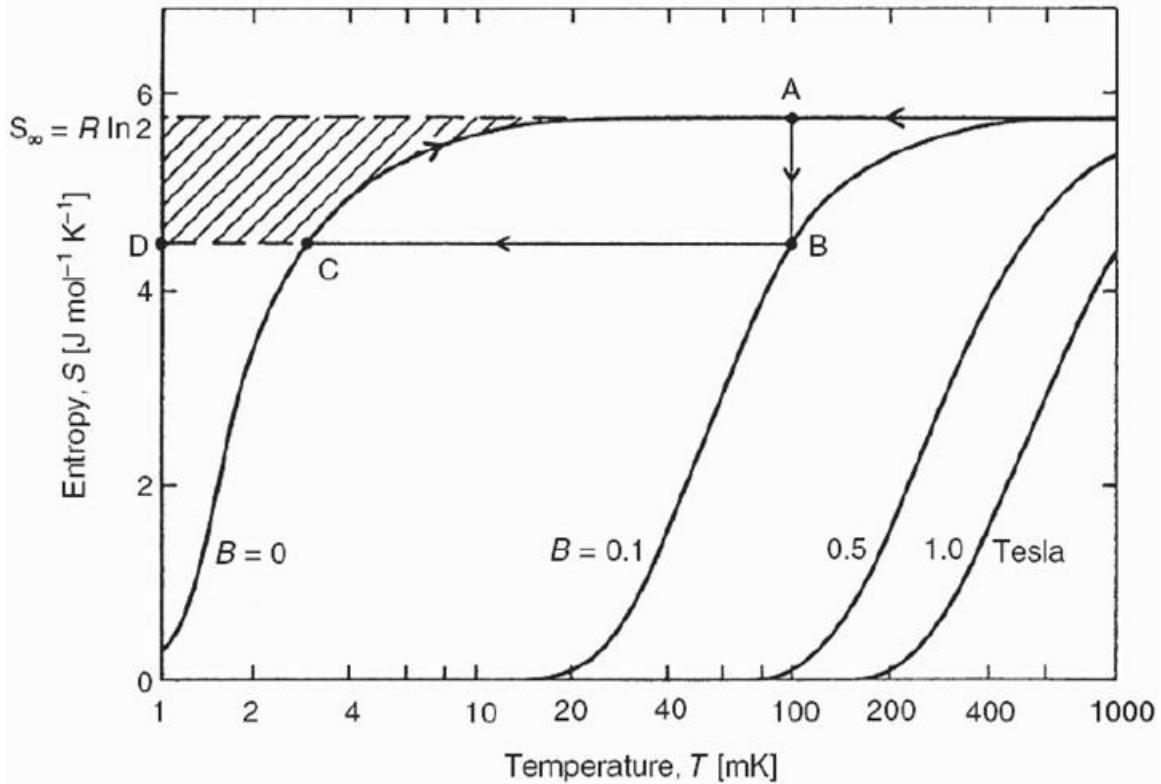


**Figure 8.15-4.** Molar entropy  $S$  versus temperature  $T$  for CMN salt, with lines of constant applied magnetic field  $B$ .

## 8.16 ADR Paramagnetic Salt Pill Manufacture

- Refrigerant (hydrated salt) is grown on a “thermal bus”
  - Efficient heat transfer from external interface
- Salt growth can take days (FAA) to weeks (CPA)
  - XRS used 930 g FAA



**Figure 8.16-1.** ADR salt pill manufacture.

## 8.17 ADR Practical Design Limits

The following are typical values based on designs for SOFIA ADR cryostats:

- Net cooling power:  $\sim 1 \mu\text{W}$ .
- Operating temperature: 80 – 100 mK.
- Heat sink temperature:  $\sim 1 \text{ K}$ .
- Magnetic field: 2 T (at a current of 2 A).
- Refrigerant mass:  $\sim 900 \text{ g}$  (FAA).
- Hold time:  $\sim 16$  hours.
- Recycle time:  $\sim 5$  hours. This includes multiple recyclings of the sorption cooler(s).

Some trends to be aware of:

- A higher heat sink temperature requires a higher magnetic field.
- A lower operating temperature requires a higher magnetic field.
- The magnet mass grows rapidly with increased bore volume and increased magnetic field:  $B \gg 2 \text{ T}$  is not practical.

## 8.18 Example: XRS ADR

Figure 8.18-1 shows the Astro-E X-Ray Spectrometer (XRS) ADR. On the left is the salt pill, heat switch, suspension, and baseplate. It was built by NASA GSFC. On the right is the magnet—a superconducting NbTi magnet made by Cryomagnetics, Inc. It generated a 2 T central field at a current of 2 A. The bore was 3 inches in diameter and 6 inches in length. The total mass of the assembled refrigerator was 15 kg. The ADR was staged off of a helium bath at  $\sim 1.5 \text{ K}$ . The operating temperature was 60 mK and the hold time was 30 hours.



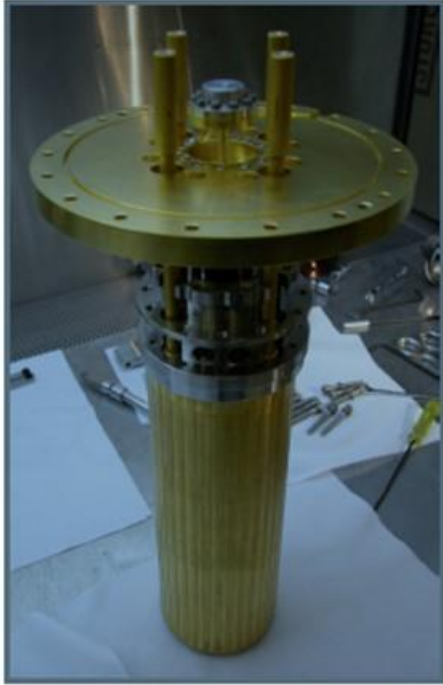


*Figure 8.18-1. XRS ADR. Left: the salt pill removed from the bore of the magnet; Right: Superconducting magnet made by Cryomagnetics, Inc.*

### **8.19 Example: HAWC+ ADR**

The HAWC+ ADR (Figure 8.19-1) is pre-cooled to  $\sim 1$  K, from the LHe bath temperature by a custom  $^4\text{He}$  SR from Chase Research Cryogenics. The SR contains  $\sim 33$  STP liters of  $^4\text{He}$ .

The ADR (Tuttle, 2002), built by NASA GSFC, uses a 920-gram FAA salt pill, within a stainless steel tube for stiffening, and suspended within the bore of a superconducting magnet by a low-conductance Kevlar<sup>®</sup> suspension system (Voellmer, 2003).

The ADR and  $^4\text{He}$  SR are connected by a  $^3\text{He}$  heat switch (ASTRO-H model, Kimball, 2015).

The magnet is capable of reaching 8 T but is ramped to only 2 T during operation to avoid trapping magnetic flux in the superconducting niobium magnetic shield surrounding the helium reservoir.

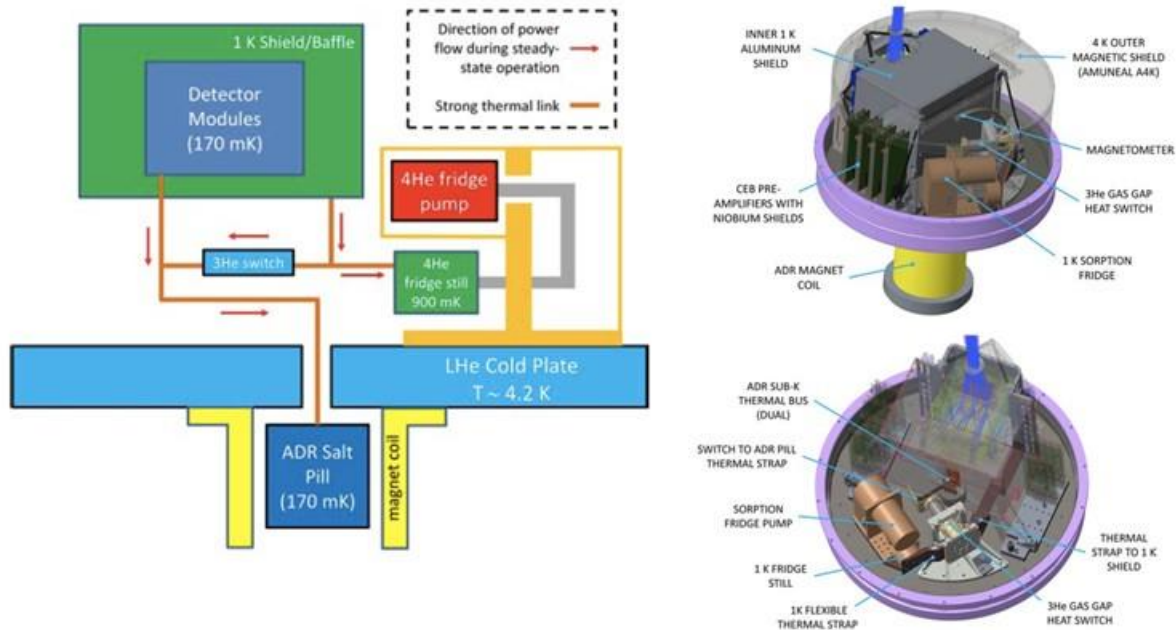


**Figure 8.19-1. The HAWC+ ADR system.**

On flight day, the following operations are performed on the 1 K and sub-K stages (Harper, 2018):

1. All components are brought to 4.2 K by heating the charcoal sorption pumps on the  $^4\text{He}$  SR and the heat switch. The heat switch connecting the SR to the 4.2 K cold plate is open.
2. The ADR magnet is ramped to  $\sim 2$  T (isothermal magnetization) and held there through step 8. The heat of magnetization is rejected to the 4.2 K cold plate via the heat switch.
3. The SR sorption pump is maintained at  $\sim 50$  K for 30 minutes while  $^4\text{He}$  condenses in the SR pot (evaporator, still).
4. The SR pump heater is turned off and the pump / cold plate switch is closed to cool the pump. The pot and connected components (1 K and sub-K stages) begin to cool.
5. The 1 K and sub-K stages continue to cool until the  $^4\text{He}$  pot is exhausted. The pill temperature is  $\sim 2.5$  K.
6. The SR / ADR switch is opened to isolate the pill and sub-K system. The SR is recycled (Steps 3. and 4.). When the SR cools to the same temperature as the thermally isolated pill, the heat switch is closed and the SR continues to cool the pill and sub-K system.
7. The temperature of the sub-K system approaches  $\sim 1$  K. After  $\sim 2.5$  hrs, the sub-K system has cooled to  $\sim 1.35$  K. The SR / ADR switch is opened and remains so for the duration of the pre-flight preparations and flight.
8. The SR is recycled a final time to act as a thermal buffer for the sub-K system.
9. When the SR cools to below the pill temperature, the ADR magnet is ramped down (adiabatic demagnetization) until the target temperature is reached, and then regulated at that temperature using a software PID loop.

A complete cooling cycle takes  $\sim 6$  hrs and is usually completed  $\sim 4$  hrs before observation begins.

## 8.20 Example: HIRMES ADR

Although the HIRMES project has been recently canceled, its cryogenic components, including the ADR, were developed to a high maturity level.

The ADR was designed by NASA GSFC and built by High Precision Devices (HPD). It is similar in design, operation, and capacity to the HAWC+ ADR.

The FAA salt pill is contained in a stainless steel tube for stiffening. This pushes the first normal mode to beyond 400 Hz, which dramatically reduces the vibrational heating at the coldest stage. Moreover, a magnetic eddy current damper is used to dissipate vibrational energy in the suspended salt pill. The pill assembly is suspended by a network of Kevlar® straps. A  $^3\text{He}$  SR (Chase Research Cryogenics) is used to intercept a large fraction of the heat leak through the straps.

A mechanical heat switch, instead of a gas gap heat switch (as in HAWC+) is used to connect the pill's thermal bus to the 1 K sink.

The HIRMES ADR was designed to operate at 70 mK with a load of  $1 - 2 \mu\text{W}$ , with a hold time of  $> 16$  hours and recycling time of  $< 1.5$  hours.

## 8.21 Dilution Refrigerator (DR): Overview

$^3\text{He} / ^4\text{He}$  DRs were developed in the 1960s and have become mainstays in low temperature laboratories world-wide, with COTS models available from several well-established vendors (e.g., Oxford Instruments, Janis Research Company, and High Precision Devices). They are capable of providing high cooling capacities at milli-Kelvin temperatures. The ultimate temperature is around 2 mK, and continuous cooling at  $\sim 10$  mK with loads of a few microwatts is routine. They are also used as precooling stages for Pomeranchuk cells or nuclear spin refrigerators to reach  $\mu\text{K}$  temperatures.

Many DR variants have been demonstrated:

- *Circulating  $^3\text{He}$  DR (Warm Cycle)*: Almost all commercially available DRs are of this type. The  $^3\text{He}$  is circulated to room temperature, using a sealed mechanical pump in conjunction with a high vacuum diffusion or turbo-pump, and then back to low temperatures via a more or less complicated series of counter-flow heat exchangers. Traditionally DRs have been packaged with a LHe Dewar, a “wet” DR, but in recent years the “dry” DR, which is pre-cooled by a two-stage commercial (e.g., Cryomech or Sumitomo) PT, has been steadily supplanting them.
- *$^3\text{He}$  Single-Shot DR*: A warm cycle DR can be run in single-shot mode by closing off the return valve and diverting the pumped  $^3\text{He}$  to a storage tank. This allows lower temperatures to be reached, but only until the  $^3\text{He}$  in the mixing chamber is exhausted, at which point the system must be recycled. A dedicated single-shot DR is an attractive option for applications that do not require continuous cooling (e.g., a SOFIA SI) as it is the simplest DR that can be constructed. In particular, the counter-flow heat exchangers are eliminated. Moreover, it is possible to replace the external pumping system by a sorption pump; all components of the DR (condenser, still, mixing chamber, and pumps) all operate below 4 K.

- *<sup>3</sup>He Cold Cycle DR*: Much of the mass, volume, and electrical power required for a warm-cycle DR can be eliminated by containing the <sup>3</sup>He circulation to cryogenic temperatures. This is done by (1) employing two sorption pumps with a network of cold valves to allow for continuous pumping, or (2) by exploiting the osmotic pressure head that naturally develops between the mixing chamber and still.
- *<sup>4</sup>He Cold Cycle DR (Leiden DR)*: It is possible to circulate <sup>4</sup>He instead of <sup>3</sup>He. Because <sup>4</sup>He is superfluid throughout the cold cycle components, a fountain pump can be used to drive the circulation.

## 8.22 DR Principles of Operation

Below ~ 0.8 K a <sup>3</sup>He – <sup>4</sup>He mixture spontaneously separates into two distinct phases: A concentrated <sup>3</sup>He phase and a dilute mixture. Referring to the phase diagram in Figure 8.22-1, the <sup>3</sup>He concentration in the dilute phase is given by the left branch of the phase separation line, and in the concentrated phase by the right branch.

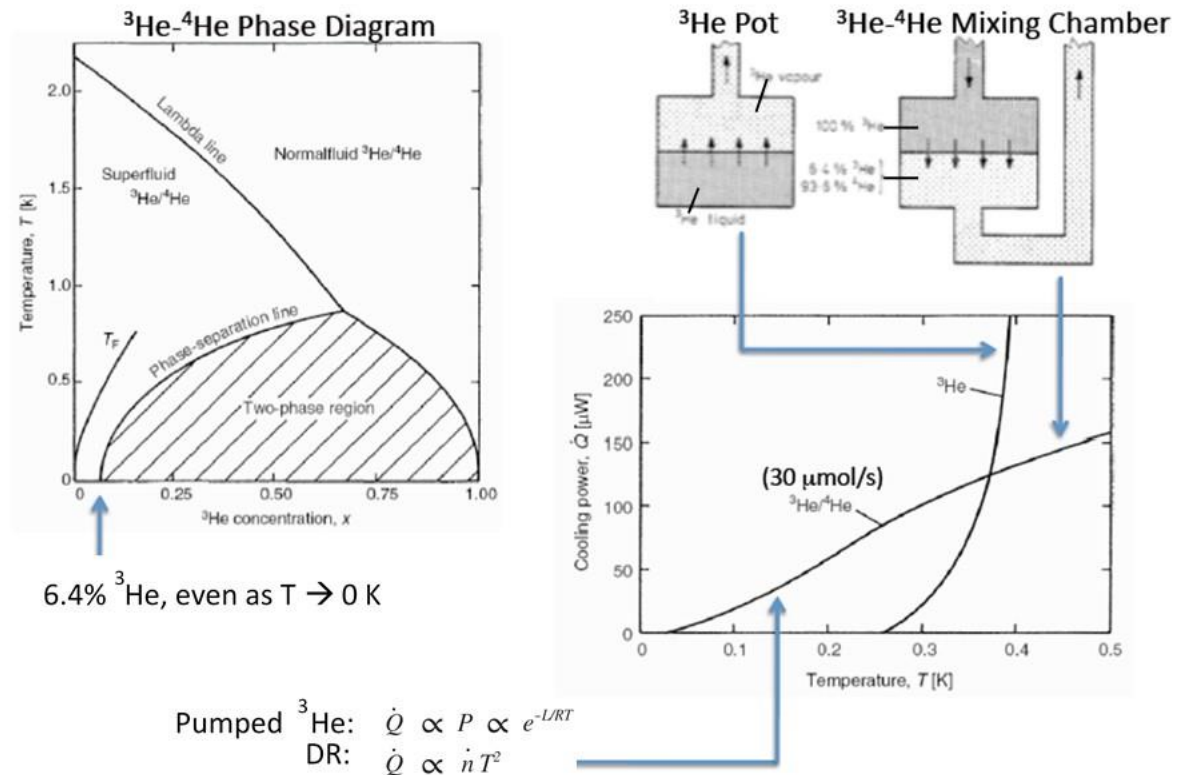


**Figure 8.22-1. <sup>3</sup>He – <sup>4</sup>He phase diagram and comparison of the DR with the pumped <sup>3</sup>He pot.**

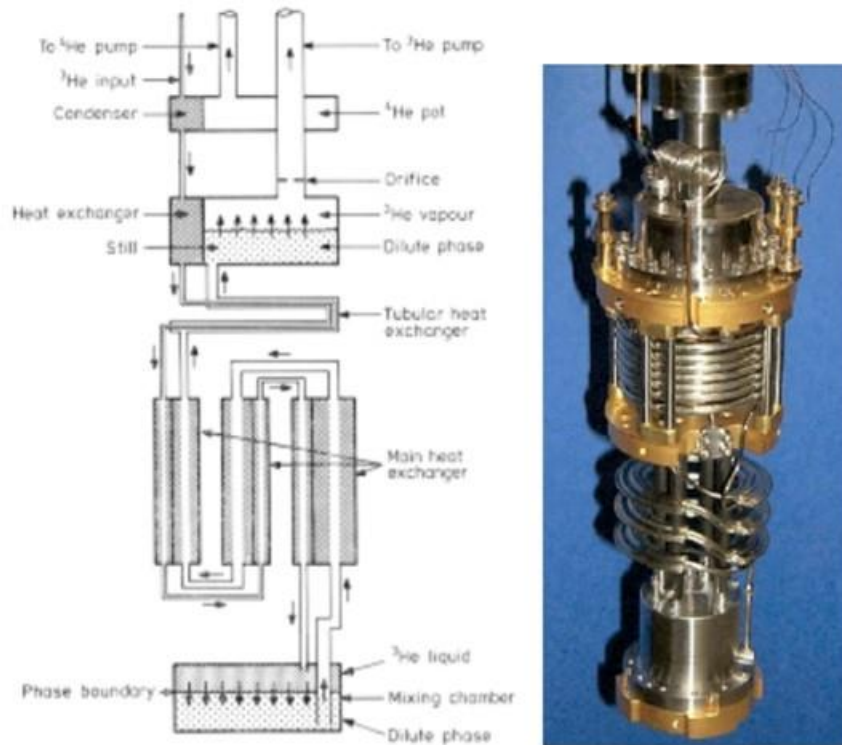
Because the concentrated phase is less dense, it floats on top of the dilute liquid, with a well-defined boundary. Maintaining this boundary in micro-gravity, or even in gravity with the cryostat tilted, can be challenging.

The mixing chamber is cooled by pumping or “evaporating” <sup>3</sup>He across the phase boundary into the “mechanical vacuum” of the superfluid <sup>4</sup>He.

Whereas, in a pumped  $^3\text{He}$  pot, the cooling power, proportional to the vapor pressure, decreases exponentially as the pot is cooled, in a DR the  $^3\text{He}$  concentration remains finite, and approaches a constant 6.4% at low temperatures. This gives a cooling capacity that is proportional to the flow rate and the square of the temperature, which explains how the DR can reach such low temperatures.

### 8.23 Traditional Wet DR

Figure 8.23-1 shows a standard DR insert (Janis Research Company, LLC) for a LHe Dewar.



$$\dot{Q}_M = \dot{n} (96T_M^2 - 12T_i^2)$$

**Figure 8.23-1. Left: Schematic of a  $^3\text{He}$ -circulating DR; Right: Janis Research Company DR insert for a LHe Dewar. Also given is the expression for the refrigeration capacity (bottom).**

The thermal load is attached to the mixing chamber at the bottom, where the cooling effect is produced by pumping  $^3\text{He}$  across the phase boundary.

The pumped mixture moves upward toward the still through the heat exchangers, precooling the returning  $^3\text{He}$ .

Applying heat to the still drives off nearly pure  $^3\text{He}$ , which is then removed to room temperature by a vacuum pump. The orifice in the pump line suppresses superfluid film flow.

The  $^3\text{He}$  is then passed through an  $\text{LN}_2$  cold trap before returning to the cryostat.

The returned  $^3\text{He}$  is condensed at the pumped  $^4\text{He}$  pot (maintained at  $\sim 1$  K). The  $^4\text{He}$  pot is serviced by its own mechanical pump at room temperature. It is continually replenished via a capillary from the LHe bath.



The return stream is pre-cooled by exchanging heat with the out-going stream at the still and in the heat exchangers, reaching a temperature  $T_i$  before being injected into the mixing chamber. The return temperature  $T_i$  is greater than the mixing chamber temperature  $T_M$ . It is a measure of the overall ineffectiveness of the heat exchanger chain. The expression for the cooling power reflects this.

## 8.24 Dry DR

Figure 8.24-1 shows a commercial (Oxford Instruments) dry DR. It is functionally the same as the wet DR described above, with two exceptions:

1. The main difference is that the LN<sub>2</sub> jacket and LHe bath have been replaced by the first and second stages of a commercial PT refrigerator.
2. There is no pumped helium pot, and the nominally 4 K second stage of the PT is too warm to condense the returning <sup>3</sup>He. One solution is to use a Joule-Thomson expander in line with the return stream.

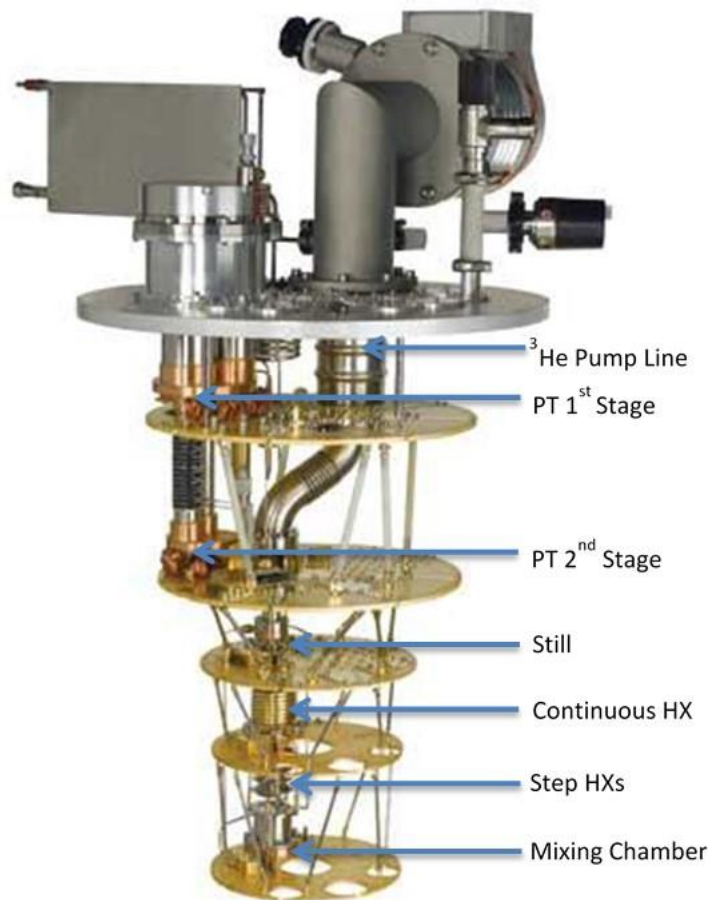


**Figure 8.24-1. A dry DR (Oxford Instruments).**

A laboratory dry DR usually employs an external LN<sub>2</sub> cold trap on the <sup>3</sup>He return line, so it is not completely dry, although a closed cycle cryopump could be used instead.

It is conceivable that a scaled-down version of such a DR could be used on SOFIA. The vacuum pump in the VPS would need to be replaced by a sealed <sup>3</sup>He pump, and a return line to the

cryostat provided. Both the pumping and return lines must wrap around the CLA. It is not apparent that such a long and narrow pumping line could accommodate the flow rate necessary to reach sub-100 mK temperatures with appreciable loads.

## 8.25 Single-Cycle DR

Figure 8.25-1 shows a simple, but elegant single-cycle DR that was developed at Argonne National Laboratory (Roach, 1987). It was offered commercially by RMC Cryosystems. RMC was later acquired by Janis, but the model was soon discontinued due to limited marketing potential.

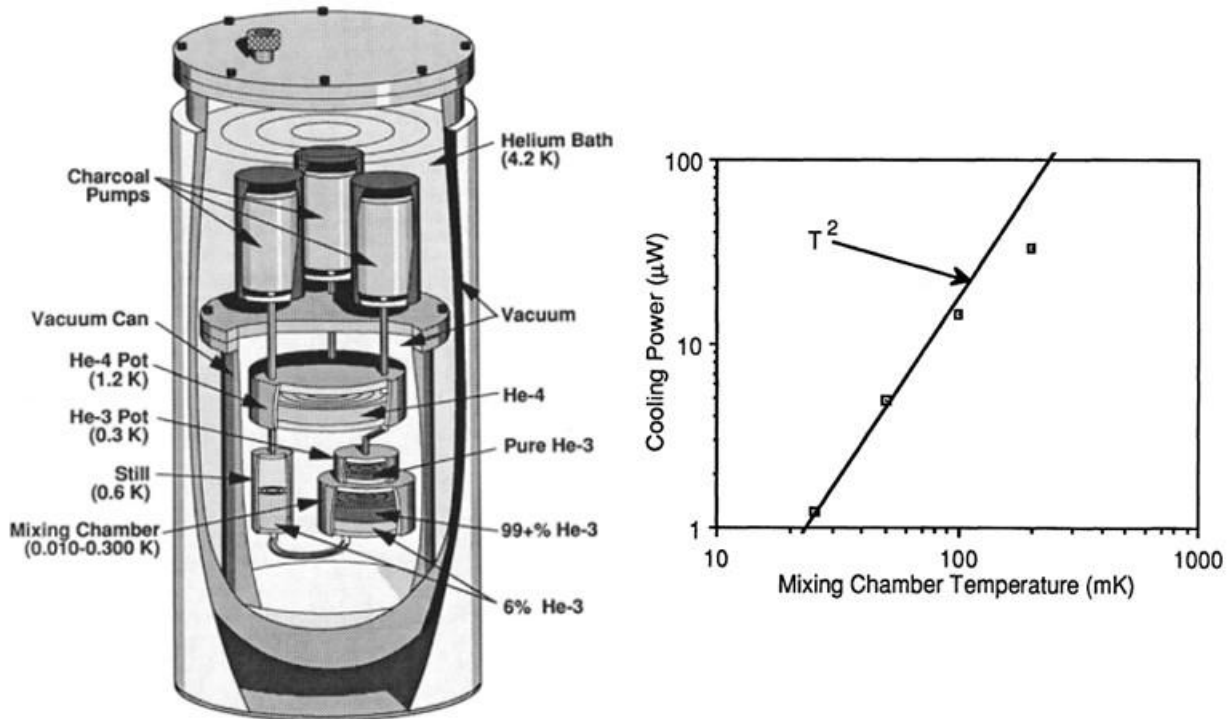


**Figure 8.25-1. Left: A single cycle DR; Right: The measured cooling power at the mixing chamber showing a  $T^2$  dependence, in agreement with theory.**

It was compact, fitting inside a 6-inch ID LHe Dewar.

Roughly, it was operated as follows:

1.  $^4\text{He}$  was condensed in the  $^4\text{He}$  pot and then pumped by a sorption pump to give a 1.2 K stage.
2. This allowed for the condensation of  $^3\text{He}$  in the  $^3\text{He}$  pot. Pumping on it allow for condensation and phase separation of the mixture in the mixing chamber.
3.  $^3\text{He}$  was then pumped across the phase boundary via the still.
4. The mixing chamber cooled and remained cold until the  $^3\text{He}$  was exhausted.

It could run for 10 hours at 20 mK with a heat load of  $\sim 1 \mu\text{W}$ . About  $1 \text{ cm}^3$  of liquid  $^3\text{He}$  is required for 1 hour of run time. Therefore, the DR is scalable to a point; eventually the required quantity of  $^3\text{He}$  becomes prohibitive.

A single-cycle DR of this type would seem to be the most obvious approach for an SI cryostat. The DR could be precooled by the 4 K stage of a two-stage PT or GM. A micro-gravity version, with demonstrated tiltability, was later developed at NASA ARC (Roach, 1999).

## 8.26 Tiltable Single-Cycle DR

This single-cycle DR depicted in Figure 8.26-1 was developed at the University of Manchester (Melhuish, 2013) for ground-based and balloon-borne astrophysical applications and was required to operate at cryostat tilts of up to 60°. It appears to have only been demonstrated in a laboratory environment

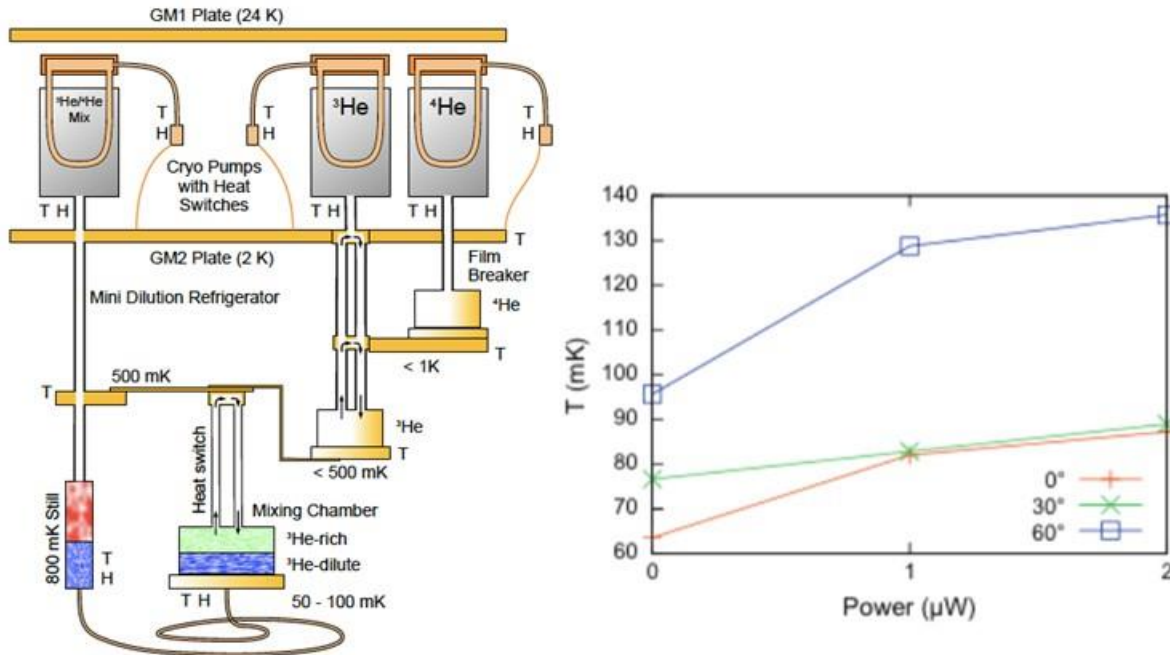


**Figure 8.26-1. A tiltable DR developed for astrophysical applications.**

It is similar to the RMC refrigerator described in the previous section, with some refinements, including the use of passive <sup>3</sup>He heat pipe diodes, which allow for SR recycling without warming the lower stages.

It was found that if the system was oriented so that the still and mixing chamber remained at the same level while tilting, then the performance of the DR was minimally affected. A cooling power of 1 μW was measured at tilts of 0° and 30°.

Note that the DR is precooled by a two-stage GM cryocooler. Use of a PT cold head, with its lower vibration, would presumably result in some improvement in performance.



## 8.27 Continuously Operating Cold Cycle DR

A cold cycle DR does not require external vacuum pumps and can be precooled by a 4 K PT and a collection of  $^3\text{He}$  and  $^4\text{He}$  SRs.

For SOFIA SI applications, indefinite operation is not required. The DR would need to operate during preflight and during the observation phase of the flight.

The advantage of a continuously circulating DR is that it would require much less  $^3\text{He}$ . This in turn would reduce the size and mass of the mixing chamber, especially if it is partially filled with copper sinter or other porous medium. A mixing chamber is subject to the same vibrational heating as an ADR salt pill. A lighter mixing chamber would be easier to support and mechanically isolate.

A schematic of a novel cold cycle DR (Mohandas, 1994) is shown in Figure 8.27-1. Two sorption pumps are used to alternately pump  $^3\text{He}$  from the still and return it to the mixing chamber. The periodic flow reversals are controlled using cryogenic valves.

A continuous version (Roach, 1998) of the tiltable single-cycle DR was developed at NASA ARC. See Figure 8.27-2. It was designed for micro-gravity operation: fine-pore copper sinters hold the liquids in place. Circulation is driven by the osmotic pressure head and cryopumping at the condenser.

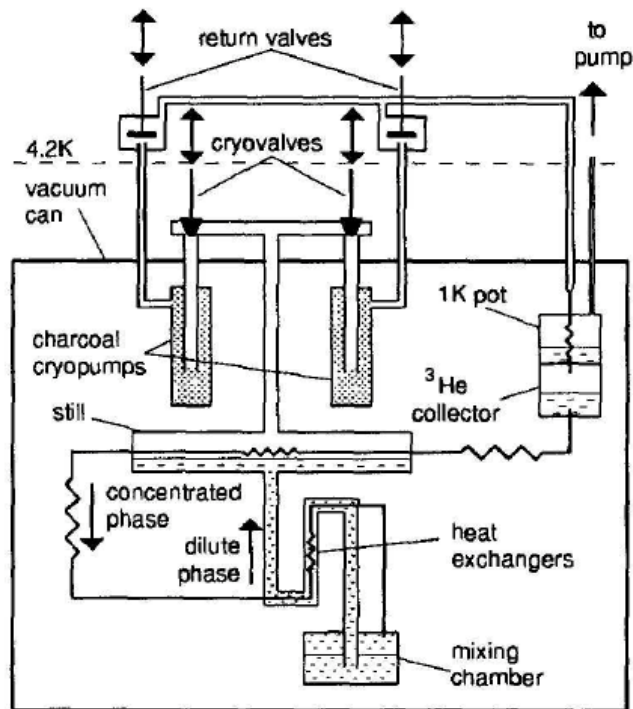


*Figure 8.27-1. A continuously operating cold cycle DR (Mohandas, 1994).*

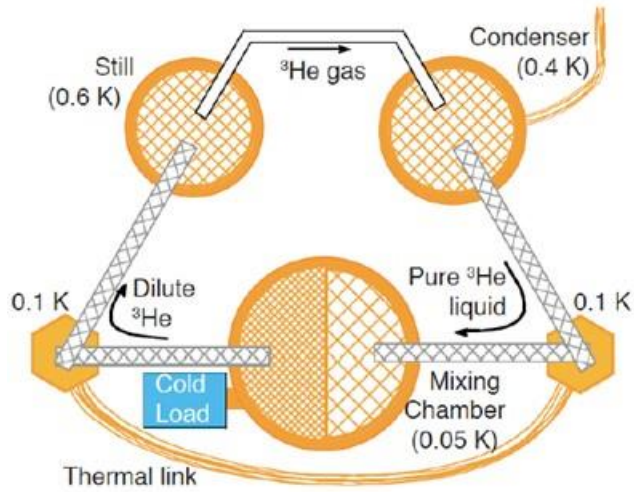


**Figure 8.27-2. A continuously operating cold cycle DR (Roach, 1998).**



**Figure 8.28-1. The MUSCAT DR developed by Chase Research Cryogenics.**

## 8.28 Example: MUSCAT Cold Cycle DR

The Mexico-UK Sub-millimeter Camera for AsTRonomy (MUSCAT) (Brien, 2019) for the Large Millimeter Telescope (LMT) is built around the continuously operating DR (Figure 8.28-1) built by Chase Research Cryogenics. It is supported by a complicated assembly of  $^3\text{He}$  and  $^4\text{He}$  SRs, also built by Chase.

The DR is capable of cooling below 100 mK with a load of  $\sim 3 \mu\text{W}$ , while using only 9 STP liters of  $^3\text{He}$ .

## 8.29 Example: Planck Open Cycle DR

The Institut Neel (Grenoble) and Air Liquide developed a flight DR (Figure 8.29-1) to support the Planck mission. Launched in May 2009, it is the only DR to have flown in space. It operated successfully for 2.6 years. The cooling power at 100 mK was  $0.2 \mu\text{W}$ . The helium flow rate was  $6 \mu\text{moles/s}$  ( $^3\text{He}$ ) and  $18 \mu\text{moles/s}$  ( $^4\text{He}$ ). This was an open cycle system, meaning that the helium mixture was vented to space. This design is obviously not an option for SOFIA SI application. A continuous, closed cycle version is currently in development.

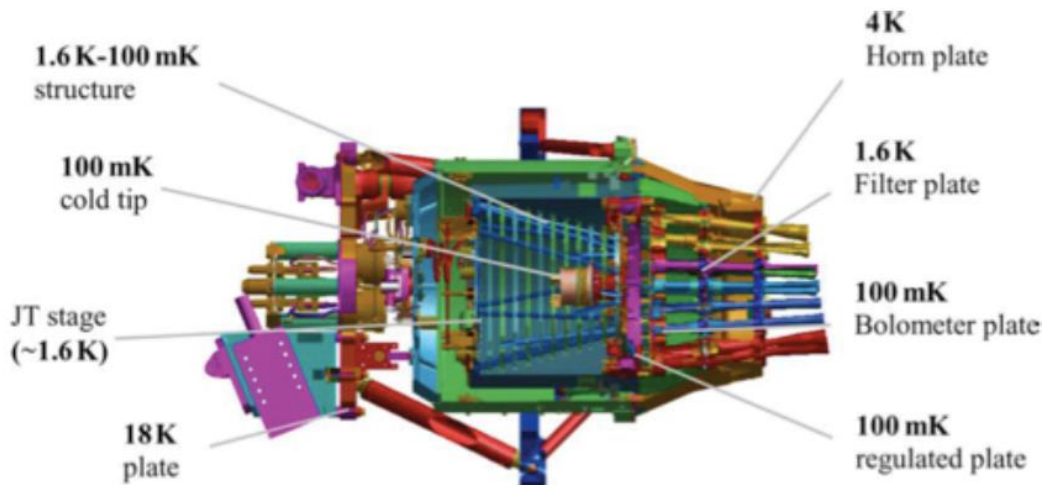


*Figure 8.29-1. Planck open cycle DR developed by Institut Neel and Air Liquide (Ade, 2011).*

## 8.30 Heat Switches: Overview

Low temperature heat switches are important components in many cryogenic applications. As discussed, for SI applications (HAWC+ and HIRMES) they are used in conjunction with single-cycle refrigerators (ADRs and SRs), to make and break thermal contact with a heat sink for pumping / recycling.

For the SI developer, some important factors to be considered in the selection of a switch are:

- Its operating temperature range;
- The on/off switching ratio;
- The actuation method (reliability and thermal dissipation);
- Its mass and size;
- Its sensitivity to vibrational loads;
- Its sensitivity to tilt; and

- Availability: most of the variants discussed are commercially available.

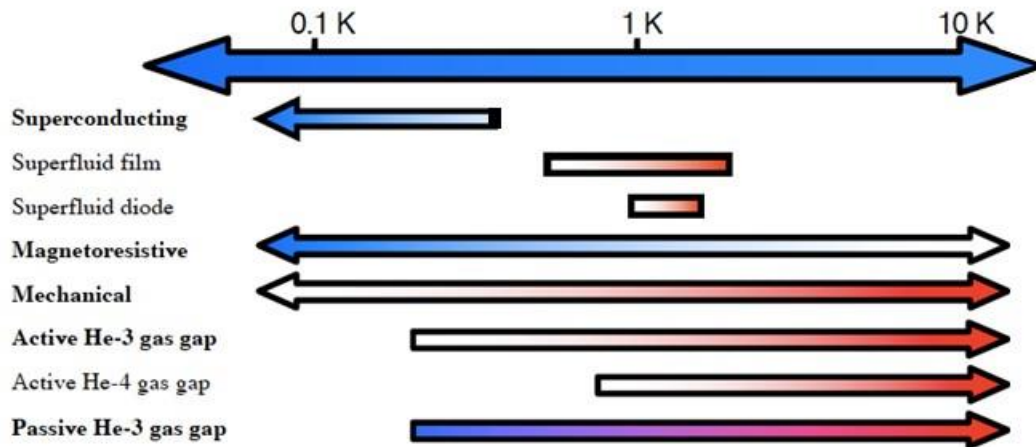


*Figure 8.30-1. Various cryogenic heat switches with ranges of applicability.*

### 8.31 Mechanical Heat Switches

Shown in Figure 8.31-1 is a mechanical switch used for HIRMES to connect the ADR salt pill to the 1 K heat sink.

Mechanical heat switches work by making and breaking a mechanical high thermal conductance contact. The contact must have a considerable force between thermally conductive surfaces. For the contacting surfaces gold-plated copper is the most suitable material.

These switches have fast switching times and a very high on/off conductance ratio.

There are a variety of actuation approaches, including stepper motors, piezoelectric or magnetostrictive actuators, shape memory alloys, etc.

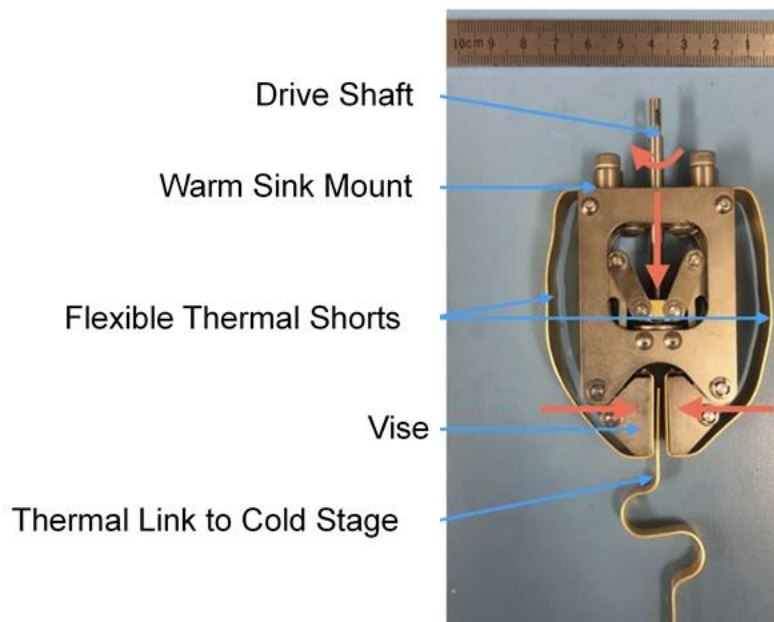


*Figure 8.31-1. Mechanical heat switch as used in HIRMES.*

### 8.32 Gas Gap Heat Switches

Gas gap heat switches (Figure 8.32-1) have been developed for operation at various temperatures. In all of these the thermal conduction is controlled entirely by variation of the gas pressure within a narrow gap between two mating surfaces (usually copper). At modest pressures, the gas is in the continuity regime where its thermal conductivity is relatively high and independent of pressure. The heat flow across the gap is inversely proportional to the gap width, thus calling for a narrow gap. At sufficiently low pressure the gas enters the free molecular regime where thermal conductivity is low and linearly proportional to both the gap width and the pressure. Consequently, the heat flowing across the gap in the off-state is independent of the gap width, but proportional to the gas pressure. Thus, a high level of isolation requires ultra-low off pressure, which limits how narrow the gap can be so as not to preclude rapid pump-out of the gas. Setting the pressure in gas gap heat switches is often controlled with a sorption pump that employs a material such as activated carbon, which when cold adsorbs the gas; upon heating, the gas is released.

Operation of the pump merely requires an electrical heater and a weak thermal link to cool it back down. Gas-gap heat switches with on/off transition times of less than 1 minute have been developed.

For very low temperature applications it is critical to minimize the off conductance of a gas gap switch. Several approaches have been devised for the switch shell that contains the gas to meet this requirement. One such approach developed for the Hitomi (Astro-H) mission is a shell using welded Ti 15-3-3-3. This material has a superconducting transition temperature near 3.8 K resulting in a very low thermal conduction at lower temperatures.

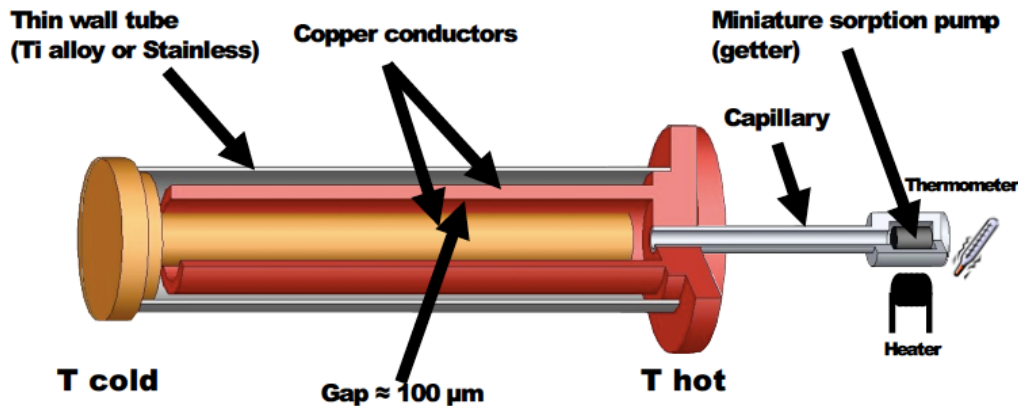
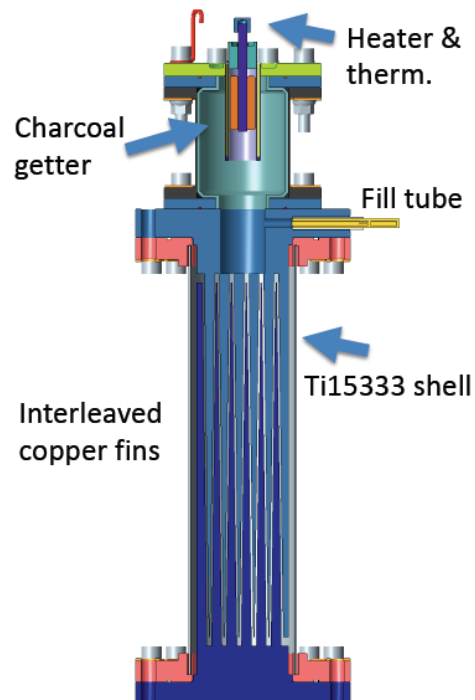


Figure 8.32-1. Gas gap heat switch.

### 8.33 Example: Astro-H Gas Gap Heat Switch

Some characteristics of this switch (Figure 8.33-1) are:

- Low conductance between the getter and the switch body. It requires only 0.3 mW to reach 10 K.
- The low mass getter reduces turn on/off time to less than 60 seconds.
- The superconducting Ti 15-3-3-3 shell has an extremely low off state conductance below 1 K.



*Figure 8.33-1. The Astro-H gas gap heat switch.*

### 8.34 Passive Gas Gap Heat Switch

In a passive gas-gap heat switch (Figures 8.34-1 and 8.34-2) the heated sorption pump is replaced by a passive getter that is placed at the cold side of the heat switch. In the OFF mode the gas is adsorbed at the cold end of the switch by the cold getter. The switch turns ON when the getter is warmed up to an activation temperature  $T_{ON/OFF}$ , which can be between 0.2 K to > 20 K.

The pressure in the switch is a strong function of the getter temperature. Depositing thin frozen gas ( $H_2$ , Ne) films onto the getter substrate changes the binding energy; this allows for the ability to tune the heat switch performance for a specific application.

Some advantages of a passive gas gap heat switch:

- No control electronics.
- Practically instantaneous transition between on / off states.
- No thermal dissipation.



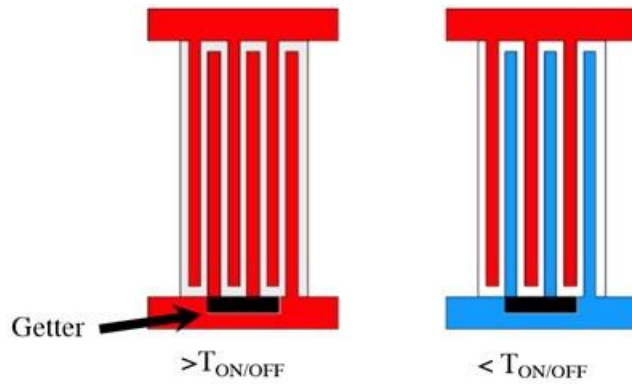


**Figure 8.34-1. Passive gas gap heat switch. Left: ON; Right: OFF.**

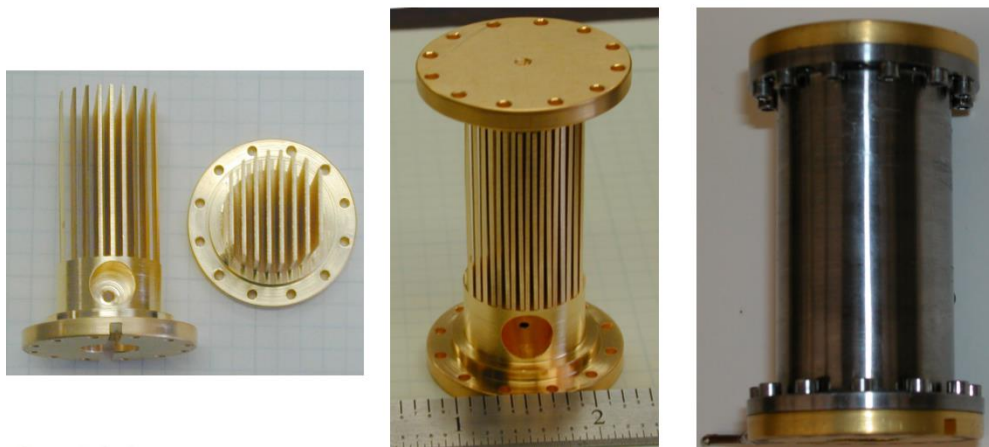


**Figure 8.34-2. Passive gas gap heat switch. Fully disassembled on the left; fully assembled on the right.**

### 8.35 Thermal Straps

*Metal Thermal Straps.* Because of their high thermal conductivity and desirable mechanical properties, metal thermal straps are made from aluminum foil or copper in wire or foil form. They are most useful in low-temperature applications (below 100 K) and are sometimes used at warmer temperatures when mass is not a significant performance driver.

*Carbon, Graphite, or Graphene Thermal Straps.* Carbon-based materials have lower density and higher thermal conductivity than copper or aluminum at temperatures above  $\sim 100$  K. High conductivity carbon materials (in the form of pyrolytic graphite or graphene) have been commercially available in fiber and sheet configurations. Recent developments in graphene have led to carbon materials that have better thermal and mechanical properties as compared to fibers. If density is taken into consideration, there is an even more dramatic benefit to the carbon-based materials for straps.





*Figure 8.36-1. Commercially available carbon, copper, and aluminum thermal straps.*

## 9.0 Thermal Conductance at Low Temperatures

### 9.1 Thermal Conductivity of Aluminum and Copper: Overview

Metals with high thermal conductivity are copper, aluminum, silver, and gold. Aluminum provides the highest conductance per unit mass, making it attractive in aerospace applications where mass must be minimized.

Aluminum has two drawbacks at low temperatures. Below 1.2 K, aluminum becomes superconducting; superconductors are poor thermal conductors. It is also hard to make good thermal contact to aluminum because of the insulating oxide layer which forms rapidly on bare aluminum surfaces; the effect of the oxide layer is much greater at low temperatures than near room temperature.

Copper is usually used when a good low temperature thermal conductor is required, since it suffers from neither of these problems. In addition, unlike aluminum, it can be used structurally in the pure form. Aluminum alloys can be used structurally but have much poorer conductivity than pure aluminum.

At low temperatures the thermal and electrical conductivity of pure metals varies over many orders of magnitude, depending on the temper (history of cold work and annealing) and chemical purity.

Measurements of single samples of copper and aluminum, either made directly, or obtained from literature are often used for design. Due to the large variation possible between samples, this can lead to poor design assumptions.

Aluminum offers the advantages of better availability in high purity form, lower density, less reduction of conductivity by deformation and no requirements for annealing in vacuum. For cryogenic thermal links above 1.2 K, it is necessary to use of Five-Nine (5N) pure copper with

good conductivity, to be able to oxygen-anneal copper, or to have a method for reliably making good thermal contact to aluminum.

Gold plating and various types of welding help overcome oxidation of aluminum. However, gold-plating aluminum is not necessarily reproducible, and welding is not always practical.

At sufficiently low temperatures, the thermal conductivity of aluminum or copper is a linear function of temperature. To good approximation, the electrical resistivity is constant over a similar temperature range; the constant value is known as the residual resistivity. The low temperature conductivity of a given sample can be categorized by the thermal conductivity at a particular temperature or the residual resistivity, or rather the residual resistance ratio, RRR—that is,

$$RRR = R_{room\ temperature} / R_{residual} = R_{300\ K} / R_{\rightarrow 0\ K}.$$

(Source: Woodcraft, 2005).

## 9.2 Thermal Conductivity of Copper as a Function of RRR

Electrons in metals are primarily responsible for electrical and thermal conduction.

In most metals, the thermal conductivity  $k$  increases with decreasing temperature due to decreasing interactions between charge carriers and lattice vibrations.

At around 20 K,  $k$  reaches a maximum and then begins to fall off. In this low temperature regime, impurities and lattice defects become the dominant factors in determining the electrical and thermal resistance.

There is a strong correlation between electrical and thermal conductivity, so the RRR value is often used as an indicator of the thermal conductivity (Figure 9.2-1).

In a copper thermal conductor, there is a strong dependence on the history of annealing and cold working. At low temperatures  $k$  can vary by orders of magnitude. *Even minimal cold working of a copper strap can significantly decrease its thermal conductance.*

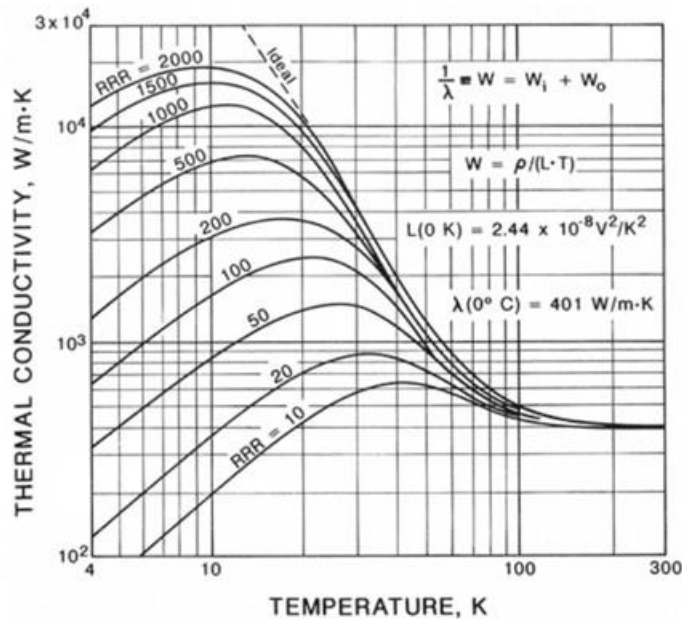


*Figure 9.2-1. Thermal conductivity of copper: Dependence on residual resistance ratio RRR.*

### 9.3 Effects of Annealing on Thermal Conductivity

For each purity range and condition, there is considerable scatter in the values of thermal conductivity. For the annealed samples the difference may be in purity of the original material and/or in the annealing conditions. It is established that the improvements due to annealing depend on annealing time and temperature.

There are conflicting results concerning annealing of aluminum. For aluminum no improvement in RRR was seen for 5N purity by annealing in vacuum. Air annealing is found to produce higher RRR values than vacuum annealing for anneal times of a few minutes, but for longer times, vacuum annealing produced better results in another work.

Even for 5N purity aluminum results, for samples obtained from different sources, the thermal conductivities do not seem to correlate with the annealing conditions. It seems likely that the annealing conditions are not the dominant cause of the scatter in the data. Material purity or perhaps the types of internal impurities or external contamination introduced by the annealing furnace are probably more important.

The conductivity of copper can be improved by annealing at temperatures just below the melting point in the presence of trace quantities of oxygen, a process usually known as oxygen annealing. It is well established that significantly higher conductivity values can be produced than by vacuum annealing. While the exact mechanism is not certain, the improvement seems to largely come about by reducing the effect of impurities.

RRR values of over 2000 could be produced by oxygen annealing copper samples with an initial RRR as low as 5.

Thermal conductivity values for 5N purity vacuum-annealed and oxygen-annealed copper at a temperature of 1 K are plotted in Figure 9.3-1. The results labelled 'other' are for copper samples that were cold worked before measurement, or where the heat treatment is unknown. The

annealed aluminum values are shown. The error bar shows the range of results obtained for copper from a single supplier over time.

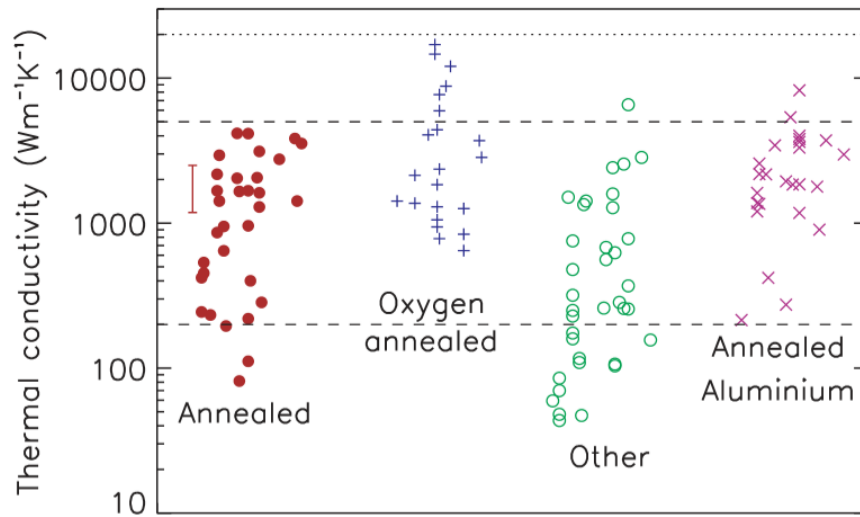


**Figure 9.3-1. Thermal conductivity values for 5N purity vacuum-annealed and oxygen-annealed copper at a temperature of 1 K. (Woodcraft, 2005).**

In Figure 9.3-1, the values for annealed copper cover a larger range than for aluminum. This is probably due to the large reduction in conductivity caused by even a few ppm (parts per million) of magnetic impurities in copper. Since the 5N specification only describes the total impurity content and not the quantity of individual elements, different samples of the same purity range can have variable conductivities. The amount of magnetic impurities is likely to depend on the copper ore used and the purification process, suggesting that the range of conductivity values of material produced by a given supplier will be smaller. This explains why samples from a single supplier over a period of 10 years were found to have RRR values which varied only between 900 and 1900.

Oxygen-annealed copper samples are likely to show much less sample to sample (and supplier to supplier) variation than vacuum annealed copper. Oxygen annealing is not a process that is generally offered commercially. It should be noted that oxygen annealing is not a useful method for improving the conductivity of aluminum.

The lower density of aluminum gives it a considerable advantage, but for temperatures below 4 K, oxygen annealed copper can outperform 5N aluminum.

(Source: Woodcraft, 2005).

### 9.4 Thermal Conductivity of Aluminum and Copper: Summary

For both copper and aluminum, 5N is the highest purity that is readily available. The range of conductivity values for annealed 5N copper is somewhat greater than that for aluminum, with the upper limits being similar.

Much of the variation for copper is likely to be due to the use of different ore and processing methods, and the variation for samples from a given manufacturer is probably considerably smaller. If a source of 5N copper with consistently high conductivity can be found, then 5N aluminum and copper can be assumed to have similar conductivity.

Oxygen-annealing of copper can give conductivity values somewhat higher than for aluminum of the same purity.

The conductivity of oxygen-annealed copper is likely to be much less sensitive to the copper source than vacuum-annealed copper, reducing the need to choose an appropriate supplier. This process is not generally offered commercially.

Copper has the advantage that it is relatively easy to make good thermal contact; it is more difficult for aluminum, where there is no established procedure.

(Source: Woodcraft, 2005).

## 9.5 Thermal Contact Resistance: Constriction

Thermal contact resistance depends on the applied force and *not* the apparent contact area. This is because thermal contact resistance is determined by the actual area of physical contact (i.e., the area available for heat transfer).

Constriction thermal resistance (Figure 9.5-1) arises when pressed solids make physical contact at the microscopic surface asperities and heat is constricted to flow across these contacts. It is due to thinning of the heat flow channels at the contacting asperities.

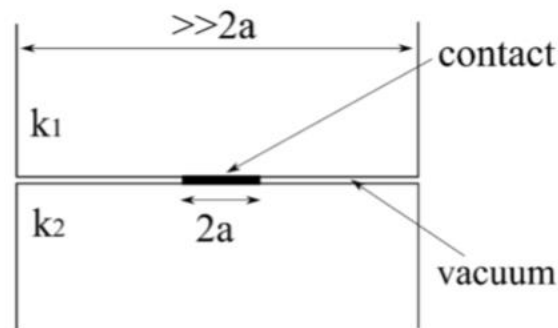


*Figure 9.5-1. Two solids with thermal conductivities  $k_1$  and  $k_2$  making contact over a circular region of radius  $a$ . (Dhuley, 2019).*

Some aspects of thermal constriction resistance:

1. Geometry: How two surfaces touch each other on the microscopic level at the surface asperities.
2. Mechanical: Deformation of the contacting asperities is characterized based on surface hardness, material elastic modulus, and applied pressure.
3. Thermal: Equation for heat diffusion through the narrow contacting asperities.

(Source: Dhuley, 2019).

## 9.6 Thermal Contact Resistance: Thermal Boundary

The second component of thermal contact resistance deals with the interaction of the heat carriers with the physical boundary of the contacting solids.

This component is usually insignificant for contacts at room temperature. The mean free path of the heat carriers is small compared to the asperity size and the definition of thermal conductivity in the diffusion limit is valid.

At cryogenic temperatures, the mean free path of the heat carriers can become comparable to the asperity size and there can occur ballistic transport or scattering at the physical interface.

(Source: Dhuley, 2019).

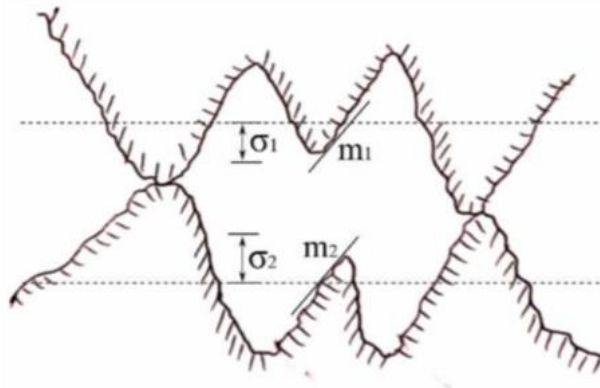


**Figure 9.6-1. Contact of two surfaces at a microscopic level ( $\sigma$  is the surface roughness and  $m$  is the asperity slope).**

## 9.7 Thermal Boundary Resistance Models

For contacts where phonons carry heat across the interface, the phonons are assumed to transmit either in a specular or a diffuse manner.

For the specular case the acoustic mismatch model (AMM) of interfacial thermal resistance has been developed. This prevails at very low temperatures, typically below 1K where the dominant phonon wavelength is large (several mm) compared to the surface roughness of practical finishes (several micrometers).

At higher temperatures, the phonon wavelength may become comparable to the surface roughness and in this case, it is hypothesized that the interface would diffusively transmit the phonons. This is described by the phonon diffuse mismatch model (DMM).

The DMM methodology for phonons is employed at an interface between two metals to describe thermal resistance of electrons carrying heat diffusively.

The total resistance to heat flow is due to the constrictions and the physical interface between contacting surfaces. Thus, adding these resistances in series gives the total thermal contact resistance for a joint made of the same material.

(Source: Dhuley, 2019).

## 9.8 Thermal Contact Resistance at Room Temperature

Figure 9.8-1 shows the contact conductance of various alloys of aluminum and copper at room temperature. The variation in the measured data shows how challenging it is for any model to predict contact resistance of most practical metal contacts.

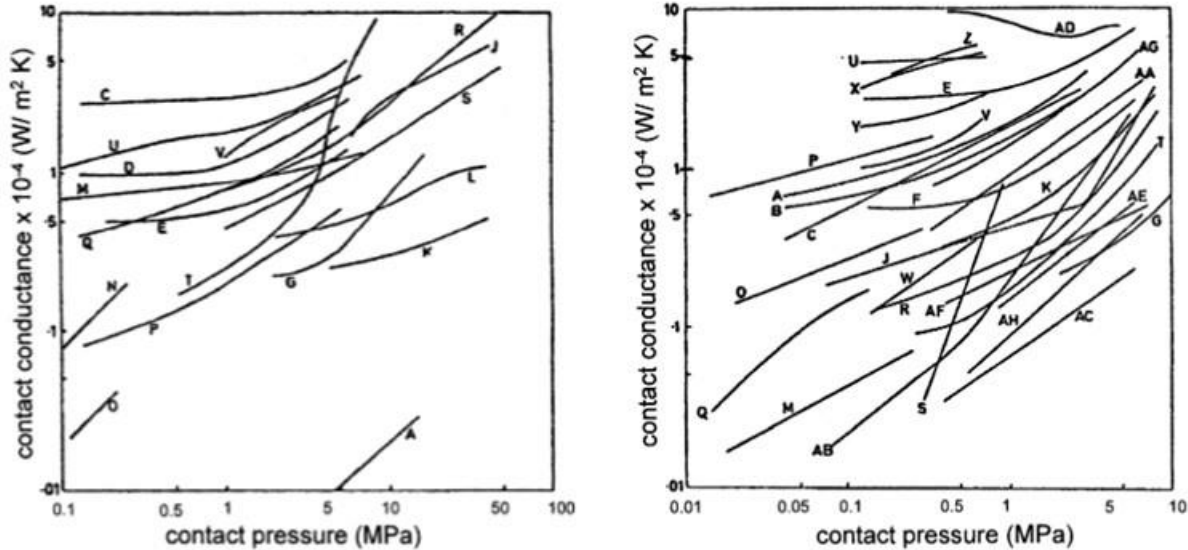


*Figure 9.8-1. Contact conductance of copper (left) and aluminum (right) alloys near room temperature. (Yovanovich, 2005; Lambert, 1997).*

## 9.9 Thermal Contact Resistance at Low Temperatures

The temperature dependence of the contact resistance of metallic joints depends on the surface condition and electron wavelength.

At 4.2 K, in a copper-copper joint made of OFHC copper, the constriction and thermal boundary resistance contributions are expected to be comparable. If the metallic surfaces are clean of surface oxides, the contact resistance follows a  $T^{-1}$  dependence similar to the bulk thermal resistance. In case the oxide layer is thick enough not to allow passage of electrons but thin enough to be transparent to phonons, the contact resistance will be governed by the phonon thermal conductivity of the metal, which varies as  $T^{-2}$ .

In several experiments, the contact resistance across copper-copper pressed contacts is seen to follow a power law  $T^n$  where  $1 < n < 2$  depending on surface cleanliness. However, due to a native oxide layer on copper,  $n$  is expected to be close to 2. Finally, when the oxide thickness is much greater than the phonon wavelength in the metal, the contact resistance is determined by the bulk thermal conductivity of the oxide.

Gold plating of copper is an effective approach to preventing surface oxides and achieving electronic thermal conductance across pressed contacts. The native surface oxide of gold breaks at low applied load giving a larger probability of achieving a metallic contact. The thermal resistance for gold-plated copper-copper contacts vary as  $T^{-1}$ , which is a signature of clean metal-metal contacts.

(Source: Dhuley, 2019).



## 9.10 Copper Contact Conductance with Several Interface Materials

Use of interface materials such as indium foil, thermal grease, gold plating can enhance the contact conductance at the interface of pressed contacts between 2 and 20 K (Figure 9.10-1) and between 40 and 90 K (Figure 9.10-2).

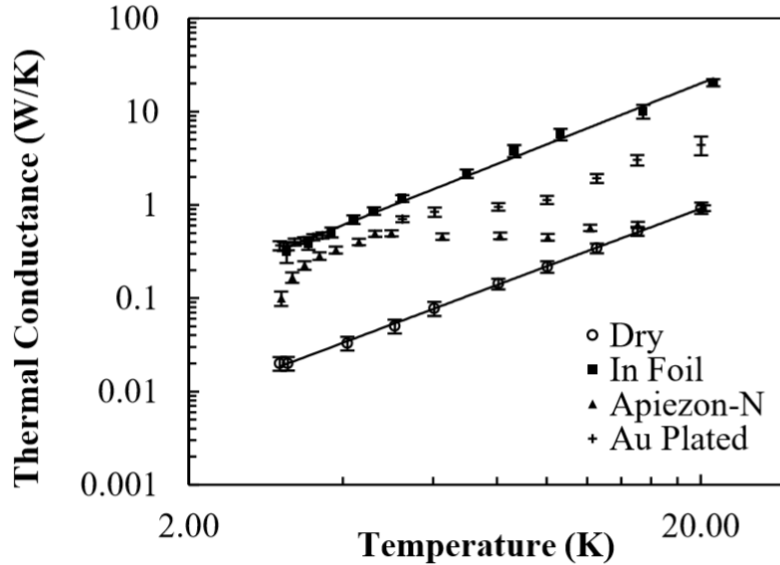


*Figure 9.10-1. Copper-copper pressed contact conductance between 2 and 20 K using various interface materials. (Dillon, 2017).*

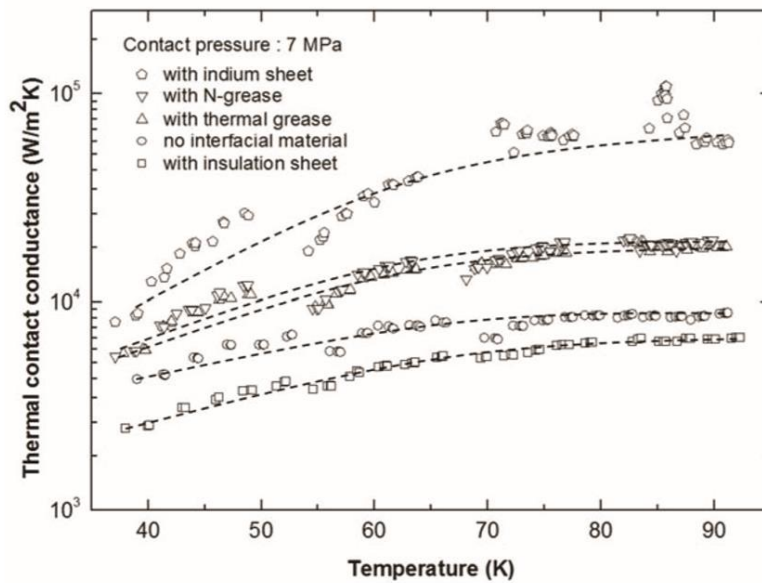


*Figure 9.10-2. Copper-copper pressed contact conductance between 40 and 90 K using various interface materials. (Choi, 2014).*

**Table 9.10-1. Contact resistance values of bolted joints at room temperature. (Gluck, 2002).**

Bolt	Diam (mm)	Resistance Values from Several Sources ( $^{\circ}\text{C}/\text{W}$ ) <sup>a</sup>					TRW Small Stiff Surfaces <sup>b</sup>
		TRW Large Thin Surfaces <sup>b</sup>	LM Plate Thickness (mm) <sup>c</sup>				
			(1.57)	(3.18)	(6.35)	(9.53)	
2-56	—	9.48	—	—	—	—	4.74
NC 4-40	2.8	7.59	12.6	—	—	—	3.79
NC 6-32	3.5	5.69	6.61	2.2	—	—	2.37
NC 8-32	4.2	3.79	4.5	1.5	0.75	—	1.25
NF 10-32	4.8	1.90	3.0	1.0	0.5	0.333	0.76
NF 1/4-28	6.4	0.95	2.1	0.7	0.35	0.233	0.28
NF 5/16-24	7.9	—	1.5	0.5	0.25	0.167	—
NF 3/8-24	9.5	—	—	0.39	0.194	0.128	—
NF 7/16-20	11.1	—	—	—	0.16	0.106	—
NF 1/2-20	12.7	—	—	—	—	0.089	—

<sup>a</sup>Bolted aluminum interface in vacuum, bare clean mill rolled surface finish (LM), standard steel bolts torque to specification (LM), primary heat transfer through compressed area near bolt (LM).

<sup>b</sup>TRW, March 1984.

<sup>c</sup>LM, George D. Rhoads, 20 July 1988.

### 9.11 Copper Contact Conductance of Bolted Joints

At the macroscopic level, bolted plates deform elastically, as shown in Figure 9.11-1. Separation of plates (exaggerated in the figure) occurs and at relatively small distances from the bolt. The bolted-joint problem can be considered the contact conductance problem for a non-uniform interface pressure.

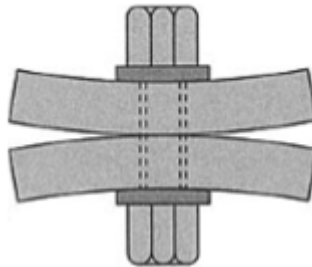


**Figure 9.11-1. Exaggerated depiction of elastic deformation in bolted plates. (Gluck, 2002).**

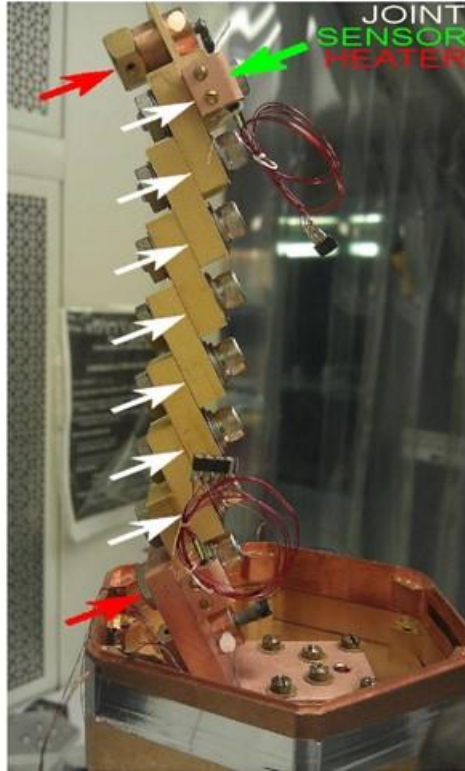


**Figure 9.11-2. Experimental set-up for measuring the contact resistance of bolted joints at cryogenic temperatures. (Schmittab, 2005).**

In one study (Schmittab, 2005) bolted joints were set up and measured at cryogenic temperatures as follows:

- Seven gold plated single screw joints in series (as shown in Figure 9.11-2):
    1. Between 60 mK and 130 mK using a DR
    2. Between 5.9 K and 26.4K using a PT cryocooler
    3. Between 190 mK and 1 K using an ADR
    4. Between 6.8 and 8.9K using a PT
  - One gold plated single screw joint between 100 and 470 mK using an ADR.
  - One gold plated single screw joint between 4.0 and 14.0 K using a PT.
  - One gold plated six-screw joint between 3.6 and 9.4 K using a PT (results obtained for this test are presented on a per screw basis).
- Bolted-joint specifications:
- Non-annealed HDHC (hard drawn, high conductivity) copper was used.
  - Machining to 0.002-inch flatness, 16 $\mu$ -inch surface finish for test group A, 8  $\mu$ -inch surface finish for test groups B through D.
  - Gold plating for test groups A through D was 20  $\mu$ -inch thick over a 50  $\mu$ -inch layer of nickel.
  - All tests used #10-32x 0.75 in 316 stainless steel socket head cap screws with a #10-32 18-8 stainless steel machine screw hex nut tightened to 25 in-lbf (estimated clamping force of 3 kN).

- Two nested 0.190-inch ID, 0.375-inch OD, 0.020-inch-thick 110 lbf flat load 300 series stainless steel Belleville washers were used with each screw to maintain the bolt preload as the temperature decreased.
- #10 screw size, 7/16-inch OD, 316 stainless steel flat washers were used in between the Belleville washers and the copper surfaces to prevent surface scours as bolt load is applied.

Contact conductance test results of the bolted joints at cryogenic temperatures are shown in Figure 9.11-3. The relationship  $K = 0.1161 * T^{1.1111}$  is an acceptable fit to the results obtained for tests A through D (Figure 9.11-3).

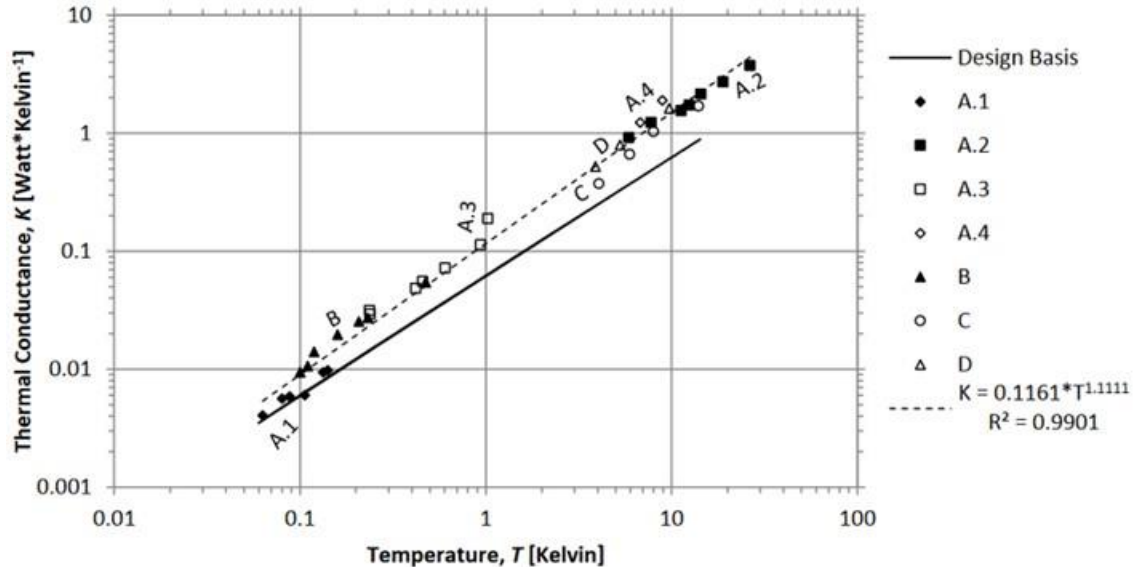


Figure 9.11-3. Measured contact resistance values of bolted joints at cryogenic temperatures. (Schmittab, 2005).

## 10.0 Summary of Cryogenic Technologies and General Guidance

### 10.1 PT and GM Refrigerators

PT and GM refrigerators are reliable COTS components. A wide range of cold heads from various manufacturers are compatible with the SOFIA Cryocooler System's compressors and helium flex lines. PTs and GMs are continuous cycle refrigerators.

- **Required for dry cryostats.** Replaces the LN<sub>2</sub> and LHe reservoirs of a traditional wet cryostat.
- **Only two-stage refrigerators are considered:** The high-capacity first stage cools the thermal radiation shield that envelops the colder stages and provides a heat sink for support structures, piping, and wiring. The second, nominally 4 K stage cools the instrument itself (e.g., the GREAT cryostats) or pre-cools colder stages (e.g., SRs, magnetic, or DRs).
- **Mechanical components?** Yes. Both employ room temperature valves that operate at ~ 1 Hz. Vibrational input to the cryostat can be reduced by selecting the remote motor option

offered by most manufacturers. In addition, the GM refrigerator contains a displacer within the cold head, which also oscillates at ~ 1 Hz.

- **Vibrational source?** Yes, for both, but lower for the PT. For this reason, designers tend to shy away from GMs. However, this factor should be weighed against the GM's advantages (lower cost and insensitivity to tilt).
- **Environmental temperature sensitivity?** No, within SOFIA operational parameters.
- **Potential safety issues?** Yes: Both types contain pressurized helium gas, and may require retrofitting with pressure relief valves, depending on internal configurations. As with all components, they require Airworthiness Certification. Thus far, only TransMIT PTs have been used for SOFIA SIs. Use of the same may simplify certification, but this should be weighed against possible advantages (e.g., performance, mass, and power requirements) of other manufacturers' products.
- **Sensitivity to cryostat tilt?** GM: None. PT: Yes, but typically acceptable, given proper margin control. Tilt dependence is readily measured, and manufacturers may have data available upon request.
- **Maturity and SOFIA flight heritage:** Many commercial models, compatible with the on-board Cryomech compressors, are available (e.g., TransMIT, Cryomech, Sumitomo). They require little to no modification. TransMIT PTs have flown (GREAT).
- **TRL 9- :** May require modifications or "tuning" to maximize performance when paired with on-board compressors.

## 10.2 $^4\text{He}$ and $^3\text{He}$ SRs

A SR can be used to directly cool an instrument, intercept heat leaks to magnetic or DRs, or precool a DR stage. Both types reject heat to the 4 K stage. For most SI applications, a single-cycle version would be the logical choice because of its simplicity, sufficiently long hold time, and high duty cycle.

- **Mechanical components?** None.
- **Vibrational source?** No.
- **Environmental temperature sensitivity?** No, within SOFIA operational parameters.
- **Potential safety issues?** Yes: Contains pressurized gas when warm. However, the working fluid is entirely contained within the unit (i.e., external expansion chambers are not required).
- **Sensitivity to cryostat tilt?** Yes, but typically acceptable, given adequate margin control. Tilt dependence is relatively easy to measure, and manufacturers may have in-house data available upon request.
- **Maturity and SOFIA flight heritage:** A  $^4\text{He}$  SR has flown on HAWC+, and both  $^4\text{He}$  and  $^3\text{He}$  SRs are slated to fly on HIRMES. The go-to commercial source has been Chase Research Cryogenics, although other manufacturers, such as Oxford Instruments, possess the expertise to build custom units as well. Chase has also built continuously operating 1 K and 300 mK SR systems, as have other cryogenics laboratories around the world. The

SI developer should not rule out such systems, as they could simplify the operation of the cryostat.

- **TRL 4 – 9- :** TRL 9- if Chase SRs are used that are of the same design as those used on HAWC+ and HIRMES, although modifications may be required to tailor to the specific application. If a substantially different design is required, or if another manufacturer is contracted, then it is likely that, at best, only laboratory validation will have been performed.

### 10.3 ADRs

The ADR is the only technology that has been used to reach sub-100 mK temperatures in SOFIA SIs. Only single-stage versions have been used. The SI developer might consider multi-stage configurations if higher capacities are required. As the ADR uses a superconducting magnet, magnetic shielding may be required.

- **Mechanical components?** None. HIRMES uses a mechanical heat switch, but it is not actuated during the ADR hold time.
- **Vibrational source?** No.
- **Environmental temperature sensitivity?** Possibly, depending on the refrigerant (salt pill material). The SI developer should review SOFIA thermal data, especially for the cargo hold. *Excessive heat can damage the pill.*
- **Potential safety issues?** None.
- **Sensitivity to cryostat tilt?** None, except insofar as it may affect the vibrational spectrum. The authors are unaware of any such problem having been observed.
- **Maturity and SOFIA flight heritage:** An ADR flew with the HAWC+ SI; it was designed and built by NASA GSFC. A similar ADR was developed for HIRMES; it was built by HPD with input from NASA GSFC. Both projects faced difficult challenges, especially those related to vibrational heating.
- **TRL 4 – 9- :** TRL 9- if the ADR is of the same design as that used on HAWC+, or on HIRMES. However, the SI developer would want to incorporate lessons learned, and that could require extensive modifications.

### 10.4 DR: Overview

A DR could be used instead of an ADR to reach sub-100 mK temperatures. Thus far they have not been used for SOFIA SIs. Compared with the ADR, its advantages and disadvantages are:

**Advantages:** (1) Magnetic shielding is not required. (2) Potential to reach lower temperatures and/or higher capacities.

**Disadvantages:** (1) May require expansion chambers outside the cryostat, which could complicate Airworthiness Certification. (2) The maturity level is lower.

#### Variants:

**DR 1:** Circulating  $^3\text{He}$ , warm continuous cycle.

**DR 2:** Pumped  $^3\text{He}$ , cold single-cycle.

**DR 3:** Circulating  $^3\text{He}$ , cold continuous cycle with reciprocating sorption pumps and cryovalves.

**DR 4:** Circulating  $^3\text{He}$ , cold continuous cycle with osmotic pumping.

**DR 5:** Circulating  $^4\text{He}$ , cold continuous cycle with fountain effect pump.

**The following apply to all variants, with exceptions noted.**

- **Mechanical components?** None, except for DR 1 (external  $^3\text{He}$  pump), and DR 3 (two cryovalves operating at very low duty cycle).
- **Vibrational source?** No, except for DR 3 (level of vibration unknown).
- **Environmental temperature sensitivity?** No, within SOFIA operational parameters.
- **Potential safety issues?** Yes, all variants contain pressurized gas when warm. Because of the relatively large quantity of working fluid required, variant DR 2 might require expansion chambers outside the vacuum shell. This could complicate Airworthiness Certification.
- **Sensitivity to cryostat tilt?** Yes, all variants; but should be acceptable, given adequate design and margin control.
- **Maturity and SOFIA flight heritage:** Prototypes of all variants have been tested successfully in laboratory environments. Variants DR 2 and DR 4 have been subjected to tilt, with performance degradation measured. Commercial models of all variants, except for DR 3 and 5, have been developed. The expertise required to develop a custom DR exists within a number of long-established companies, including Oxford, Janus, Chase, and HPD. As mentioned, no DRs have flown on SOFIA. Only one DR has flown in space, but it was an open-cycle design, and therefore not appropriate for SOFIA SO application.
- **TRL 4 – 6- :** Prototypes of variants DR 2 and 4, with sizes and capacities appropriate for SI applications, have been successfully tested in laboratory environments while subjected to tilts beyond the required  $\pm 20^\circ$ . None have been subjected a simulated SOFIA vibrational environment. Any existing prototype design would need to be modified with appropriate mechanical suspension.

## 10.5 DRs: Discussion of Variants

**DR 1:** Circulating  $^3\text{He}$ , warm continuous cycle.

Implementation of such a system would require the use of an external mechanical pump, as with the FIFI-LS SI, which used the SOFIA Vacuum Pump System. However, a dedicated, sealed  $^3\text{He}$  pump would need to be installed. In addition, a pumping and return line, running between the cryostat and the pump around the CLA, would be required as well. This would result in a pumping line with a high flow impedance, so it is not clear whether this approach could achieve lower temperatures or higher capacities than the other variants. *This is the only DR option discussed that would require modifications to the SOFIA platform.*



**DR 2:** Pumped  $^3\text{He}$ , cold single-cycle.

This is the simplest option, requiring only four liquid chambers and three sorption pumps. Its only disadvantage is that in order to achieve the required hold time, a large quantity (compared with the circulating options) of working fluid is necessary. This could result in a bulky and heavy mixing chamber. In addition, an external expansion chamber, at least for the  $^3\text{He}/^4\text{He}$  mixture would likely be needed.

**DR 3:** Circulating  $^3\text{He}$ , cold continuous cycle with reciprocating sorption pumps and cryovalves.

By circulating, and thus achieving continuous refrigeration, the quantity of working fluid in the system can be greatly reduced. This applies to DR 1, 4, and 5 as well. The  $^3\text{He}$  is sorption-pumped as in DR 2. However, two pumps are used: While one is pumping on the mixing chamber, the other is recycling and returning  $^3\text{He}$  to the condenser. Flow is controlled by two cold valves, which could affect reliability. This variant and DR 5 are the lowest TRL options.

**DR 4:** Circulating  $^3\text{He}$ , cold continuous cycle with osmotic pumping.

This variant has no moving parts, is based on proven sorption pumping technology, and Chase Research Cryogenics has built and tested a prototype that is adaptable to an SI. This variant and DR 2 would seem to be the most promising options.

**DR 5:** Circulating  $^4\text{He}$ , cold continuous cycle with fountain effect pump.

Documented reliability issues, low TRL, and a low level of expertise in industry make this an unlikely option.

## 10.6 Heat Switches

Given its high TRL, proven reliability, and reasonably high on/off conductance ratio, the gas gap heat switch is an excellent option. The SI developer should also consider the mechanical clamping switch, which has a higher on/off conductance ratio. More exotic switches might be considered for specialized applications.

**Mechanical components?** Yes, for the mechanical heat switches. These are not actuated while observations are conducted. The gas gap heat switch has no moving parts.

**Vibrational source?** Not during observation.

**Environmental temperature sensitivity?** No, within SOFIA operational parameters.

**Safety issues?** Minimal. The small quantity of working fluid in a gas gap heat switch does not require an expansion chamber.

**Sensitivity to cryostat tilt?** None.

**Maturity and SOFIA flight heritage:** A gas gap heat switch is used with the HAWC+ ADR and HIRMES is using the mechanical switch. No issues have been reported. Both types are commercially available in various sizes.

**TRL 9- :**

## 10.7 General Guidance Concerning SI Cryostat Design

1. The SI developer should adhere to established best practices in cryostat design and fabrication. This requires a broad knowledge base related to the behavior of materials at low temperatures (mechanical properties, thermal conductance, thermal contraction, heat

capacity, outgassing, etc.); multi-layer insulation (MLI) design and layout; heat sinking techniques (i.e., thermal intercepts on support structures, piping, and wiring); potential sources of parasitic heat loads; and refrigeration techniques. Any established low temperature laboratory should possess this knowledge base. Early partnering with such a laboratory will reduce the risk of running into significant challenges during cryostat development.

2. The design process should begin with a clear understanding of the instrument’s thermal requirements, including desired goals and acceptable limits, and all SOFIA-specific constraints, including size, mass, center-of-gravity, safety, etc. For sub-1 K cryostats, special attention must be devoted to the vibrational environment.
3. Thorough trade studies should be conducted, including a wide range of available technologies—at least those technologies discussed in this document.
4. Perform quantitative mechanical analyses (normal mode and forced vibration) as the design and build proceeds. A SME with experience in this field should be brought on as soon as possible.
5. No amount of analysis or modeling can substitute for testing in a relevant environment. A rigorous test campaign should be conducted in parallel with the cryostat development. Components and assemblies should be tested in a simulated SOFIA vibrational environment as soon as is feasible.
6. Conservative thermal margins should be established. This is especially important at very low temperatures. Between room temperature and ~ 80 K, standard margin schemes (Goddard, JPL, military, etc.) can be useful guides. However, below 4 K, it is difficult to systematize thermal margins because of heavily design-dependent factors such as parasitics (which will typically be comparable to the gross refrigeration capacity) and large variations in materials properties. A good example is the thermal conductance of high-RRR copper straps. Cold working of such a strap, even with careful handling, can dramatically lower its conductance. An experienced low-temperature thermal team is critical to navigate development risk versus design conservatism.

## 11.0 Acronyms List

ADR	Adiabatic Demagnetization Refrigerator
AFR	Air Force Base
ARC	Ames Research Center
AFRC	Armstrong Flight Research Center
ALMA	Atacama Large Millimeter/submillimeter Array
CCA	Chromic Cerium Alum
CFHX	Counter-Flow Heat Exchanger
CG	Center of Gravity
CLA	Cable Load Alleviator
CMN	Cerium Magnesium Nitrate
CoC	Certificate of Compliance
ConOps	Concept of Operations
COTS	Commercial-Off-The-Shelf
CPA	Chromic Potassium Alum

CWR	Counterweight Rack
DR	Dilution Refrigerator
ECS	Environmental Control System
EXES	Echelon-Cross-Echelle Spectrograph
FAA	Ferric Ammonium Alum
FC	Frequency Converter
FIFI-LS	Field Imaging Far Infrared Line Spectrometer
FLL	Forward Lower Lobe
FORCAST	Faint Object Infrared Camera for the SOFIA Telescope
FP	Fountain Pump
FS	Factor of Safety
Ge-Ga	Germanium Gallium-doped
GGG	Gadolinium Gallium Garnet
GLF	Gadolinium Lithium Fluoride
GM	Gifford-McMahon
GREAT	German Receiver for Astronomy at Terahertz Frequencies
GSE	Government Supplied Equipment
GSFC	Goddard Space Flight Center
H/W	Hardware
HAWC	High Resolution Airborne Wideband Camera
HDHC	Hand Drawn High Conductivity
HIRMES	High Resolution Mid-Infrared Spectrometer
HMI	Human Machine Interface
HPD	High Precision Devices
HX	Heat Exchanger
ICD	Interface Control Document
IRR	Instrument Readiness Room
IRTS	Infrared Telescope for Space
JT	Joule-Thomson
JWST	James Webb Space Telescope
LHe	Liquid Helium
LMT	Large Millimeter Telescope
LN <sub>2</sub>	Liquid Nitrogen
MD	Mission Director
MS	Margin of Safety
MUSCAT	Mexico-UK Sub-millimeter Camera for Astronomy
NBP	Normal Boiling Point
OFHC	Oxygen Free High Conductivity
MNOP	Maximum Normal Operating Pressure
PID	Proportional Integral Differential
PIF	Preflight Integration Facility
PLC	Programmable Logic Controller
PRV	Pressure Relief Valve
PT	Pulse Tube
PTC	Pulse Tube Cooler (or Coldhead)
PSD	Power Spectral Density

PVS	Pressurized Vessels and Systems
QD	Quick Disconnect
RRR	Residual Resistance Ratio
SI	Science Instrument
SME	Subject Matter Expert
SOFIA	Stratospheric Observatory For Infrared Astronomy
SR	Sorption Refrigerator
STP	Standard Temperature and Pressure
TA	Telescope Assembly
UPS	Uninterruptible Power Supply
VPS	Vacuum Pump System
XRS	X-Ray Spectrometer

## 12.0 References

- Ade, P. A. R., et al., Planck Early Results. II. The Thermal Performance of Planck, *Astronomy and Astrophysics*, 536, A2, 2011.
- Brien, T. L. R., et al., A Continuous 100-mK Helium-Light Cooling System for MUSCAT on the LMT, *Journal of Low Temperature Physics*, preprint.
- Canavan, E. R., et al., A Magnetoresistive Heat Switch for the Continuous ADR, *Adv. Cryo. Eng. B*, 47, 2002.
- Choi, Michael K., et al., Thermal Design and Analyses of Cooling SOFIA HIRMES to 4K Cryogenic Temperature using Cryocooler, 49<sup>th</sup> International Conference on Environmental Systems, 2019.
- Choi, Yeon Suk, et al., Experiments on Thermal Contact Conductance Between Metals below 100 K, *AIP Conference Proceedings*, 1573, 2014.
- Dhuley, R. C., et al., Pressed Copper and Gold-Plated Copper Contacts at Low Temperatures—A Review of Thermal Contact Resistance, *Cryogenics* 101, 2019.
- Dillon, A., et al., Thermal Interface Material Characterization for Cryogenic Electronic Packaging Solutions, *CEC*, 2017.
- DiPirro, M. J., et al., Heat Switches for ADRs, *Cryogenics* 62, 2014.
- Duband, L., et al., Helium Adsorption Coolers for Space, *Proc. 30<sup>th</sup> ESLAB Symp.*, Submillimeter and Far-Infrared Space Instrumentation, 1996.
- Fischer, Christian, et al., FIFI-LS: The Field-Imaging Far-Infrared Line Spectrometer on SOFIA, *Journal of Astronomical Instrumentation* 7, 4, 2018.
- Gluck, D. E. and Baturkin, V., Mountings and Interfaces. In D.G. Gilmore (Ed.), *Spacecraft thermal control handbook*, Vol. I. The Aerospace Press, 2002.
- Harper, Doyal A., et al., HAWC+, the Far-Infrared Camera and Polarimeter for SOFIA, *Journal of Astronomical Instrumentation* 7, 4, 2018.
- Herter, T. L., et al., FORECAST: A Mid-Infrared Camera for SOFIA, *Journal of Astronomical Instrumentation* 7, 4, 2018.
- Heyminck, S., et al., GREAT: The SOFIA High-Frequency Heterodyne Instrument, *Astronomy and Astrophysics*, 2014.
- Kashani, A., et al., Helium Liquid and Gas Gap Heat Switches for Applications at 2 K, *Advances in Cryogenic Engineering* 39, 1994
- Kimball, M., et al., Heat Switches Providing Low Activation Power and Quick Switching Time for Use in Adiabatic Demagnetization Refrigerators, *Adv. Cryo. Eng. B*, 47, 2002.

Kimball, M. O., et al., JOP Conf. Ser. Mater. Sci. Eng., 101, 012157, 2015.

Kittel, P., et al., Thermal Conductance of Gold Plated Metallic Contacts at Liquid Helium Temperatures, *Advances in Cryogenic Engineering* 34, 1987.

Kittel, Peter, et al., *Cryocoolers for Space*, 2004.

Lambert, M. A., et al., Review of Models for Thermal Contact Conductance in Metals, *Journal of Thermophysics and Heat Transfer*, 11, 2, 1997.

Lounasma, O. V., *Experimental Principles and Methods Below 1K*, Academic Press, 1974.

Martins, D., et al., Customizable Gas-Gap Heat Switch, *Advances in Cryogenic Engineering* 55, 2009.

Melhuish, Simon J., et al., A Tilttable Single-Shot Miniature Dilution Refrigerator for Astrophysical Applications, *Cryogenics*, 55-56, 2013.

Mohandas, P., et al., Continuously Operating Cryogenic Cycle Dilution Refrigerator, *Physica B*, 194-196, 1994.

Nilles, M. J., Effects of Oxidation and Roughness on Cu Contact Resistance from 4 to 290 K, *Advances in Cryogenic Engineering* 34, 1987.

Piccirillo, L., et al., *Miniature Sorption Coolers: Theory and Applications*, CRC Press, 2018.

Pobel, Frank, *Matter and Methods at Low Temperatures*, Springer-Verlag, 2007.

Richards, Samuel N., et al., SOFIA-HIRMES: Looking Forward to the High-Resolution Mid-infrared Spectrometer, *Journal of Astronomical Instrumentation* 7, 4, 2018.

Richter, M. J., et al., EXES: The Echelon-Cross-Echelle Spectrograph for SOFIA, *Journal of Astronomical Instrumentation* 7, 2018.

Risacher, C., First Supra-THz Heterodyne Array Receivers for Astronomy with the SOFIA Observatory, *IEEE Trans. On TeraHertz Science & Technology*, 6, 2, 2016.

Risacher, C., et al., The upGREAT Dual Frequency Heterodyne Arrays for SOFIA, *Journal of Astronomical Instrumentation* 7, 4, 2018.

Roach, P. R., et al., Compact Dilution Refrigerator, *Japanese Journal of Applied Physics*, 26, 1987.

Roach, P. R., et al., A 3He-Gap Heat Switch for Use below 2 K in Zero G, *Advances in Cryogenic Engineering B*, 37, 1992.

Roach, P. R., et al., Development of a Dilution Refrigerator for Low-Temperature Microgravity Experiments, *Cryocoolers* 10, 1998.

Schmittab, R. L., et al., Thermal Conductance Measurements of Bolted Copper Joints for SuperCDMS, FERMILAB-PUB-14-522-PDD.

Shirron, P., et al., Heat Switches Providing Low Activation Power and Quick Switching Time for use in Cryogenic Multi-Stage Refrigerators, *Advances in Cryogenic Engineering A*, 57, 2012.

Shirron, Peter J., McCammon, Dan, *Salt Pill Design and Fabrication for Adiabatic Demagnetization Refrigerators*, 2019.

Tomaru, T., et al., Vibration Analysis of Cryocoolers, *Cryogenics* 44, 309-317, 2004.

Voellmer, G. M., et al., *Proc. Spie* 4850, 1070-1079, 2003.

White, Guy K., *Experimental Techniques in Low-Temperature Physics*, 3<sup>rd</sup> Edition, Oxford University Press, 1979.

Woodcraft, Adam L., Recommended Values for the Thermal Conductivity of Aluminum of Different Purities in the Cryogenic to Room Temperature Range, and a Comparison with Copper, *Cryogenics*, 45, 9, 2005.

## **SOFIA Documents**

SOF-DA-PLA-PM17-2000, *Concept of Operations (ConOps) for SOFIA.*  
SOF-NASA-REP-SV03-2115, *2016 Cabin Temperature Characterization Results.*  
SOF-AR-SPE-SE01-2028, *SOFIA Science Instrument (SI) System Specification.*  
APP-DF-PRO-OP02-2043, *Procedure for Crossing the TA Barrier during Flight.*  
APP-DA-PLA-PM17-2076, *Cryocooler System Concept of Operations (ConOps).*  
SOF-AR-ICD-SE03-2029 (MCCS\_SI\_05), *Principal Investigator Patch Panel to PI Equipment Rack(s) ICD.*  
SOF-DA-ICD-SE03-036 (TA\_SI\_01), *Cable Load Alleviator Device / Science Instrument Cable ICD.*  
APP-DF-ICD-SE03-2038 (GLOBAL\_POWER\_BUDGET), *Global Power Budget ICD.*  
SOF-NASA-ICD-SE03-2066 (CRYO\_SI\_02), *Phase 2 Cryocooler System to Science Instrument (SI) ICD.*  
SOF-DA-ICD-SE03-037 (TA\_SI\_02), *Telescope Assembly / Science Instrument Mounting ICD.*  
SOF-AR-ICD-SE03-2027 (SI\_CWR\_01), *Science Instrument Equipment to Counterweight Rack (CWR) ICD.*  
SOF-DA-ICD-SE03-051 (TA\_SI\_05), *SI Equipment Rack / TA Counterweight ICD.*  
SE03-2015 (SI\_AS\_01), *Principal Investigator Equipment to PI Rack to Aircraft System ICD.*  
SE03-002 (GLOBAL\_09), *Science Instrument Envelope ICD.*

**REPORT DOCUMENTATION PAGE**

*Form Approved  
OMB No. 0704-0188*

The public reporting burden for this collection of information is estimated to average 1 hour per response, including the time for reviewing instructions, searching existing data sources, gathering and maintaining the data needed, and completing and reviewing the collection of information. Send comments regarding this burden estimate or any other aspect of this collection of information, including suggestions for reducing the burden, to Department of Defense, Washington Headquarters Services, Directorate for Information Operations and Reports (0704-0188), 1215 Jefferson Davis Highway, Suite 1204, Arlington, VA 22202-4302. Respondents should be aware that notwithstanding any other provision of law, no person shall be subject to any penalty for failing to comply with a collection of information if it does not display a currently valid OMB control number.  
**PLEASE DO NOT RETURN YOUR FORM TO THE ABOVE ADDRESS.**

<b>1. REPORT DATE</b> (DD-MM-YYYY) 10/15/2020	<b>2. REPORT TYPE</b> Technical Memorandum	<b>3. DATES COVERED</b> (From - To)
--------------------------------------------------	-----------------------------------------------	-------------------------------------

<b>4. TITLE AND SUBTITLE</b> Cryogenic Technologies for the Stratospheric Observatory for Infrared Astronomy (SOFIA) Science Instruments	<b>5a. CONTRACT NUMBER</b>
	<b>5b. GRANT NUMBER</b>
	<b>5c. PROGRAM ELEMENT NUMBER</b>

<b>6. AUTHOR(S)</b> Richards, W. Lance; Meyer, Michael L.; Feller, Jeffrey R.; Rhodes, Alan C.; Rosner, Stefan; Stevanovic, Dejan; Kashani, Ali	<b>5d. PROJECT NUMBER</b>
	<b>5e. TASK NUMBER</b>
	<b>5f. WORK UNIT NUMBER</b> 860921.01.23.01.01

<b>7. PERFORMING ORGANIZATION NAME(S) AND ADDRESS(ES)</b> NASA Langley Research Center Hampton, VA 23681-2199	<b>8. PERFORMING ORGANIZATION REPORT NUMBER</b> NESC-NPP-18-01305
---------------------------------------------------------------------------------------------------------------------	----------------------------------------------------------------------

<b>9. SPONSORING/MONITORING AGENCY NAME(S) AND ADDRESS(ES)</b> National Aeronautics and Space Administration Washington, DC 20546-0001	<b>10. SPONSOR/MONITOR'S ACRONYM(S)</b> NASA
	<b>11. SPONSOR/MONITOR'S REPORT NUMBER(S)</b> NASA/TM-2020-5008777

**12. DISTRIBUTION/AVAILABILITY STATEMENT**  
Unclassified - Unlimited  
Subject Category Astronomy  
Availability: NASA STI Program (757) 864-9658

**13. SUPPLEMENTARY NOTES**

**14. ABSTRACT**  
This work was performed at the request of the Program Chief Engineer for Stratospheric Observatory for Infrared Astronomy (SOFIA). The intended audience for this position paper is the prospective SOFIA Science Instrument (SI) developer, who may not have extensive experience with cryogenics or cryostat design. The objective is to provide an introductory handbook that (1) concisely summarizes SOFIA requirements, (2) describes components and techniques that enable cryostats to reach temperatures ranging from 4 K to 50 mK, and (3) warns of common pitfalls that an SI developer might encounter.

**15. SUBJECT TERMS**  
Stratospheric Observatory for Infrared Astronomy; Science Instrument; Cryogenic Technologies; NASA Engineering and Safety Center

<b>16. SECURITY CLASSIFICATION OF:</b>			<b>17. LIMITATION OF ABSTRACT</b>	<b>18. NUMBER OF PAGES</b>	<b>19a. NAME OF RESPONSIBLE PERSON</b>
<b>a. REPORT</b>	<b>b. ABSTRACT</b>	<b>c. THIS PAGE</b>			STI Help Desk (email: help@sti.nasa.gov)
U	U	U	UU	108	<b>19b. TELEPHONE NUMBER</b> (Include area code) (443) 757-5802